Thesis presented to the Instituto Tecnológico de Aeronáutica, in partial fulfillment of the requirements for the degree of Doctor of Science in the Graduate Program of Physics, Field of Nuclear Physics.

Geanderson Araújo Carvalho

WHITE DWARFS IN GENERAL RELATIVITY, MODIFIED THEORIES OF GRAVITY AND BINARY SYSTEMS

Thesis approved in its final version by signatories below:

Prof. Dr. Rubens de Melo Marinho Jr.

Advisor

Prof. Dr. Jorge Armando Rueda

Co-advisor

Prof. Dr. Pedro Teixeira Lacava

Pro-Rector of Graduate Courses

Campo Montenegro
São José dos Campos, SP - Brazil
2019

Cataloging-in Publication Data
Documentation and Information Division

Carvalho, Geanderson Araújo
White dwarfs in general relativity, modified theories of gravity and binary systems / Geanderson Araújo Carvalho.
São José dos Campos, 2019.
98f.

Thesis of Doctor of Science – Course of Physics. Area of Nuclear Physics – Instituto Tecnológico de Aeronáutica, 2019. Advisor: Prof. Dr. Rubens de Melo Marinho Jr.. Co-advisor: Prof. Dr. Jorge Armando Rueda.

1. Relativistic Astrophysics. 2. White Dwarfs. 3. Modified Theories of Gravity. 4. Chandrasekhar Limit. 5. Binary Systems. I. Instituto Tecnológico de Aeronáutica. II. Title.

BIBLIOGRAPHIC REFERENCE

CARVALHO, Geanderson Araújo. **White dwarfs in general relativity, modified theories of gravity and binary systems**. 2019. 98f. Thesis of Doctor of Science – Instituto Tecnológico de Aeronáutica, São José dos Campos.

CESSION OF RIGHTS

AUTHOR'S NAME: Geanderson Araújo Carvalho
PUBLICATION TITLE: White dwarfs in general relativity, modified theories of gravity and binary systems.
PUBLICATION KIND/YEAR: Thesis / 2019

Geanderson Araújo Carvalho
Praça Marechal Eduardo Gomes, 50
12.228-900 – São José dos Campos–SP

WHITE DWARFS IN GENERAL RELATIVITY, MODIFIED THEORIES OF GRAVITY AND BINARY SYSTEMS

Geanderson Araújo Carvalho

Thesis Committee Composition:

Prof. Dr.	Wayne Leonardo Silva de Paula	Chairman	-	ITA
Prof. Dr.	Rubens de Melo Marinho Jr.	Advisor	-	ITA
Prof. Dr.	Jorge Armando Rueda	Co-advisor	-	UNIROMA
Prof. Dr.	César Henrique Lenzi	Internal member	-	ITA
Prof. Dr.	Oswaldo Duarte Miranda	External member	-	INPE
Prof. Dr.	Márcio Eduardo da Silva Alves	External member	-	UNESP

ITA

To my family.

Acknowledgments

First of all, I would like to thank God for all the blessings bestowed and for given me the capability to finish this work.

I would like also to thank all the professors who participated of my academic training, in special, Dr. Rubens Marinho Jr. for guidance, oportunity and patience during all of those years, I have learned so much with him, not only about physics. I would like to give a special thanks to Dr. Manuel Malheiro with whom I have learned so much and for his incentive, to teach me how to be persistent and to give me a lot of opportunities. Among many others professors with whom I have learned infinitely. To professor Dr. Andrey Martins for having encouraged my academic career. To Dr. Jorge Rueda for months of orientation and learning at the Sapienza University of Rome and its students for kind reception.

To all the friends who helped effectively or indirectly, being with me along all of those years of graduation.

I would like to thank my fiancee Flavia Rocha for all the support, help and companionship without which it would not be possible the conclusion of this work.

Last but not least, I would like to thank to my family. My mother Nilva, for giving me all the backing I could have, for always encouraging me to study, and for all her years of struggle and sweat so that I could get here. To my brothers, George and Gedson, for the great help, encouragement and years of play.

To CAPES for financial support.

"Study hard what interests you the most in the most undisciplined, irreverent and original manner possible.
— Richard Feynman

Resumo

Neste trabalho de tese realizamos primeiramente um estudo comparativo do equilíbrio hidrostático de estrelas anãs brancas em diferentes abordagens, a saber, Newtonianas e relativísticas. Comparando os modelos obtivemos que a estrutura destas estrelas sofrem efeitos tanto de Relatividade Geral quanto de Relatividade Restrita para massas acima de $1{,}3M_{\odot}$, necessitando assim de uma abordagem estritamente relativística. Consideramos a inclusão do efeito de campos elétricos para anãs brancas, para tal supomos uma distribuição de carga superficial. Encontramos neste caso que a carga total necessária para induzir efeitos na estrutura de anãs brancas é da ordem 10^{19-20}C, cujos campos elétricos de superfície $E \sim 10^{17-18}$V/m são majoritariamente abaixo do limite de campo crítico de Schwinger $1{,}3 \times 10^{18}$V/m. Neste caso, mesmo com campos elétricos abaixo do valor de campo crítico obtemos anãs brancas super-Chandrasekhar com massas da ordem $M \sim 2M_{\odot}$, desta forma sendo compatíveis com as massas estimadas encontradas a partir de observações de supernovas Ia. Consideramos também um modelo de extensão de Relatividade Geral, no qual na Lagrangiana de Einstein-Hilbert o escalar de curvatura é substituído por uma função arbitrária do tipo $f(\mathcal{R}, \mathcal{T})$, onde $\mathcal{R}$ e $\mathcal{T}$ são o escalar de curvatura e o traço do tensor energia-momento, respectivamente. Mostramos, a partir da nova equação de equilíbrio hidrostático para o funcional específico $f(\mathcal{R}, \mathcal{T}) = \mathcal{R} + 2\lambda\mathcal{T}$, que a massa máxima de anãs brancas é alterada conforme variamos a magnitude do parâmetro λ. Quanto maior a magnitude de λ estrelas maiores e mais massivas são encontradas. Também encontramos para o modelo sugerido que as densidades centrais das anãs brancas de massa máxima são bem menores que as densidades centrais encontradas em Relatividade Geral e em outras teorias modificadas de gravidade. Investigamos também algumas propriedades do gás de Fermi em D dimensões para mostrar que anãs brancas são gravitacionalmente instáveis dada a presença de dimensões espaciais extras. Além disso, mostramos que o campo elétrico induzido devido a fricção magnética em sistemas binários de anãs brancas pode levar a uma emissão eletromagnética elevada para campos $B > 10^{9}$G, o que poderia também afetar a evolução orbital de tais sistema binários.

Abstract

In this work we perform, initially, a comparative study of the hydrostatic equilibrium of white dwarfs (WD) in different approaches, namely, Newtonian and general relativistic. We obtain that the structure of these stars suffer effects from both special and general relativistic corrections for stars with mass $M > 1.3M_{\odot}$. We also consider the inclusion of effects in the structure of WD from strong electric fields, for such we suppose a superficial net charge distribution in those stars. We find that the total charge necessary to appreciate considerable effects in the structure of WD is of the order of 10^{19-20}C, whose electric fields at the surface $E \sim 10^{17-18}$V/m are mostly below the Schwinger critical field limit 1.3×10^{18}V/m. In this case, even with fields smaller than the critical one we obtain super-Chandrasekhar WD masses in the order of $\sim 2M_{\odot}$, being in this way consistent with estimated masses measured from supernova Ia observations. We consider also a modified gravity model, in which in the Einstein-Hilbert Lagrangian the Ricci scalar is replaced by an arbitrary function of the form $f(\mathcal{R}, \mathcal{T})$, where $\mathcal{R}$ and $\mathcal{T}$ represent the Ricci scalar and trace of the energy-momentum tensor, respectively. We showed from the hydrostatic equilibrium, for the specific functional form $f(\mathcal{R}, \mathcal{T}) = \mathcal{R} + 2\lambda\mathcal{T}$, that the maximum mass of WD is modified according to the variation of the parameter λ. The larger the magnitude of λ the larger and more massive stars are found. We also find for the suggested model that the maximum mass stars' central densities are smaller than the ones obtained in General Relativity and other modified theories of gravity. We investigated also some properties of the D-dimensional Fermi gas to show that WD are gravitationally unstable due the presence of extra spatial dimensions. Moreover, we showed that the electric field induced by magnetic friction in double WD binaries can power a high electromagnetic emission (for $B > 10^{9}$G) and it can also change the orbital evolution of the binaries.

List of Figures

FIGURE 2.1 – Pressure as function of the energy density for fully degenerate relativistic Fermi gas in D-dimensions. As one can see the pressure decreases as the number of dimensions increase, which can be see also from Eqs. (2.37) and (2.38). 29

FIGURE 4.1 – a) Mass-radius relation and b) mass-central mass density relation for general relativistic and Newtonian cases. In both plots the solid black line represents the outcomes for general relativistic WD, the dashed-dotted magenta line represents Newtonian results with special relativistic corrections and the dashed gray line represents the Newtonian results. It is also displayed in a) the non-relativistic mass-radius relation (dotted orange line), in which $M \propto 1/R^3$. . . . 44

FIGURE 4.2 – Mass-radius relation of massive WD. The curves follow the same representation as in Fig. 4.1. The full blue circles mark the maximum masses. The dotted red line represents the measured mass of the most massive white dwarf ($M = 1.41 M_\odot \pm 0.04$) found in literature (VENNES *et al.*, 1997) and the shaded orange region corresponds to its estimated error. 45

FIGURE 4.3 – From top to bottom: a) mass profiles, b) energy density profiles and c) gradient of pressure profiles. All profiles correspond to a fixed total star mass of $M = 1.415 M_\odot$. 47

FIGURE 4.4 – General relativistic and Newtonian gravitational fields as a function of radial coordinate for a fixed total star mass of $1.415 M_\odot$. 48

FIGURE 4.5 – General relativistic and Newtonian gravitational potentials as a function of radial coordinate for a fixed total star mass of $1.415 M_\odot$. . . . 48

FIGURE 4.6 – General relativistic gravitational fields as a function of radial coordinate for a total mass of $1.415 M_\odot$, calculated with and without correction terms. 49

FIGURE 4.7 – Radius relative difference ΔR versus fixed total star mass. 50

FIGURE 4.8 – Surface gravity versus fixed total star mass. The dotted red line is the measurement of mass of the most massive white dwarf ($EUVE\ J\ 1659+440$) found in literature (VENNES *et al.*, 1997) and the shaded orange region is its estimated error. 51

FIGURE 4.9 – Relative difference between Newtonian surface gravity and general relativistic surface gravity against fixed total star mass. 51

FIGURE 4.10 –Fit of the general relativistic mass-radius diagram with Eq.(4.8) (red dashed line) and the non-relativistic limit (dotted orange line). . . . 53

FIGURE 4.11 –Total mass, in Solar masses $M_\odot$, versus central mass density of the star for six values of σ. The unit for the constant σ is [C]. 55

FIGURE 4.12 –The radius of the charged white dwarf as a function of the mass for different values of σ. 55

FIGURE 4.13 –Profile of the pressure inside the star as a function of the radial pressure for five different values of σ and for $\rho_c = 10^{10}[\mathrm{g/cm^3}]$. . . . 56

FIGURE 4.14 –Electric field as a function of the radial coordinate inside the charged white dwarf, for five values of σ and one of ρ_c. The central energy density $10^{10}[\mathrm{g/cm^3}]$ is considered. 57

FIGURE 4.15 –Total electric charge against the central energy density for some values of σ. 58

FIGURE 4.16 –Independent total mass $MG_D^{(D-1)/2}$ as function of the central energy density for white dwarfs in D-dimensions, for $D = 4$ (4.16a) and $D = 5$ (4.16b). As one can see the case $D = 5$ does not present any stability region. It is worth to cite that $G_D = l_D G_4$, where l_D is a parameter with dimension km^{D-4} and G_4 is the Newton's gravitational constant. We also have used natural units $c = 1 = G_4$ with $M_\odot = 1.47\mathrm{km}$. 60

FIGURE 4.17 –Energy conditions: in (4.17a) we have the null energy condition (NEC), $p + \rho \geq 0$. In (4.17b) we have the weak energy condition (WEC), $\rho \geq 0$. In (4.17c) the strong energy condition (SEC), $T \geq 0$. And finally in (4.17d) we have the last one, the dominant energy condition (DEC), $\rho \geq |p|$, one can see that for any dimensions, the energy conditions are respected for any value of energy density and pressure. 62

FIGURE 5.1 – Total mass as a function of the total radius for different values of λ. The full magenta circles indicate the maximum mass points. 66

FIGURE 5.2 – Mass as a function of the radius for massive WDs with different values of λ. The blue circles with error bars represent the observational data of a sample of massive WDs taken from the catalogs (VENNES *et al.*, 1997; NALEŻYTY *et al.*, 2004). 66

FIGURE 5.3 – On the top panel it is presented the star energy density as a function of the radial coordinate, on the central panel we show the star pressure fluid against the radial coordinate and on the bottom panel we display the mass (in solar masses, $M_\odot$) inside the star versus the radial coordinate. We consider $\rho_c = 10^9$ [g/cm^3] and the displayed values of λ. 68

FIGURE 5.4 – The dependence of the total mass of the white dwarfs on central density for different values of λ. 69

FIGURE 5.5 – The total star radius versus central density for different values of λ. 69

FIGURE 6.1 – Schematic representation of the unipolar inductor model. As the secondary star is a conductor moving in the primary star's magnetosphere an electric field is induced inside the secondary. This electric field could thus accelerate particles from the secondary's surface. In a situation of equilibrium a closed circuit could be set with the charged particles following the magnetic field lines' path. Source: (WU *et al.*, 2002). 73

FIGURE 6.2 – Luminosity as a function of the orbit's angular frequency using the results of (WU *et al.*, 2002) (see also Eq. (6.6)). The value of α is 0.9. The masses are $M_1 = M_2 = 0.6M_\odot$ and their respective radii are taken from (CARVALHO *et al.*, 2018). The magnetic field strength ranges from 10^6G to 10^9G. According to the model of Wu et al. the luminosity can be very high at moments close to merger. . 74

FIGURE 6.3 – Parameterized luminosity as a function of orbital angular frequency (see Eq. 6.9). The masses are $M_1 = M_2 = 0.6M_\odot$. The mass-radius relation is taken from (CARVALHO *et al.*, 2018). 75

FIGURE 6.4 – Orbital evolution for two values of magnetic field. The parameters were choose such as in Fig. 6.3. The initial period is 4 hours. 76

FIGURE 6.5 – Intrinsic time-domain phase evolution normalized by $Q_\omega^{\rm GW}$, $\hat{Q}_\omega \equiv Q_\omega/Q_\omega^{\rm GW}$. 76

FIGURE 6.6 – Left: Evolution of the separation distributions n for WD-WD binaries with an initial power-law where $\alpha = -2$. Red, black and blue lines correspond to magnetic fields of 0, 10^9G and 10^{10}G, respectively. Solid, dotted and dashed-dotted lines corresponds to a time t of 1Myr, 100Myr and 10Gyr. Right: Present day distributions N for a timescale $t_0 = 10$Gyr. Colors follow the same representation as in the left panel, solid, dashed-dotted and dotted lines now represent α equals to 1, -1 and -3, respectively. 79

List of Tables

TABLE 4.1 – Maximum mass and minimum radius for the static models of WD stars. 45

TABLE 4.2 – Corresponding radii to fixed total star masses in Newtonian and general relativistic cases. $R_{\rm Newton}$ means the radius predicted by Newtonian case, $R_{\rm SR}$ is the radius given by special relativistic case, and $R_{\rm GR}$ is the radius calculated in the general relativistic case and the $R_{\rm NR}$ is the radius supplied by non-relativistic approximation, where the mass follows the relation $M/M_{\odot} \propto 1/R^3$. 46

TABLE 4.3 – Corresponding central mass densities to fixed total masses in Newtonian and general relativistic cases. $\rho_C^{\rm Newton}$ means the central density achieved in Newtonian case, $\rho_C^{\rm SR}$ is the central density given by SR case, $\rho_C^{\rm GR}$ is the central density found for the general relativistic case. 46

TABLE 4.4 – Values of the constants for the analytic mass-radius relations. 52

TABLE 4.5 – The constant σ and the maximum masses of the electrically charged white dwarfs with their respective radii, central densities, charges and electric fields at the surface of the stars. 56

TABLE 5.1 – The maximum masses of the white dwarfs found for each value of λ with their respective total radii and central energy densities. 70

TABLE 6.1 – Parameterized orbital evolution, separation distribution and delay time distribution for WD-WD binaries. 78

List of Abbreviations and Acronyms

General Relativity	GR
Special Relativity	SR
Super-Chandrasekhar	SC
White Dwarf	WD
Equation of State	EoS

List of Symbols

$M_\odot$	Mass of the Sun
$R_\odot$	Radius of the Sun
R_s	Schwarzschild Radius

Contents

1 Introduction 18

2 Review about the Equation of State of White Dwarfs 22

2.1 Chandrasekhar Equation of State 22

2.2 Salpeter Equation of State 25

2.2.1 Electrostatic Corrections 25

2.2.2 Inverse beta decay 27

2.3 Generalization of the Chandrasekhar Equation of State for a D-dimensional space-time 28

3 Field Equations from a Variational Principle 31

3.1 General Relativity 31

3.1.1 Schwarzschild Solution 33

3.1.2 Tolman-Oppenheimer-Volkoff Equation 35

3.1.3 Reissner-Nordström Solution 35

3.1.4 Bekenstein Equation 37

3.1.5 Field equations for a D-dimensional space-time with spherical symmetry 38

3.2 $f(\mathcal{R},\mathcal{T})$ Gravity 40

3.2.1 Stellar structure equations in $f(\mathcal{R},\mathcal{T})$ gravity 41

4 White Dwarfs in General Relativity 43

4.1 Comparison between Newtonian and general relativistic cases . . 43

4.1.1 Fixed total star mass 45

4.2 Fit of the general relativistic mass-radius relation 52

4.3 Stellar equilibrium configurations of charged white dwarfs 53

4.4 About the radial stability of charged white dwarf 58

4.5 Universal charge-radius relation and maximum total charge of white dwarfs 59

4.6 Gravitational instability of white dwarfs in D-dimensions 59

4.6.1 Energy conditions 61

4.6.2 Lane-Emden equation in D-dimensions (Newtonian instability) 62

5 White Dwarfs in $f(\mathcal{R},\mathcal{T})$ Gravity 65

6 White Dwarfs in Binary Systems 71

7 Conclusions 80

Bibliography 85

Appendix A – Some derivations and important mathematical identities 97

1 Introduction

White dwarf stars, object of study of this work, are stars that have their beginning in the "death" of ordinary stars of up to $8 - 10M_{\odot}$ (WOOSLEY; HEGER, 2015), here $M_{\odot}$ represents the mass of the Sun. This "death" is determined by the gravitational collapse of stars in the so called main sequence phase of evolution, such as the Sun. When this collapse occurs we have an event named in the literature as supernova (WANG; WHEELER, 2008). Since the matter that constitutes a white dwarf star is made up of "heavy" elements, such as carbon and oxygen, fusion reactions do not occur in its interior as it happens in ordinary stars (main sequence stars), consequently, there is no thermal pressure that supports the star against the gravitational collapse (HILLEBRANDT; NIEMEYER, 2000).

Indeed, up to 1926, more than a decade after the first detection of a white dwarf, the physical mechanism that supports such stars against gravitational collapse was unknown (SHAPIRO; TEUKOLSKY, 1983). Only after the development of the Fermi-Dirac statistics it was possible to understand that white dwarfs can withstand gravitational attraction due to electron degeneracy pressure, which originates from the Pauli exclusion principle.

Chandrasekhar then theorized that white dwarf stars would be constituted by a crystalline lattice of fully ionized ions immersed in a degenerate electron gas (CHANDRASEKHAR, 1967). In case of total degeneracy - considering that the star has undergone a long cooling process, i.e., irradiated its residual thermal energy mainly due to neutrino emission - the star temperature is considered sufficiently small, such that $T \to 0$, and the star is supported mainly due degeneracy pressure. In this limiting case the degeneracy pressure could sustain a mass of up to $1.44M_{\odot}$, the so-called Chandrasekhar mass limit, which Chandrasekhar derived in the 1930s using the Newtonian theory of gravitation (CHANDRASEKHAR; S., 1935).

Currently, there are no observations or concrete evidence of white dwarfs with masses exceeding the Chandrasekhar limit, which makes this limit one of the most well-established theoretical constraints in the field of astrophysics. In the Sloan Digital Sky Survey (SDSS) catalog, which has several data of white dwarfs, both isolated and in binary systems, as well as magnetized and nonmagnetized white dwarfs, the most massive white dwarf quoted has a mass of $1.34M_{\odot}$ and a rotation period of 725 seconds (KEPLER *et al.*, 2017;

KLEINMAN *et al.*, 2013). In reference (VENNES *et al.*, 1997) the most massive white dwarf reported has a mass $M = 1.41 \pm 0.04 M_{\odot}$ and magnetic field $B \sim 10^9$G. With respect to the study of magnetized white dwarfs, the scientific community has shown renewed interest in the subject, due to the increasing number of magnetic white dwarfs observed and the possible description of soft gamma-ray repeaters (SGR) and anomalous x-ray pulsars (AXP) as white dwarf pulsars with short rotation periods (in the order of $P \sim 1 - 10$ seconds) and high magnetic fields ($B \sim 10^{12-14}$G) (LOBATO *et al.*, 2015; MALHEIRO *et al.*, 2011b; COELHO; MALHEIRO, 2014).

Magnetic white dwarfs have also been used as an attempt to explain some indirect evidence of white dwarfs with mass above the Chandrasekhar mass limit (DAS; MUKHOPADHYAY, 2013; DAS; MUKHOPADHYAY, 2014; FRANZON; SCHRAMM, 2015), or simply referred in the literature as super-Chandrasekhar white dwarfs (HOWELL *et al.*, 2006; HICKEN *et al.*, 2007; YAMANAKA *et al.*, 2009; SCALZO *et al.*, 2010; SILVERMAN *et al.*, 2011; TAUBENBERGER *et al.*, 2011; TANAKA *et al.*, 2010). Those evidence were the detection of type Ia supernovae[1] with certain peculiar characteristics, such as, low velocity curves and high luminosities. In several works those characteristics are put forward as indicative that super-Chandrasekhar white dwarfs are the most likely progenitors of such peculiar supernovae (HOWELL *et al.*, 2006; TANAKA *et al.*, 2010).

Supernova events are of great importance for the understanding of our universe. The events $SN1937C$, $SN1960F$, $SN1990N$, $SN1991T$, among others, are used as standard candles serving as a reference for carrying length measurements on cosmological scales, see, for example, (BRANCH; TAMMANN, 1992) and references therein. In 1998 observations of type Ia supernovae also led to the discovery that our universe is gradually expanding faster (RIESS *et al.*, 1998; PERLMUTTER *et al.*, 1999).

The most accepted model currently describing the cosmological history of our universe - including the current accelerated expansion phase - using General Relativity theory is the ΛCDM (Cold Dark Matter) model, that associates this accelerated expansion of the universe to a negative energy density, which in turn would be related to the zero point energy. This energy responsible for such phenomena is commonly called in the literature as dark energy (FRIEMAN *et al.*, 2008). However, despite describing well our universe on cosmological scales, the ΛCDM model has its flaws. The cosmological constant Λ - often associated with vacuum energy - is not compatible with the values predicted by any quantum field theory, the so-called "fine-tuning problem of the cosmological constant", in addition to having certain discrepancies with observational data, for example, the cosmic microwave background anomalies (Del Popolo; Le Delliou, 2017).

In this sense new theories have been developed in attempt to solve such problems from

[1]Type Ia supernovae are the gravitational collapse of a white dwarf, probably due to mass accretion of a companion star.

the cosmological point of view, for example: the theory called modified Newton dynamics (MOND) and extended theories of General Relativity. Extended theories of General Relativity (EGR) or modified theories of gravity are theories that have as their base the usual general relativistic formulation, starting from the Einstein-Hilbert Lagrangian. However, modifications in this Lagrangian are made in order to obtain new field equations that describe the cosmological history of the universe without the need to introduce the concepts of dark matter and dark energy. In addition, due to certain supernova observations indicate the existence of super-Chandrasekhar white dwarfs, several theoretical models, both in General Relativity and modified theories of gravity, were constructed in an attempt to obtain white dwarfs with masses of the order of $2M_{\odot}$, thus being compatible with observations.

In the scope of General Relativity, super-Chandrasekhar white dwarfs were obtained by taking into account magnetic field effects (DAS; MUKHOPADHYAY, 2013; DAS; MUKHOPADHYAY, 2014; FRANZON; SCHRAMM, 2015), rotation as a rigid body (BOSHKAYEV *et al.*, 2013; BOSHKAYEV *et al.*, 2014), differential rotation (OSTRIKER; BODENHEIMER, 1968) and electric field (LIU *et al.*, 2014). In (LIU *et al.*, 2014) white dwarfs with a charge distribution in their interior were studied. Such a charge distribution was assumed to follow a linear relationship with the matter distribution $\rho_e \propto \rho$. For this distribution a total charge of the order of $Q \sim 10^{20}$ C was shown to be able to raise the gravitational mass of the star up to about $3M_{\odot}$. In (LIU *et al.*, 2014) the stability condition via virial theorem was generalized by including the electric field energy, thus demonstrating that charged white dwarfs are stable according to this theorem.

We will consider here that the charge distribution in a white dwarf is similar to a charge distribution in a conductor, that is, the charge is considered to be concentrated on the surface of the star. This assumption is reasonable given the fact that it is shown in the literature that the greater the degree of degeneracy of matter the larger the thermal and electrical conductivity (YAKOVLEV; URPIN, 1993; BAIKO; YAKOVLEV, 1995). Therefore, we model the surface charge distribution as a Gaussian distribution on the surface of the star $\rho_e = ke^{\frac{(r-R)^2}{b^2}}$. We find in this case that the amount of charge required to significantly change the gravitational mass of the star is in the range of 10^{20}C. It is important to note that this order of magnitude is the same found for several types of distributions considered for neutron stars and quark stars (NEGREIROS *et al.*, 2009; RAY *et al.*, 2003; ARBAÑIL *et al.*, 2013; ARBAÑIL; MALHEIRO, 2015; JING *et al.*, 2015). Instability due to radial oscillations and the electric field screening caused by vacuum polarization are discussed later in the present work.

Extended Theories of General Relativity have also recently been applied to white dwarfs in order to theoretically predict the existence of super-Chandrasekhar white dwarfs (DAS; MUKHOPADHYAY, 2015b; BANERJEE *et al.*, 2017; JAIN *et al.*, 2016; JING;

WEN, 2016; DAS; MUKHOPADHYAY, 2015a; CARVALHO *et al.*, 2017). At the same time, due to the variety of observational data, white dwarfs can be used to restrict the free parameters of these theories (see, for example, (JAIN *et al.*, 2016; BANERJEE *et al.*, 2017)). In (JING; WEN, 2016) the authors obtained super-Chandrasekhar white dwarfs for a Born-Infield type theory, as well as the restriction to the maximum value of the model parameter according to observational data. Super-Chandrasekhar and sub-Chandrasekhar white dwarfs were also obtained in the Starobinsky's gravity (DAS; MUKHOPADHYAY, 2015b; DAS; MUKHOPADHYAY, 2015a). In (CARVALHO *et al.*, 2017) we study the effects of a specific model of modified theory of gravity on the structure of white dwarfs in order to both restrict the free parameters of the theory and to analyze the possibility of predicting stable super-Chandrasekhar white dwarfs.

In the next chapter, we will briefly review the equation of state used in this work. In the chapter 3 we derive the field equations in order to obtain the hydrostatic equilibrium equations for each approach we used. The solutions for the field equations are: the Schwarzschild solution and the Reissner-Nordstrom solution, as well as the equilibrium equations related to these solutions, which are the Tolman-Oppenheimer-Volkof and Bekenstein equations, respectively. In the chapter 3 we also derive the equilibrium equation for an object with spherical symmetry in a spacetime with arbitrary dimension D, as well as derive the hydrostatic equilibrium equation for a modified theory of gravity, namely, the $f(\mathcal{R},\mathcal{T})$ gravity. In chapters 4 and 5 we outline our results for white dwarfs in the scope of General Relativity and $f(\mathcal{R},\mathcal{T})$ gravity, respectively. In chapter 6 we introduce a model of electromagnetic emission in double white dwarf binary systems and study its consequences for the evolution and gravitational wave emission of those binaries. Finally, in chapter 7 we conclude and make a prognosis of our work in progress.

2 Review about the Equation of State of White Dwarfs

Equation of state (EoS) plays a crucial role in determining the macroscopic properties of compact stars, whether treating white dwarfs, neutron stars or quarks stars. Hydrostatic equilibrium solutions can be constructed if an EoS relating pressure and energy density of the fluid constituting the star is provided. For white dwarfs, we can find in the literature several EoS that take into account, for instance, magnetic field effects and temperature effects (CHAMEL *et al.*, 2013; CARVALHO *et al.*, 2014).

One of the most seminal works about the white dwarf EoS was the work of Fowler who first introduced the concept of degenerate stars (FOWLER, 1926). Following Fowler's work, Chandrasekhar in 1931 took into account relativistic effects for the EoS and showed that white dwarf stars have a maximum mass value at which degeneracy pressure can withstand and counterbalance gravity (CHANDRASEKHAR; S., 1931). The EoS derived by Chandrasekhar is based on a relativistic formulation and the Fermi-Dirac quantum statistic for an ideal gas.

Corrections due to electrostatic interactions between the gas particles were derived by Salpeter for a zero temperature plasma (SALPETER; E., 1961). In a later study this EoS was applied to the study of the macroscopic properties of white dwarfs in (HAMADA; SALPETER, 1961), in which it was shown that the maximum mass of white dwarfs depends in a non-trivial way not only on the ratio A/Z between mass number and atomic number; as Chandrasekhar has shown; but also explicitly depends on the atomic number Z of the constituent elements present in the white dwarf. The EoS derived by Chandrasekhar and Salpeter, used hereinafter in this work, are discussed in the following sections.

2.1 Chandrasekhar Equation of State

As fermions, electrons obey the Fermi-Dirac statistis and its pressure is determined almost solely by the Pauli exclusion principle. As an ideal gas in thermal equilibrium the

number of electrons in the gas can be calculated as (PATHRIA, 1996)

$$N \equiv \sum_{E} f(E), \tag{2.1}$$

where E represents energy, μ the chemical potential, k_B is the Boltzman constant and T is the temperature. The Fermi-Dirac distributions $f(E)$ is

$$f(E) = \frac{1}{e^{(E-\mu)/k_B T} + 1}. \tag{2.2}$$

We can write Eq.(2.1) in its integral form and divide by the volume to obtain the particle number density n as

$$n = \frac{N}{V} = \frac{g}{h^3} \int f(E) d^3p, \tag{2.3}$$

where h^3 is the volume of a cell in the phase-space, and g is the spin-degeneracy factor ($g = 2s + 1$ for particles with mass and spin s).

For white dwarf stars that have undergone a long cooling process we can consider that the Fermi energy E_F is much larger than the thermal energy $k_B T$, so that $\mu - m_e c^2 >> k_B T$, where m_e is the electron mass and c is the speed of light.

Consequently, the Fermi-Dirac distribution function can be approximated by a step function for the limit $T \to 0$

$$f(E) = \begin{cases} 1, & \text{para} \quad E \leq \mu, \\ 0, & \text{para} \quad E > \mu. \end{cases} \tag{2.4}$$

In this limiting case all energy levels up to the maximum level are fullfilled. As all energy levels below the Fermi energy are fullfilled, we have by definition $E_F = \mu$. Using (2.3) and (2.4) we have (PATHRIA, 1996)

$$N = \int_0^{E_F} a(E) dE, \tag{2.5}$$

where $a(E)$ represents the density of states and it is given by (PATHRIA, 1996)

$$a(E)dE = \frac{gV}{h^3} d^3p. \tag{2.6}$$

Then substituting (2.6) into (2.5) we obtain the electron number density

$$\begin{aligned} n &= \int_0^{p_F} \frac{g}{h^3} d^3p, \\ &= \frac{p_F^3}{3\pi^2\hbar^3}. \end{aligned} \tag{2.7}$$

As the white dwarf is essentially composed of an ionic lattice immersed in the electron gas we can calculate the mass density as a contribution only of the ions. This assumption is valid once the nucleon mass is about a thousand times greater than the mass of the electron. Then we have

$$\rho_0 = \frac{N_i m_i}{V}, \tag{2.8}$$

where N_i is the number of ions and m_i its mass. The number of ions is

$$N_i = \frac{N_p}{Z} \tag{2.9}$$

where Z is the atomic number and N_p is the proton number. The ion mass is

$$m_i = m_N A, \tag{2.10}$$

where m_N is the nucleon mass and A is the nucleon number of the ions. Replacing (2.9) and (2.10) into (2.8), and assuming charge neutrality $N_p = N_e$, we obtain

$$\begin{aligned} \rho_0 &= \frac{N_e m_N A}{ZV}, \\ &= n_e m_N \frac{A}{Z}, \\ &= \frac{p_F^3}{3\pi^2\hbar^3} m_N \frac{A}{Z}, \end{aligned} \tag{2.11}$$

the ratio A/Z depends on the internal composition of the star. It is generally assumed that the star is mainly constituted by elements, such as, ^{4}He, ^{16}O or ^{12}C, hence $A/Z = 2$ (GLENDENNING, 2000).

On the other hand, since the ions are heavier than electrons their momentum are negligible when compared to the degenerate electrons' ones, in this case the energy density can be calculated as

$$\begin{aligned} \epsilon &= \rho c^2 + \epsilon_{ele}(p_F), \\ &= n m_N \frac{A}{Z} c^2 + \epsilon_{ele}(p_F). \end{aligned} \tag{2.12}$$

The electron relativistic energy is

$$E(p) = \sqrt{p^2c^2 + m_e^2c^4}. \tag{2.13}$$

Hence, the electron energy density ϵ_{ele} becomes

$$\begin{aligned} \epsilon_{ele}(p) &= \frac{2}{(2\pi\hbar)^3}\int_0^{p_F} E(p)d^3p, \\ &= \frac{1}{\pi^2\hbar^3}\int_0^{p_F}(p^2c^2 + m_e^2c^4)^{\frac{1}{2}}p^2dp, \end{aligned} \tag{2.14}$$

and making the change of variable $x = p/m_ec$, one find

$$\epsilon_{ele}(x) = \frac{\epsilon_0}{8}\left[(2x^3 + x)(1 + x^2)^{1/2} - \text{asenh}(x)\right], \tag{2.15}$$

where ϵ_0 is a constant that has the dimension of energy density and is defined as

$$\epsilon_0 = \frac{m_ec^2}{\lambda_e^3\pi^2}, \tag{2.16}$$

being λ_e the electron Compton wavelength, therefore, ϵ_0 can be physically interpreted as the electron rest mass energy per wave packet.

The electron degeneracy pressure for zero temperature and isotropic moment distribution can be written as

$$p_e = \frac{1}{3}\frac{2}{(2\pi\hbar)^3}\int_0^{p_F} pvd^3p, \tag{2.17}$$

this gives pressure as a moment flow, with the factor 1/3 coming from isotropy. The electron relativistic velocity is

$$v = \frac{pc^2}{E}, \tag{2.18}$$

so the pressure becomes

$$\begin{aligned} p_e &= \frac{1}{3}\frac{2}{(2\pi\hbar)^3}\int_0^{p_F} ppc^2(p^2c^2 + m_e^2c^4)^{-1/2}4\pi p^2dp, \\ &= \frac{\epsilon_0}{24}\left[(2x^3 - 3x)(1 + x^2)^{1/2} + 3\text{asenh}(x)\right]. \end{aligned} \tag{2.19}$$

2.2 Salpeter Equation of State

2.2.1 Electrostatic Corrections

The nature of matter over the wide range of densities that is covered in white dwarfs can vary largely due to several effects that may be important depending on the density

regime, such as effects from Coulomb interactions between particles. Considering also that the constitution of the white dwarf is largely determined by its progenitor star (LIEBERT, 1980; GLENDENNING, 2000), and that effects from Coulomb interactions depend on the atomic number Z, the white dwarf structure will be affected by the evolution history of its progenitor star.

At higher densities the atoms become progressively more ionized and the electrons fill the empty spaces between them. So, the energy is minimized to a clustering of ionic lattice immersed in the electron gas soup (GLENDENNING, 2000). Originally the idea of the ionic lattice, applied in the form of Wigner-Seitz cells by Salpeter, was introduced by Frenkel in (FRENKEL, 1928). This idea basically consists of consider a sphere (cell) around each nucleus, and as an approximation the spheres do not interact with each other since it is considered that each sphere has a quantity of electrons that neutralizes it. It is possible to show that for each interaction energy between electron-electron and electron-ion we have, respectively (GLENDENNING, 2000)

$$E_{e-e} = \frac{3}{5}\frac{Z^2e^2}{R}, \tag{2.20}$$

$$E_{e-i} = -\frac{3}{2}\frac{Z^2e^2}{R}, \tag{2.21}$$

where R is the radius of the Wigner-Seitz cell that can be calculated from

$$n_e = \frac{Z}{\frac{4}{3}\pi R^3}, \tag{2.22}$$

summing equations (2.20) and (2.21) and dividing it by the atomic number Z, one can calculate the electrostatic energy per electron as

$$\frac{E_C}{Z} = -\frac{9}{10}\left(\frac{4\pi}{3}\right)^{1/3} Z^{2/3}e^2n_e^{1/3}. \tag{2.23}$$

The thermodynamic pressure $p = -\partial E/\partial V$ associated with the electrostatic interactions becomes (SHAPIRO; TEUKOLSKY, 1983)

$$\begin{aligned} p_C &= n_e^2\frac{\partial E_C/Z}{\partial n_e}, \\ &= -\frac{3}{10}\left(\frac{4\pi}{3}\right)^{1/3} Z^{2/3}e^2n_e^{4/3}. \end{aligned} \tag{2.24}$$

The pressure resulting from the Coulomb interaction is negative, which is a reasonable result, since the attractive force between electrons and ions is greater than the electron-electron interaction force, because on average the distance between electrons is greater

than the distance between electrons and nuclei. As total pressure we have

$$p_T = p_e + p_C, \tag{2.25}$$

where p_e is given by (2.19). We can use (2.7) to find the Coulomb pressure term as a function of the parameter x, which is

$$p_C = -3.802 \times 10^{-4}\ \epsilon_0 Z^{2/3} x^4. \tag{2.26}$$

2.2.2 Inverse beta decay

With increasing density it is also possible to occur neutronization, in which the Fermi energy of the electrons reaches a value where the process of capture of electrons by the nuclei may start to happen. The main interest is to know for which values of density the nuclei are still beta stable. This type of consideration was first analyzed in (SALPETER; E., 1961), and, more recently, in several works such as (CHAMEL *et al.*, 2013; CARVALHO *et al.*, 2014; OTONIEL *et al.*, 2016).

Inverse beta decay becomes important with increasing energy density of the electrons,

$${}^{A}_{Z}X + e \ \rightarrow \ {}^{A}_{Z-1}Y + \nu_e, \tag{2.27}$$

the neutronization process is generally ignored, however, the higher the electron energy density the greater the probability of the inverse beta decay to occur, since the condition for decaying $E_F \geq \epsilon_Z$ can be satisfied , where ϵ_Z is the beta decay energy for electron capture (taking into account only the kinetic energy) (SALPETER; E., 1961). For high energy densities in which inverse beta decay may occur the star will gradually become unstable and will collapse to a more dense state of matter in which it must be a mixture of neutron rich nuclei, electrons, and neutrons.

The mass density threshold for the inverse beta decay according to (SHAPIRO; TEUKOLSKY, 1983) is

$$\rho_N = \frac{\mu_e m_N}{3\pi^2 \hbar^3 c^3} \left(\epsilon_Z^2 + 2 m_e c^2 \epsilon_Z\right)^{3/2}, \tag{2.28}$$

the energy ϵ_Z is obtained experimentally and is listed in (CAMERON, 1957). For certain nuclei, the density threshold for neutronization can be calculated from (2.28). The maximum stellar mass calculated from the equilibrium equations may have very high densities in its center where inverse beta decay processes may occur. In this case, this process is expected to decrease the electron number density in the star, which in turn would decrease the degeneracy pressure, consequently the star may have a stable maximum mass configured by the neutronization threshold.

2.3 Generalization of the Chandrasekhar Equation of State for a D-dimensional space-time

Let's consider the equation of state of an ideal fully relativistic degenerate Fermi gas in the presence of extra dimensions, such that the energy density and particle number density are written, respectively, as follows

$$\begin{aligned} \epsilon &= \frac{g}{(2\pi\hbar)^{D-1}}\int_0^{\mathrm{k_F}} E(k)d^{D-1}k, \\ &= \frac{g\,c\,(mc)^D\Omega_{D-2}}{(2\pi\hbar)^{D-1}}\int_0^{x_{\mathrm{F}}}\sqrt{x^2+1}x^{D-2}dx, \\ \epsilon(x_{\mathrm{F}}) &= \epsilon_0^{(D)}\frac{x_{\mathrm{F}}^{D-1}\,{}_2F_1(\alpha,\beta;\sigma;-x_{\mathrm{F}}^2)}{D-1}, \end{aligned} \tag{2.29}$$

$$\begin{aligned} n &= \frac{g}{(2\pi\hbar)^{D-1}}\int_0^{k_F} d^{D-1}k, \\ &= \frac{\epsilon_0^{(D)}}{mc^2}\frac{x_{\mathrm{F}}^{D-1}}{D-1}, \end{aligned} \tag{2.30}$$

where $\epsilon_0^{(D)} = \frac{g\,c\,(mc)^D\Omega_{D-2}}{(2\pi\hbar)^{D-1}}$, $\alpha = -1/2$, $\beta = (D-1)/2$, $\sigma = \beta + 1$, $x_{\mathrm{F}} = k_{\mathrm{F}}/mc$, ${}_2F_1$ represents the hyper-geometric function ("Hypergeometric Functions" in Handbook of Mathematical Functions with Formulas, Graphs, and Mathematical Tables (ABRAMOWITZ; STEGUN, 1965, Ch. 15)), k_F represents the Fermi momenta and $E(k)$ is the relativistic energy that depends on the rest mass of the fermion. It is worth to cite that the analytical expression for the energy density Eq. (2.29) is a new expression to calculate the energy density of a Fermi gas in the presence of extra dimensions, and it is the energy calculated in respect to the vacuum since the integral goes from $k = 0$ to $k = k_{\mathrm{F}}$. The above relations can be used to study white dwarfs and pure neutron stars once they can be modeled with the Fermi gas equation of state. For $D = 4$, i.e., the usual four dimensional spacetime, equations (2.29) and (2.30) give the standard Chandrasekhar EoS (CHANDRASEKHAR, 1964).

In the case of white dwarfs the contribution for the total energy density from ions can be calculated by supposing local charge neutrality, such that, we have

$$\epsilon_{\mathrm{ion}} = nm_N\mu_e c^2, \tag{2.31}$$

being m_N the nucleon mass and μ_e the ratio between the atomic and baryon numbers. The fluid pressure can be calculated from thermodynamics as

$$\begin{aligned} p &= n\frac{d\epsilon}{dn} - \epsilon, \\ p &= \frac{g\,c\,(mc)^D\Omega_{D-2}}{(2\pi\hbar)^{D-1}\,(D-1)}\int_0^{x_{\rm F}}\frac{x^D}{\sqrt{x^2+1}}dx, \\ p(x_{\rm F}) &= \epsilon_0^{(D)}\frac{x_{\rm F}^{D+1}{}_2F_1(-\alpha,\sigma;\sigma+1;-x_{\rm F}^2)}{(D-1)^2}. \end{aligned} \tag{2.32}$$

The analytical expression above gives the degeneracy pressure of a D-dimensional free relativistic Fermi gas, and it has been also obtained here for the first time. It is worth to cite that although the energy density of the ions $\epsilon_{\rm ion}$, to be non-negligible for the star mass, it does not contribute for the thermodynamic pressure as one can check from (2.32).

From our assumptions the realization of extra dimensions imply that energy density and pressure of the fluid are drastically changed depending on the number of dimensions D of the space-time. The generalized energy density and pressure of an ideal Fermi gas in D dimensions were casted into the form of Eqs. (2.29) and (2.32). The pressure versus energy density is presented in Fig. 2.1 for different values of D showing that the pressure decreases as the number of dimensions increase (the change of pressure in terms of D was already discussed in the context of charged gravastars (GHOSH *et al.*, 2017), see figure 1 of this reference).

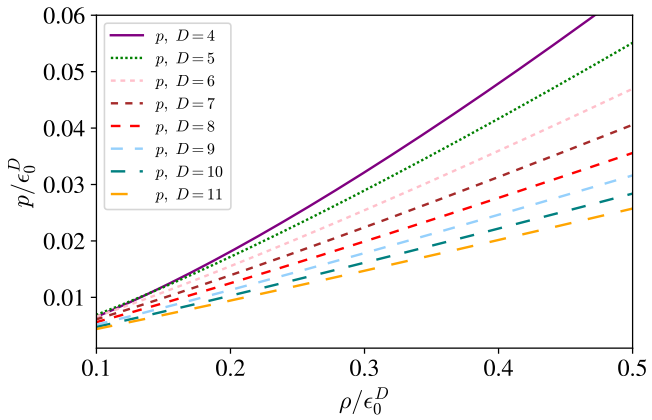

FIGURE 2.1 – Pressure as function of the energy density for fully degenerate relativistic Fermi gas in D-dimensions. As one can see the pressure decreases as the number of dimensions increase, which can be see also from Eqs. (2.37) and (2.38).

It is also possible to obtain a correlation between the sound velocity v_s and the number of space-time dimensions in the ultra-relativistic regime (when $x >> 1$ or $k >> mc$), which is

$$\left(\frac{v_s}{c}\right)^2 = \frac{1}{D-1}. \tag{2.33}$$

Another important limit is when the fermions are non-relativistic, which is characterized by $x << 1$ or $k << mc$, i.e., a limit of low particle energy. The above limits yield to a simplification of the equation of state (EOS), thus being rewritten in an adiabatic form

$$p = K\rho^{\gamma}, \tag{2.34}$$

where γ is the adiabatic index, K is the proportionality constant and ρ represents the mass density. In general, the adiabatic index can be rewritten as $\gamma = 1 + 1/n$, where n is the so-called polytropic index. The generalized form in D-dimensions of the non and ultra-relativistic approximations of the degenerate relativistic free Fermi gas can be showed to be written, respectively as

$$p = K\rho^{\frac{D+1}{D-1}}, \tag{2.35}$$

$$p = K\rho^{\frac{D}{D-1}}. \tag{2.36}$$

Eqs. (2.35) and (2.36) provide, respectively, the well-known non and ultra-relativistic limits $p = K\rho^{5/3}$ and $p = K\rho^{4/3}$, for the standard four dimensional space-time. We highlight that this result is similar to that ones of (BECHHOEFER; CHABRIER, 1993) which have used energy minimization and dimensional analysis.

It is worth noting that the above non and ultra-relativistic polytropic EOS limits, by the first law of thermodynamics can be written always as a linear relation between the pressure and the energy density $p = (\gamma - 1)\epsilon$, that yields to,

$$p = \frac{2}{D-1}\epsilon, \tag{2.37}$$

$$p = \frac{\epsilon}{D-1}, \tag{2.38}$$

respectively, where ϵ is the energy density of the fermions. The first equation also gives us the sound velocity in the non-relativistic regime as

$$\left(\frac{v_s}{c}\right)^2 = \frac{dp}{d\epsilon} = \frac{2}{D-1}. \tag{2.39}$$

Thus, comparing Eqs. (2.39) and (2.33) we conclude that in the non relativistic limit, the value of the constant sound velocity in D-dimensions is always the double of the ultra-relativistic one, because in the dispersion relation of the non-relativistic case the energy is quadratic in the momentum and not linear as in the relativistic case.

3 Field Equations from a Variational Principle

The Lagrangian formalism can be applied in several areas of physics, from the description of motion of particles in classical and quantum systems to the description of the motion of astrophysical and astronomical systems. Therefore, in the following subsections we use the Lagrangian formalism to derive the field equations. It is worth mentioning that throughout this chapter we will use the CGS unit system where $4\pi\varepsilon_0 = 1$, where ε_0 is the vacuum permittivity constant, together with the natural unit system, where $c = G = 1$.

3.1 General Relativity

The General Relativity theory (GR) formulated by Einstein in 1916, as well as any other classical field theory, can be derived from a Lagrangian formalism. The Lagrangian formulation of the Einstein field equations was performed by Hilbert and consists of the development of a Lagrangian density that describes the gravitational field as

$$\delta s = \delta \int d^4x \mathcal{L} = 0. \tag{3.1}$$

In the absence of matter the Lagrangian is represented only by the curvature scalar, so we have $\mathcal{L} = \sqrt{-g}\mathcal{R}$, where $\mathcal{R}$ is the curvature scalar and g is the determinant of the metric tensor $g_{\mu\nu}$. Our notation of tensor indices will always follow the pattern: Latin indices are representative only for spatial coordinates and Greek indices for space-time.

Taking the variation of the action we obtain

$$\delta s = \delta \int d^4x \sqrt{-g}\mathcal{R} = \int d^4x \left(\sqrt{-g}R_{\mu\nu}\delta g^{\mu\nu} + \sqrt{-g}g^{\mu\nu}\delta R_{\mu\nu} + g^{\mu\nu}R_{\mu\nu}\delta\sqrt{-g}\right), \tag{3.2}$$

where in (3.2) we adopt the Einstein's sum convention and $R_{\mu\nu}$ is the Ricci tensor.

Since the Ricci tensor can be set as $R_{\mu\nu} = \nabla_\alpha \Gamma^\alpha_{\mu\nu} - \nabla_\nu \Gamma^\alpha_{\mu\alpha}$, where $\Gamma^\alpha_{\mu\nu}$ represent the

Christoffel symbols, the equation (3.2) becomes

$$\delta s = \delta \int d^4x\sqrt{-g}\mathcal{R} = \int d^4x \left(\sqrt{-g}R_{\mu\nu}\delta g^{\mu\nu} + \sqrt{-g}g^{\mu\nu}\left(\nabla_\alpha \delta\Gamma^\alpha_{\mu\nu} - \nabla_\nu\delta\Gamma^\alpha_{\mu\alpha}\right) + g^{\mu\nu}R_{\mu\nu}\delta\sqrt{-g}\right), \quad (3.3)$$

taking into account that the metric $g_{\mu\nu}$ commutes with the covariant derivative ∇_ν, we obtain for the second term of (3.2)

$$\begin{aligned}
\sqrt{-g}g^{\mu\nu}\delta R_{\mu\nu} &= \sqrt{-g}\left(\nabla_\alpha(g^{\mu\nu}\delta\Gamma^\alpha_{\mu\nu}) - \nabla_\nu(g^{\mu\nu}\delta\Gamma^\alpha_{\mu\alpha})\right) && (3.4)\\
&= \sqrt{-g}\left(\nabla_\alpha(g^{\mu\nu}\delta\Gamma^\alpha_{\mu\nu}) - \nabla_\alpha(g^{\mu\alpha}\delta\Gamma^\nu_{\mu\nu})\right) && (3.5)\\
&= \sqrt{-g}\nabla_\alpha J^\alpha, && (3.6)
\end{aligned}$$

where in (3.6) we define $J^\alpha = g^{\mu\nu}\delta\Gamma^\alpha_{\mu\nu} - g^{\mu\alpha}\delta\Gamma^\nu_{\mu\nu}$, being $\nabla_\alpha J^\alpha$ the divergence of the vector field J, we can use the Stokes theorem

$$\int d^4x\sqrt{-g}\nabla_\alpha J^\alpha = \int d^4x\sqrt{-g}\partial_\alpha J^\alpha = \int d\Sigma_\alpha\sqrt{-g}J^\alpha = 0, \quad (3.7)$$

where $d\Sigma_\alpha$ represents the hyper-surface of d^4x. Since this hyper-surface is set at infinity we can assume that the contribution of the vector field J^α is zero for the boundary condition of $d\Sigma$, such that the term proportional to $\delta R_{\mu\nu}$ can be neglected (D'INVERNO, 1992).

In this case we obtain for the variation of the action

$$\delta s = \int d^4x \left(\sqrt{-g}R_{\mu\nu}\delta g^{\mu\nu} + g^{\mu\nu}R_{\mu\nu}\delta\sqrt{-g}\right). \quad (3.8)$$

Now considering that the variation δg can be given by $\delta g = g g^{\mu\nu}\delta g_{\mu\nu}$ (D'INVERNO, 1992), we have

$$\begin{aligned}
\delta s &= \int d^4x \left(\sqrt{-g}R_{\mu\nu}\delta g^{\mu\nu} - g^{\mu\nu}R_{\mu\nu}\frac{1}{2\sqrt{-g}}\delta g\right) && (3.9)\\
&= \int d^4x \left(\sqrt{-g}R_{\mu\nu}\delta g^{\mu\nu} - \mathcal{R}\frac{1}{2\sqrt{-g}}g g^{\mu\nu}\delta g_{\mu\nu}\right) && (3.10)\\
&= \int d^4x \left(\sqrt{-g}R_{\mu\nu}\delta g^{\mu\nu} + \mathcal{R}\frac{1}{2\sqrt{-g}}(-g) g^{\mu\nu}\delta g_{\mu\nu}\right) && (3.11)\\
&= \int d^4x \left(\sqrt{-g}R_{\mu\nu}\delta g^{\mu\nu} + \mathcal{R}\frac{\sqrt{-g}}{2} g^{\mu\nu}\delta g_{\mu\nu}\right) && (3.12)\\
&= \int d^4x \left(\sqrt{-g}R_{\mu\nu}\delta g^{\mu\nu} - \mathcal{R}\frac{\sqrt{-g}}{2} g_{\mu\nu}\delta g^{\mu\nu}\right) && (3.13)\\
&= \int d^4x\sqrt{-g}\left(R_{\mu\nu} - \mathcal{R}\frac{1}{2}g_{\mu\nu}\right)\delta g^{\mu\nu} = 0 && (3.14)
\end{aligned}$$

where we use the following properties $g_{\mu\nu} = g_{\nu\mu}$ and $\delta(g^{\mu\nu}g_{\mu\nu}) = \delta(\delta^{\mu}_{\mu}) = 0$, where δ^{α}_{γ} is the Kronecker Delta. From (3.14) we obtain the gravitational field equation for vacuum as

$$R_{\mu\nu} - \frac{1}{2}g_{\mu\nu}\mathcal{R} = 0. \tag{3.15}$$

Considering now that the Lagrangian has a source term L_m

$$s = \int d^4x\sqrt{-g}\left(\frac{\mathcal{R}}{16\pi} + L_m\right), \tag{3.16}$$

and that the derivative of the action satisfies the relation

$$\delta s = \int d^4x\Sigma_i\left(\frac{\delta s}{\delta\phi^i}\delta\phi^i\right), \tag{3.17}$$

we can take the variation of s with respect to the metric and divide it by $\sqrt{-g}$ to obtain

$$\frac{1}{\sqrt{-g}}\frac{\delta s}{\delta g^{\mu\nu}} = \int d^4x\left[\frac{1}{16\pi}\left(R_{\mu\nu} - \frac{1}{2}g_{\mu\nu}\mathcal{R}\right) + \frac{1}{\sqrt{-g}}\frac{\delta(\sqrt{-g}L_m)}{\delta g^{\mu\nu}}\right] = 0, \tag{3.18}$$

and introducing the definition of the energy-momentum tensor

$$T_{\mu\nu} \equiv -\frac{2}{\sqrt{-g}}\frac{\delta(\sqrt{-g}L_m)}{\delta g^{\mu\nu}} \tag{3.19}$$

we obtain the field equations of General Relativity as

$$R_{\mu\nu} - \frac{1}{2}g_{\mu\nu}\mathcal{R} = 8\pi T_{\mu\nu}. \tag{3.20}$$

3.1.1 Schwarzschild Solution

The most widely used exact solution of (3.20) is the Schwarzschild one. This solution describes the space-time around a spherically symmetry static object. Below we will make a very strict derivation of this solution.

To derive the Schwarzschild solution we assume that the metric is given by

$$ds^2 = Adt^2 - Bdr^2 - Cr^2d\theta^2 - Dr^2\text{sen}^2\theta d\phi^2, \tag{3.21}$$

and that due to spherical symmetry the coefficients A and B can be considered as a function of only the radial coordinate r, and also that $C = D = 1$.

Given the arbitrariness of referential we can rewrite the metric in its canonical form as

$$ds^2 = e^{\nu}dt^2 - e^{\lambda}dr^2 - r^2d\theta^2 - r^2\text{sen}^2\theta d\phi^2, \tag{3.22}$$

where ν and λ are functions of the radial coordinate r.

Assuming that the definition of the energy-momentum tensor (3.19) allows us to describe a perfect fluid, i.e., that the matter Lagrangian is such that we can write $T_{\mu\nu}$ as

$$T_{\mu\nu} = (p + \rho)u_\mu u_\nu - p g_{\mu\nu}, \tag{3.23}$$

where p and ρ represent the pressure and energy density of the fluid, respectively, and u_ξ is the fluid four-velocity.

Taking now the Einstein-Hilbert field equations (3.20), its components tt and rr becomes, respectively

$$\frac{e^{-\lambda}}{r^2}(e^\lambda + \lambda' r - 1) = 8\pi\rho, \tag{3.24a}$$

$$\frac{e^{-\lambda}}{r^2}(e^\lambda - \nu' r - 1) = -8\pi p, \tag{3.24b}$$

where the comma represents derivative with respect to the radial coordinate.

We can rewrite (3.24a) as

$$\frac{d}{dr}\left(r - re^{-\lambda}\right) = 8\pi\rho r^2, \tag{3.25}$$

and integrating (3.25) we obtain

$$e^\lambda = \frac{1}{\left(1 - \frac{2m}{r}\right)}, \tag{3.26}$$

where we define the gravitational mass $m(r)$ as

$$m = \int_0^{r'} 4\pi r^2 \rho dr. \tag{3.27}$$

Given the arbitrariness of the upper limit of integral in (3.27) we can interpret the gravitational mass $m(r)$ as the mass contained within a sphere of radius r', i.e., this solution for the metric coefficient g_{rr} is valid for both the interior and exterior of the object. However, in the absence of sources, we obtain by subtracting (3.24a) from (3.24b)

$$(\lambda + \nu)' = 0, \tag{3.28}$$

or simply

$$\lambda + \nu = 0. \tag{3.29}$$

Finally we obtain the external Schwarzschild solution as

$$ds^2 = \left(1 - \frac{2M}{r}\right) dt^2 - \frac{1}{\left(1 - \frac{2M}{r}\right)} dr^2 - r^2 d\theta^2 - r^2 \text{sen}^2\theta d\phi^2, \tag{3.30}$$

where M is the total mass of the object.

3.1.2 Tolman-Oppenheimer-Volkoff Equation

Tolman, Oppenheimer and Volkoff derived the general relativistic corrections for the hydrostatic equilibrium equation of an object with spherical symmetry (TOLMAN, 1939; OPPENHEIMER; VOLKOFF, 1939).

Knowing that the covariant divergence of the Einstein tensor $G_{\mu\nu} = R_{\mu\nu} - \frac{1}{2}\mathcal{R}g_{\mu\nu}$ is null due to geometric properties (D'INVERNO, 1992), i.e., $\nabla^\mu G_{\mu\nu} = 0$, we obtain directly that

$$\nabla^\mu T_{\mu\nu} = 0. \tag{3.31}$$

Using the energy-momentum tensor for a perfect fluid and choosing $\nu = 1$, we find (more details, see appendix A)

$$p' = -(p + \rho)\frac{\nu'}{2}. \tag{3.32}$$

Using (3.24b) and (3.26) one can eliminate ν' and after some algebra obtain

$$p' = -\frac{m\rho}{r^2}\left[1 + \frac{p}{\rho}\right]\left[1 + \frac{4\pi r^3 p}{m}\right]\left[1 - \frac{2m}{r}\right]^{-1}, \tag{3.33}$$

The above equation is often called Tolman-Oppenheimer-Volkoff (TOV) equation, in honor to its authors. The terms in brackets are exclusively terms derived from GR and their effects on the structure of white dwarfs will be described in detail in the next chapter. The TOV equation can be solved if coupled to the diferential form of (3.27), and for a given EoS.

3.1.3 Reissner-Nordström Solution

The electromagnetic energy-momentum tensor is described by

$$T_{\mu\nu} = (\rho + p)u_\mu u_\nu - p g_{\mu\nu} + \frac{1}{4\pi}\left(-F_\mu{}^\gamma F_{\nu\gamma} + \frac{1}{4} g_{\mu\nu} F_{\gamma\beta} F^{\gamma\beta}\right), \tag{3.34}$$

being $F^{\mu\gamma}$ the Faraday-Maxell tensor, defined as $F_{\mu\nu} \equiv \partial_\mu A_\nu - \partial_\nu A_\mu$, being A_μ the four-vector potential.

The metric is again written in its canonical form (3.22) and the field equations are

often called Einstein-Maxwell field equations.

For an electrically charged, static particle placed at the origin of the coordinate system the Faraday-Maxwell tensor $F_{\mu\nu}$ will be given by

$$F_{\mu\nu} = E(r) \begin{pmatrix} 0 & -1 & 0 & 0 \\ 1 & 0 & 0 & 0 \\ 0 & 0 & 0 & 0 \\ 0 & 0 & 0 & 0 \end{pmatrix}, \tag{3.35}$$

being $E(r)$ the electric field. Eq.(3.35) above is obtained from an *ansatz* that is after showed to work (see section 12.4 of (D'INVERNO, 1992)).

For vacuum the covariant derivative of the Faraday-Maxwell tensor is $\nabla_\mu F^{\mu\nu} = 0$, which gives us by using (3.22) and taking the indice $\nu = 0$ (see appendix A)

$$\frac{d}{dr}\left(e^{-\frac{1}{2}(\nu+\lambda)} r^2 E\right) = 0, \tag{3.36}$$

and integrating we obtain

$$E = e^{\frac{1}{2}(\nu+\lambda)} \varepsilon / r^2, \tag{3.37}$$

where ε is an integration constant. For the asymptotic conditions $\lim_{r\to\infty} \nu, \lambda \to 0$ the electric field becomes

$$E = \frac{\varepsilon}{r^2}, \tag{3.38}$$

and now we identify the quantity ε as the charge Q of the object.

Again in the absence of sources we have $\nu' + \lambda' = 0$, and, using (3.37), we can find the component $\theta\theta$ of the field equations as

$$\frac{d}{dr}\left(re^{\nu}\right) = 1 - \frac{Q^2}{r^2}, \tag{3.39}$$

which integrating gives us

$$e^{\nu} = 1 - \frac{2M}{r} + \frac{Q^2}{r^2}, \tag{3.40}$$

where M is an integration constant and it is introduced, such that, this solution can be reduced to the Schwarzschild one (3.40). From $\nu = -\lambda$ we obtain the exterior Reissner-Nordström solution as

$$ds^2 = \left(1 - \frac{2M}{r} + \frac{Q^2}{r^2}\right) dt^2 + \frac{1}{\left(1 - \frac{2M}{r} + \frac{Q^2}{r^2}\right)} dr^2 + r^2 d\Omega^2, \tag{3.41}$$

where M and Q represent the total mass and total charge of the object, respectively.

3.1.4 Bekenstein Equation

Similar to the Schwarzschild solution the metric coeficient e^{λ} can be supposed to be given such as (3.40)

$$e^{\lambda} = \left(1 - \frac{2m}{r} + \frac{q^2}{r^2}\right)^{-1}, \tag{3.42}$$

with m and q representing now the mass and charge within a sphere of radius r, respectively. The covariant derivative of the Faraday-Maxwell tensor now is $\nabla_{\mu} F^{\mu\nu} = 4\pi j^{\nu}$, which gives, for the indice $\nu = 0$

$$\nabla_1 F^{10} = \frac{d}{dr}\left(E e^{-(\lambda+\nu)/2} r^2\right) = 4\pi r^2 e^{(\lambda+\nu)/2} j^0, \tag{3.43}$$

and by considering the charge density to be $\rho_e = u_{\mu} j^{\mu} = e^{\nu/2} j^0$, we obtain the electric field $F_{10} = E$, as

$$E = \frac{e^{(\lambda+\nu)/2} q}{r^2}, \tag{3.44}$$

where $q \equiv \int 4\pi r^2 e^{\lambda/2} \rho_e dr$.

The energy-momentum tensor becomes,

$$T_{\mu\nu} = \text{diag}\left(e^{\nu}(\rho + E_c^2/8\pi), e^{\lambda}(-p + E_c^2/8\pi), r^2(-p - E_c^2/8\pi), r^2 \sin^2\theta(-p - E_c^2/8\pi)\right), \tag{3.45}$$

where $E_c = q/r^2$. Using (3.45) the tt and rr components of the field equations become, respectively

$$\frac{e^{-\lambda}}{r^2}(e^{\lambda} + \lambda' r - 1) = 8\pi\left(\rho + \frac{E_c^2}{8\pi}\right), \tag{3.46a}$$

$$\frac{e^{-\lambda}}{r^2}(e^{\lambda} - \nu' r - 1) = -8\pi\left(p - \frac{E_c^2}{8\pi}\right), \tag{3.46b}$$

From the conservation of the energy-momentum tensor $\nabla_{\mu} T^{\mu\nu} = 0$ we have

$$\frac{dp}{dr} = -(p + \rho)\frac{\nu'}{2} + \frac{q}{4\pi r^4}\frac{dq}{dr}. \tag{3.47}$$

Replacing (3.42) into (3.46a) and using (3.46b) and (3.47) we can finally obtain the

equilibrium equations for the charged case as

$$\frac{dq}{dr} = 4\pi\rho_e r^2 e^{\lambda/2}, \tag{3.48}$$

$$\frac{dm}{dr} = 4\pi r^2\rho + \frac{q}{r}\frac{dq}{dr}, \tag{3.49}$$

$$\frac{dp}{dr} = -(p+\rho)\left(4\pi rp + \frac{m}{r^2} - \frac{q^2}{r^3}\right)e^{\lambda} + \frac{q}{4\pi r^4}\frac{dq}{dr}, \tag{3.50}$$

$$\frac{d\phi}{dr} = -\frac{2}{(p+\rho)}\frac{dp}{dr} + \frac{2q}{4\pi r^4(p+\rho)}\frac{dq}{dr}. \tag{3.51}$$

3.1.5 Field equations for a D-dimensional space-time with spherical symmetry

In a spherical D-dimensional matter distribution, with energy density ϵ and radial pressure p, the space-time line element is represented as (KRORI *et al.*, 1988)

$$ds^2 = e^{a(r)}dt^2 - e^{b(r)}dr^2 - r^2 d\Omega_{D-2}^2, \tag{3.52}$$

where

$$d\Omega_{D-2}^2 = d\theta_1^2 + \sin^2\theta_1 d\theta_2^2 + \cdots + \sin^2\theta_1\cdots\sin^2\theta_{D-3}d\theta_{D-2}^2$$

is the line element on the S_{D-2}-sphere, with $x^0 = t$ and $x^i = \vec{r}$ in $D-1$-dimension, with domain (WOLF, 1991).

$$0 \leq r < \infty \tag{3.53}$$

$$0 \leq \theta_i \geq \pi \tag{3.54}$$

$$0 \leq \phi < 2\pi, \tag{3.55}$$

The Einstein equations are

$$G_{\mu\nu} = \kappa T_{\mu\nu}, \tag{3.56}$$

where $\kappa = \frac{(D-2)}{(D-3)}\Omega_{D-2}G_D$ is the coupling constant (LEMOS; ZANCHIN, 2008), being G_D the generalized Newton's constant and Ω_{D-2} the surface area of a unit sphere in the $D-1$ dimensional space, which is given by

$$\Omega_{D-2} = \frac{2\pi^{\frac{D-1}{2}}}{\Gamma\left(\frac{D-1}{2}\right)}. \tag{3.57}$$

The energy-momentum tensor is given by (3.23), but here u_μ represents the D-velocity of the fluid.

Considering the above metric (3.52) the field equations are (WOLF, 1991; HARKO,

1992)

$$\frac{(D-2)b'e^b}{2r} - \frac{(D-2)(D-3)(e^{-b}-1)}{2r^2} = \kappa\epsilon \tag{3.58}$$

$$\frac{(D-2)a'e^b}{2r} + \frac{(D-2)(D-3)(e^{-b}-1)}{2r^2} = \kappa p \tag{3.59}$$

$$e^{-b}\left[\frac{a''}{2} + \frac{a'^2}{4} - \frac{a'b'}{4} + \frac{(D-2)(a'-b')}{4r}\right] + \frac{(D-3)(D-4)(e^{-b}-1)}{2r^2} = \kappa p. \tag{3.60}$$

as before primes indicate derivatives with respect to r.

The D-divergence of $T_{\mu\nu}$ leads to

$$a' = -\frac{2p'}{\epsilon + p}. \tag{3.61}$$

Equation (3.58) can be integrated to give

$$e^{-b} = 1 - \frac{2\kappa}{(D-2)(r^{D-3})}\int_0^r \epsilon r^{D-2} dr. \tag{3.62}$$

The mass within a hypersphere of radius r, in a $D-1$ dimensional space, is defined as follows

$$m = \Omega_{D-2}\int_0^r \epsilon r^{D-2} dr, \tag{3.63}$$

such that, Eq. (3.62) becomes

$$e^{-b} = 1 - \frac{2\kappa m}{(D-2)\Omega_{D-2}r^{D-3}}. \tag{3.64}$$

For $D = 4$ one obtain from (3.64) the standard interior solution for e^{-b}, thus consistent with the four dimensional case.

Isolating a' and replacing it into (3.61) one can obtain the hydrostatic equilibrium equation as

$$\frac{dp}{dr} = -\frac{\kappa(\epsilon + p)\left[pr^{D-1} + (D-3)\frac{m}{\Omega_{D-2}}\right]}{(D-2)r^{D-2}\left[1 - \frac{2\kappa m}{(D-2)\Omega_{D-2}r^{D-3}}\right]}, \tag{3.65}$$

such that for $D = 4$ the usual Tolman-Oppenheimer-Volkoff (TOV) equation is recovered.

As we saw, there is no restriction in the field equations to have compact star in higher dimensions, everything that we need is to specify the matter-energy content to solve the system.

From (3.65) we can note the necessity of the inclusion of G_D by dimensional analyses.

More clearly, one can note that G_D may be rewritten as

$$G_D = l^{D-4}G, \tag{3.66}$$

which means $G_4 = G$, $G_5 = lG$, $G_6 = l^2G$, and so on, being l a free parameter that has dimension of length. According to (ZWIEBACH, 2009) l is related to the scale of the extra dimensions to be considered.

3.2 $f(\mathcal{R},\mathcal{T})$ Gravity

Proposed by Harko et al. (HARKO *et al.*, 2011), the $f(\mathcal{R},\mathcal{T})$ gravity is a generalization of the $f(\mathcal{R})$ theories (check, for instance, (NOJIRI; ODINTSOV, 2011)). Its gravitational action depends on an arbitrary function of both the Ricci scalar $\mathcal{R}$ and the trace of the energy-momentum tensor $\mathcal{T}$. The dependence on $\mathcal{T}$ is inspired by the consideration of quantum effects (Lobato *et al.*, 2018).

The $f(\mathcal{R},\mathcal{T})$ action reads (HARKO *et al.*, 2011)

$$s = \int d^4x\sqrt{-g}\left[\frac{f(R,T)}{16\pi} + L_m\right]. \tag{3.67}$$

In (3.67), $f(\mathcal{R},\mathcal{T})$ is the general function of $\mathcal{R}$ and $\mathcal{T}$.

The field equations of the theory are obtained by varying the action with respect to the metric $g_{\mu\nu}$ (HARKO *et al.*, 2011) (see also appendix A), yielding

$$f_{\mathcal{R}}(\mathcal{R},\mathcal{T})R_{\mu\nu} - \frac{1}{2}f(\mathcal{R},\mathcal{T})g_{\mu\nu} + (g_{\mu\nu}\Box - \nabla_\mu\nabla_\nu)f_{\mathcal{R}}(\mathcal{R},\mathcal{T}) = 8\pi T_{\mu\nu} - f_{\mathcal{T}}(\mathcal{R},\mathcal{T})(T_{\mu\nu} + \Theta_{\mu\nu}), \tag{3.68}$$

where

$$f_{\mathcal{R}}(\mathcal{R},\mathcal{T}) \equiv \frac{\partial f(\mathcal{R},\mathcal{T})}{\partial\mathcal{R}}, \quad f_{\mathcal{T}}(\mathcal{R},\mathcal{T}) \equiv \frac{\partial f(\mathcal{R},\mathcal{T})}{\partial\mathcal{T}}, \tag{3.69}$$

$$\Theta_{\mu\nu} \equiv g^{\alpha\beta}\frac{\delta T_{\alpha\beta}}{\delta g^{\mu\nu}}, \quad T_{\mu\nu} = -\frac{2}{\sqrt{-g}}\frac{\partial(\sqrt{-g}L_m)}{\partial g^{\mu\nu}}. \tag{3.70}$$

Still in Equation (3.68) above, $R_{\mu\nu}$ represents the Ricci tensor, $\Box{=}\nabla^\mu\nabla_\mu$ is the D'Alembertian and ∇_μ is the covariant derivative.

From the contravariant derivative of the field equation (3.68), one obtains (ALVARENGA

et al., 2013; BARRIENTOS; RUBILAR, 2014) (again, see also appendix A)

$$\nabla^{\mu}T_{\mu\nu} = \frac{f_{\mathcal{T}}(\mathcal{R},\mathcal{T})}{8\pi - f_{\mathcal{T}}(\mathcal{R},\mathcal{T})}\left[(T_{\mu\nu}+\Theta_{\mu\nu})\nabla^{\mu}\ln f_{\mathcal{T}}(\mathcal{R},\mathcal{T}) - \frac{1}{2}g_{\mu\nu}\nabla^{\mu}\mathcal{T} + \nabla^{\mu}\Theta_{\mu\nu}\right]. \quad (3.71)$$

We will consider the energy-momentum tensor of a perfect fluid given by (3.23). The energy-momentum tensor and the conditions aforementioned imply that

$$\mathcal{L}_m = -p, \quad (3.72)$$

$$\Theta_{\mu\nu} = -pg_{\mu\nu} - 2T_{\mu\nu}. \quad (3.73)$$

In order to obtain exact solutions in the $f(\mathcal{R},\mathcal{T})$ theory, it is necessary to consider a specific form for the function $f(\mathcal{R},\mathcal{T})$. Following a previous work (MORAES *et al.*, 2016), we will consider the functional form $f(\mathcal{R},\mathcal{T}) = \mathcal{R} + 2\,f(\mathcal{T})$ with $f(\mathcal{T}) = \lambda\mathcal{T}$ and λ a constant. Such a functional form has been broadly applied in $f(\mathcal{R},\mathcal{T})$ models (ALVARENGA *et al.*, 2013; MORAES, 2014; MORAES, 2015; SHAMIR, 2015; MORAES; SANTOS, 2016) and allows the recovering of GR by simply taking $\lambda = 0$.

By considering $f(\mathcal{R},\mathcal{T}) = \mathcal{R} + 2\lambda\mathcal{T}$ in Eqs. (3.68) and (3.71), it follows that

$$G_{\mu\nu} = 8\pi T_{\mu\nu} + \lambda[\mathcal{T}g_{\mu\nu} + 2(T_{\mu\nu} + pg_{\mu\nu})], \quad (3.74)$$

$$\nabla^{\mu}T_{\mu\nu} = -\frac{2\lambda}{8\pi + 2\lambda}\left[\nabla^{\mu}(pg_{\mu\nu}) + \frac{1}{2}g_{\mu\nu}\nabla^{\mu}\mathcal{T}\right], \quad (3.75)$$

with $G_{\mu\nu}$ in Eq. (3.74) representing the usual Einstein tensor.

3.2.1 Stellar structure equations in $f(\mathcal{R},\mathcal{T})$ gravity

The line element used to describe spherical objects in the $f(\mathcal{R},\mathcal{T})$ gravity is written once again as

$$ds^2 = e^{a(r)}dt^2 - e^{b(r)}dr^2 - r^2(d\theta^2 + \sin^2\theta d\phi^2), \quad (3.76)$$

where (t, r, θ, ϕ) are the Schwarzschild-like coordinates and the exponents $a(r)$ and $b(r)$ are functions of the radial coordinate r.

Considering the space-time metric (3.76) in the field equation (3.74) we obtain

$$\frac{e^{-b}}{r^2}\left(b'r + e^b - 1\right) = 8\pi\rho + \lambda(3\rho - p), \quad (3.77)$$

$$-\frac{e^{-b}}{r^2}\left(a'r - e^b + 1\right) = -8\pi p + \lambda(\rho - 3p), \quad (3.78)$$

$$\frac{e^{-b}}{4r}\left(\left(a'b' - 2a'' - a'^2\right)r + 2(b' - a')\right) = -8\pi p + \lambda(\rho - 3p), \quad (3.79)$$

in which primes ($'$) indicate derivatives with respect to r.

By integrating (3.77) one can obtain

$$e^{-b} = 1 - \frac{2m}{r}. \tag{3.80}$$

where the gravitational mass is given by

$$m = \int_0^r \left(4\pi\rho r^2 + \frac{\lambda}{2}(3\rho - p)r^2\right) dr, \tag{3.81}$$

for which the function $m = m(r)$ represents the gravitational mass enclosed in a surface of radius r according to the $f(\mathcal{R}, \mathcal{T})$ gravity.

An additional equation is derived from (3.75) and reads

$$\frac{dp}{dr} + (\rho + p)\frac{a'}{2} = -\frac{\lambda}{8\pi + 2\lambda}(p' - \rho'). \tag{3.82}$$

Considering the relation $\rho = \rho(p)$ and Eqs. (3.78) and (3.80) in (3.82), the hydrostatic equilibrium equation for the $f(\mathcal{R}, \mathcal{T}) = R + 2\lambda\mathcal{T}$ gravity is obtained as

$$\frac{dp}{dr} = -(p + \rho)\left[4\pi p r + \frac{m}{r^2} - \frac{\lambda(\rho - 3p)r}{2}\right]\left(1 - \frac{2m}{r}\right)^{-1} \times \left[1 + \frac{\lambda}{8\pi + 2\lambda}\left(1 - \frac{d\rho}{dp}\right)\right]^{-1}. \tag{3.83}$$

It is quite simple to recover the usual TOV equation (TOLMAN, 1939; OPPENHEIMER; VOLKOFF, 1939) in (3.83) by making $\lambda = 0$.

We remark that stellar equilibrium configurations are found only for:

$$\frac{\lambda}{8\pi + 2\lambda}\left(1 - \frac{d\rho}{dp}\right) > -1. \tag{3.84}$$

If Eq.(3.84) is not satisfied, the sign of the pressure gradient is changed, what makes the pressure to grow up from the center of the star to its surface, instead of decreasing, which is necessary for the star hydrostatic equilibrium. Since the sound velocity $v_s^2 = dp/d\rho$ is in the interval $0 < dp/d\rho < 1$, $|d\rho/dp|$ becomes much larger than unity, thus we can rewrite (3.84) as

$$\frac{\lambda}{8\pi + 2\lambda} < \frac{dp}{d\rho}. \tag{3.85}$$

Considering that $dp/d\rho$ tends to zero at the surface of the WD, we have from (3.85) that only negative values for λ are allowed.

4 White Dwarfs in General Relativity

Usually white dwarfs are not considered as a "laboratory" of test for strong field regime. However, general relativistic effects were not negligible in the case of massive white dwarfs and white dwarfs with strong magnetic fields (BERA; BHATTACHARYA, 2014; WEN *et al.*, 2014; CARVALHO *et al.*, 2017; CARVALHO *et al.*, 2016). In particluar, in (WEN *et al.*, 2014) it was shown that general relativistic effects tend to reduce the maximum stable mass of highly magnetized WD. Chandrasekhar and Tooper have also shown that the general relativistic stability criteria changes the maximum stable mass. Those general relativistic effects predict by Chandrasekhar yields also to different values of minimum radius as showed in (CARVALHO *et al.*, 2017), and these effects on the radius are important, because in the relativistic case the minimum radius predicted by the General Relativity is about three times greater than in the Newtonian case. Therefore, we show below our results of a comparative study between the stellar structure derived by Newtonian and general relativistic calculations (details about the mathematical formalism see (CARVALHO *et al.*, 2018)), details about the equations of state and Newtonian equilibrium equations can be consulted in (CHANDRASEKHAR, 1967; CARVALHO *et al.*, 2018).

4.1 Comparison between Newtonian and general relativistic cases

Using several values of central pressure p_c we construct the mass-radius and mass-central density relations which are shown in Fig. 4.1. From Fig. 4.1 it can be seen that the purely Newtonian case does not have the secular instability $\partial M/\partial R > 0$ (more details, see (CHANDRASEKHAR; TOOPER, 1964; HERRERA, 2003; PENROSE, 2002; KNUTSEN, 1988)), while in the special relativistic (SR) case - i.e., including the relativistic energy of the degenerate electrons for the EoS - presents instability when the electrons are highly relativistic. This aspect is easier to see in Fig. 4.2, where we highlight the region

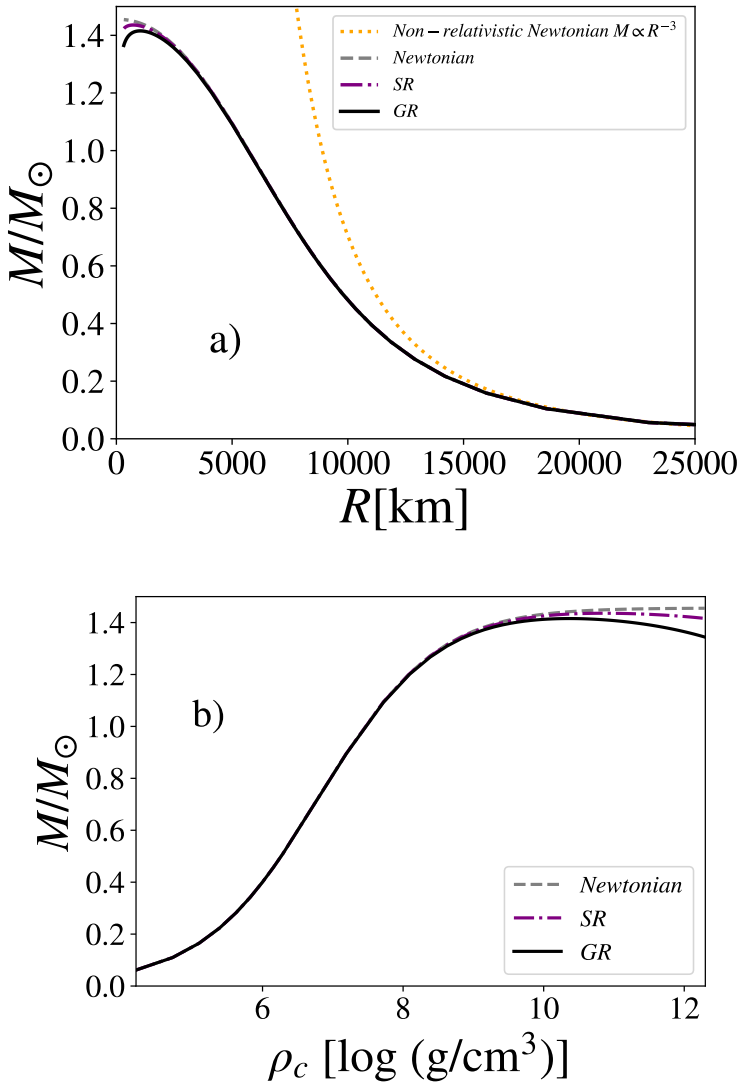

FIGURE 4.1 – a) Mass-radius relation and b) mass-central mass density relation for general relativistic and Newtonian cases. In both plots the solid black line represents the outcomes for general relativistic WD, the dashed-dotted magenta line represents Newtonian results with special relativistic corrections and the dashed gray line represents the Newtonian results. It is also displayed in a) the non-relativistic mass-radius relation (dotted orange line), in which $M \propto 1/R^3$.

of massive WD for the mass-radius relation. We also display in Fig. 4.2 the observational data of the most massive white dwarf ($M = 1.41 M_\odot \pm 0.04$) found in literature (VENNES *et al.*, 1997).

From Fig. 4.2 it is worth to note that GR does not affect greatly the maximum mass, rather it diminishes the maximum stable mass a few percents $\sim 3\%$ (see also Tab. 4.1). However, it is worthwhile to cite that the minimum radii, i.e., the radii corresponding to the predicted maximum masses, are very different. For instance, the minimum radius predicted by general relativistic calculations is about three times larger than Newtonian

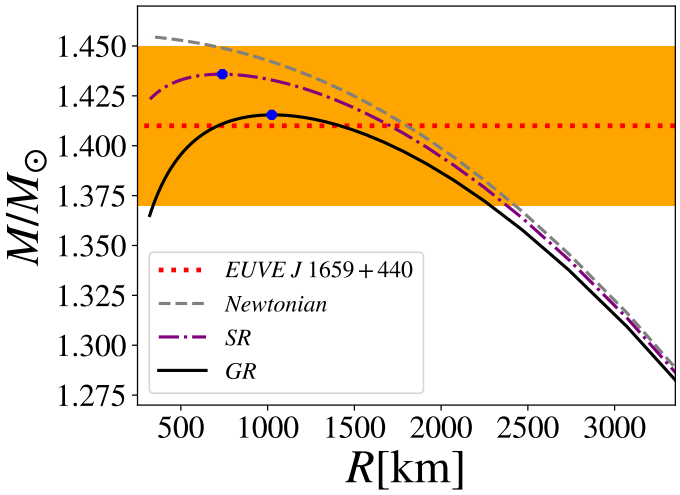

FIGURE 4.2 – Mass-radius relation of massive WD. The curves follow the same representation as in Fig. 4.1. The full blue circles mark the maximum masses. The dotted red line represents the measured mass of the most massive white dwarf ($M = 1.41 M_\odot \pm 0.04$) found in literature (VENNES *et al.*, 1997) and the shaded orange region corresponds to its estimated error.

TABLE 4.1 – Maximum mass and minimum radius for the static models of WD stars.

Model	Mass/$M_\odot$	Radius(km)
Newtonian $P = P(\rho)$	1.4546	329
Special Relativity (SR) $P = P(\epsilon)$	1.4358	739
General Relativity (GR) $P = P(\epsilon)$	1.4154	1021
Non-relativistic Newtonian $P = K\rho^{5/3}$	1.4564	7833

ones (see Tab. 4.1). Similar results can be found in (CARVALHO *et al.*, 2015; CARVALHO *et al.*, 2015; CARVALHO *et al.*, 2016; CARVALHO *et al.*, 2017).

4.1.1 Fixed total star mass

From Fig. 4.2 it can also be seen that for a fixed total star mass between $1.3 - 1.415 M_\odot$ the values of radii are very sensitive depending on the case. Tab. 4.2 shows the calculated radii for several values of total mass from Newtonian and general relativistic calculations. Tab. 4.3 presents the values of central mass density for some values of fixed total mass for the three cases, in which we can see that the GR central densities are larger than the one obtained from Newtonian calculations. In Fig. 4.3 we show, for a fixed total mass of $M = 1.415 M_\odot$, the profiles of mass, gradient of pressure and energy density for the three cases. We remark from Fig. 4.3, that in order to obtain the same total mass in

TABLE 4.2 – Corresponding radii to fixed total star masses in Newtonian and general relativistic cases. $R_{\rm Newton}$ means the radius predicted by Newtonian case, $R_{\rm SR}$ is the radius given by special relativistic case, and $R_{\rm GR}$ is the radius calculated in the general relativistic case and the $R_{\rm NR}$ is the radius supplied by non-relativistic approximation, where the mass follows the relation $M/M_\odot \propto 1/R^3$.

Mass/$M_\odot$	$R_{\rm Newton}$(km)	$R_{\rm SR}$(km)	$R_{\rm GR}$(km)	$R_{\rm NR}$(km)
1.300	3241	3222	3185	8140
1.312	3107	3081	3030	8114
1.325	2969	2937	2878	8087
1.338	2823	2788	2724	8062
1.351	2671	2633	2562	8036
1.364	2509	2467	2384	8011
1.376	2336	2286	2179	7986
1.389	2148	2085	1942	7961
1.402	1942	1859	1656	7937
1.415	1708	1595	1145	7913

TABLE 4.3 – Corresponding central mass densities to fixed total masses in Newtonian and general relativistic cases. $\rho_C^{\rm Newton}$ means the central density achieved in Newtonian case, $\rho_C^{\rm SR}$ is the central density given by SR case, $\rho_C^{\rm GR}$ is the central density found for the general relativistic case.

Mass/$M_\odot$	$\rho_C^{\rm Newton}$(g/cm^3)	$\rho_C^{\rm SR}$(g/cm^3)	$\rho_C^{\rm GR}$(g/cm^3)
1.376	3.76×10^8	9.85×10^8	1.91×10^9
1.389	2×10^9	2.05×10^9	2.28×10^9
1.402	2.28×10^9	2.82×10^9	4.51×10^9
1.415	4.08×10^9	5.05×10^9	1.61×10^{10}

all cases the structure of the stars are very distinct. From Fig. 4.3 we can note that in general relativistic case the energy density in the central region of the star is larger than in Newtonian cases. This effect at same time makes the WD's mass more concentrated at the star center and the pressure gradient to decay more sharply for the general relativistic calculations. One can calculate the Newtonian gravitational field as

$$g_{\rm Newton} = -\frac{Gm}{r^2}, \tag{4.1}$$

and the general relativistic gravitational field is $g_{\rm GR} = -\phi'/2$ (see Eq.(3.32)), thus we have

$$g_{\rm GR} = -\frac{Gm}{r^2}\left[1 + \frac{4\pi r^3 p}{mc^2}\right]\left[1 - \frac{2Gm}{c^2 r}\right]^{-1}. \tag{4.2}$$

Fig. 4.4 displays the gravitational fields of the stars with total mass $1.415M_\odot$ as a

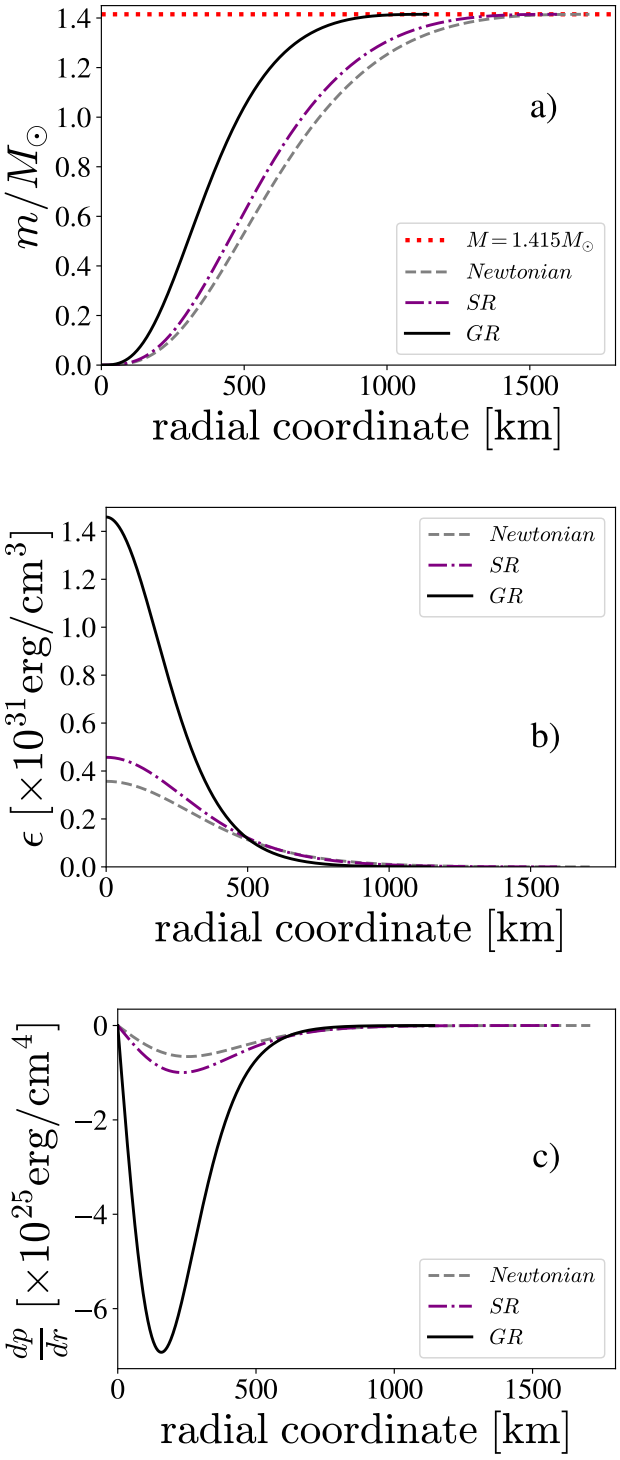

FIGURE 4.3 – From top to bottom: a) mass profiles, b) energy density profiles and c) gradient of pressure profiles. All profiles correspond to a fixed total star mass of $M = 1.415 M_\odot$.

function of radial coordinate, we can note that the gravitational fields are initially very different, however, outside the star the fields match each other, thus implying that the gravitational field outside the star can be regarded as Newtonian. In addition, inside the

star, where the gravitational fields are very different, it can be observed that there is a deviation of about $\sim 200\%$ between the correspondent highest values of the gravitational field (the minima of the curves in Fig. 4.4), this is due to the very different central densities of the three cases (see Tab. 4.3 and Fig. 4.3b). In particular, the central density ρ_C^{GR} is about 4 times larger than ρ_C^{Newton}, for the fixed total mass of $1.415 M_\odot$. We also display in Fig. 4.5 the gravitational potentials of WD with total mass $M = 1.415 M_\odot$, from which we can note a fairly difference between them.

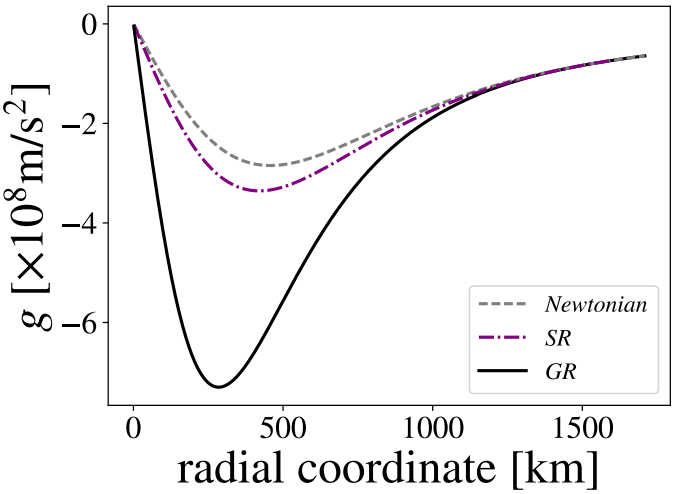

FIGURE 4.4 – General relativistic and Newtonian gravitational fields as a function of radial coordinate for a fixed total star mass of $1.415 M_\odot$.

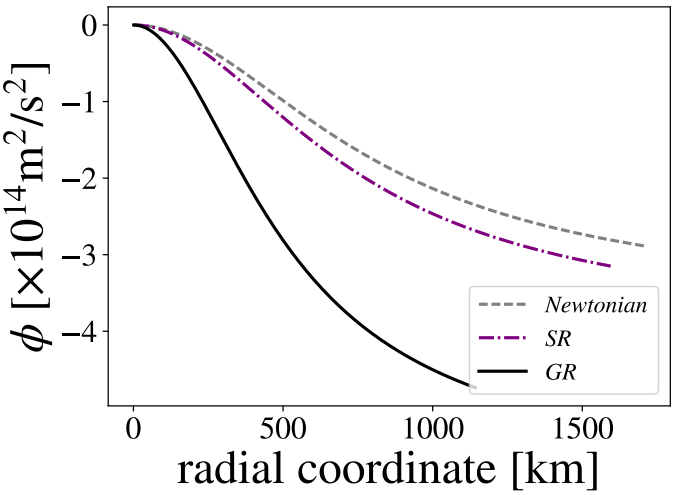

FIGURE 4.5 – General relativistic and Newtonian gravitational potentials as a function of radial coordinate for a fixed total star mass of $1.415 M_\odot$.

In Fig. 4.6 we show for the same mass of $1.415 M_\odot$ the general relativistic gravitational

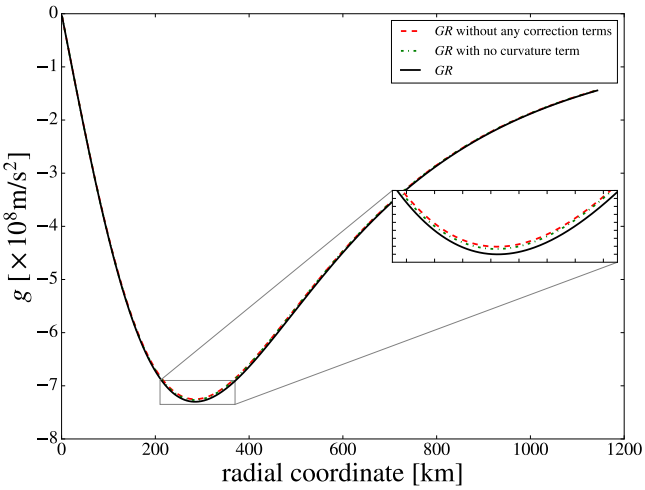

FIGURE 4.6 – General relativistic gravitational fields as a function of radial coordinate for a total mass of $1.415M_{\odot}$, calculated with and without correction terms.

field, calculated in three different ways: with all corrections terms, with no curvature term and without any correction term. *A priori*, from the Fig. 4.6 the correction terms seem to be not relevant at all, however, they yield to the important effect observed in the case of fixed total masses, thus allowing larger densities near to the center of the star $r < 300$km (see Fig. 4.3b).

4.1.1.1 Radius relative difference

Henceforth, in the present work we compare just the results of the purely Newtonian case (i.e., without special relativistic corrections) with the general relativistic outcomes for the equilibrium configurations of WD. For this purpose, we firstly define the quantity

$$\Delta R = \frac{R_{\rm Newton} - R_{\rm GR}}{R_{\rm GR}}, \tag{4.3}$$

being $R_{\rm Newton}$ and $R_{\rm GR}$ the radii given, respectively, by the Newtonian and general relativistic cases. Therefore, ΔR means the relative difference between the values of radii for fixed total masses.

In Fig. 4.7 we plot the quantity ΔR for some values of fixed total mass between $1.3 - 1.415M_{\odot}$. We can see that this quantity increases very fast when approaching $1.41M_{\odot}$. In fact, when the mass is about $1.41M_{\odot}$ we can see that the relative difference in radius is nearly 50%. It is worth to mention that the relative difference in radius is about 37% for a mass of exactly $1.41M_{\odot}$, i.e., the measured mass of the white dwarf $EUVE\ J\ 1659+440$ (VENNES *et al.*, 1997).

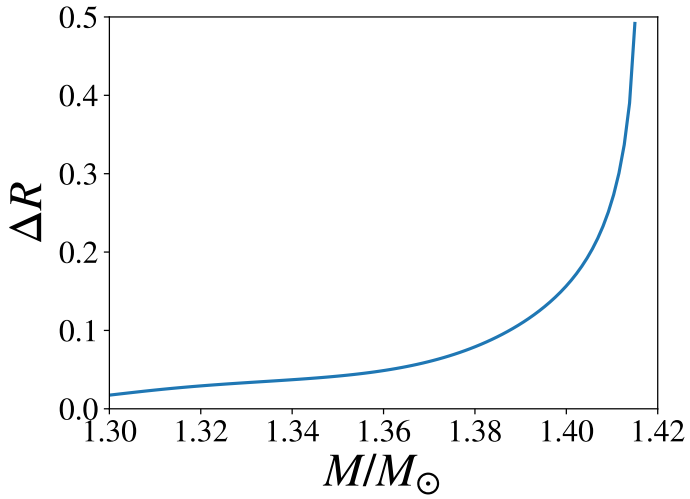

FIGURE 4.7 – Radius relative difference ΔR versus fixed total star mass.

4.1.1.2 Surface Gravity

It is worth to study the general relativistic effects on the surface gravity of the stars since this quantity can be observationally found. We calculate the surface gravity g in a Newtonian framework as

$$g_{\text{Newton}} = -\frac{GM}{R^2}. \tag{4.4}$$

To calculate the general relativistic surface gravity we use the expression given by (R. ADLER, 1975; JI *et al.*, 2008)

$$g = -\left(\frac{GM}{R^2}\right)\frac{1}{1-\frac{2GM}{c^2R}}, \tag{4.5}$$

in which is merely Eq.(4.2) for the case of zero pressure.

Using the values of Tab. 4.2 we calculate the Newtonian surface gravity and general relativistic surface gravity. In Fig. 4.8 is plotted the surface gravity against fixed total masses together with the observational data of the white dwarf $EUVE\ J\ 1659+440$. It is easy to see that using Newtonian results we are sub-estimating the surface gravity of the stars in comparison with general relativistic outcomes.

4.1.1.3 Surface gravity relative difference

Since the values for general relativistic surface gravity are much higher than Newtonian ones we define the quantity

$$\Delta g = \frac{g_{\text{Newton}} - g_{\text{GR}}}{g_{\text{GR}}}. \tag{4.6}$$

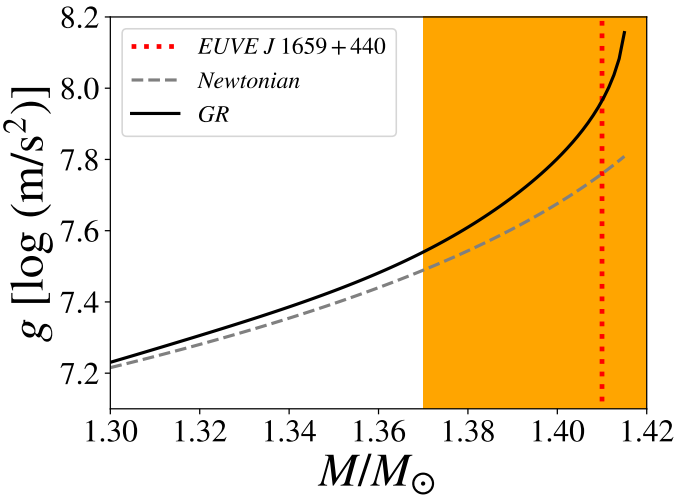

FIGURE 4.8 – Surface gravity versus fixed total star mass. The dotted red line is the measurement of mass of the most massive white dwarf ($EUVE\ J\ 1659+440$) found in literature (VENNES *et al.*, 1997) and the shaded orange region is its estimated error.

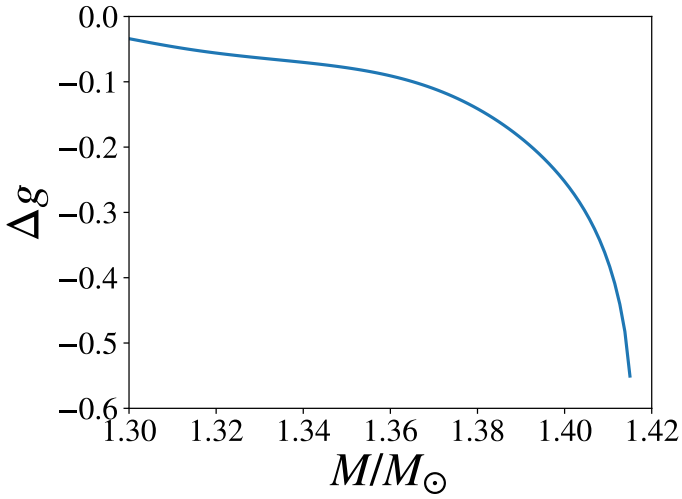

FIGURE 4.9 – Relative difference between Newtonian surface gravity and general relativistic surface gravity against fixed total star mass.

The relative difference Δg is shown in Fig. 4.9. It is interesting to note that in Fig. 4.9, for a mass of $1.415 M_{\odot}$, we have about 55% of relative difference for the values of surface gravity.

TABLE 4.4 – Values of the constants for the analytic mass-radius relations.

Model	a [km]	b	c $\left[km^{-1}\right]$	d $\left[km^{-2}\right]$
$\mu_e = 2$	20.86	0.66	2.48×10^{-5}	2.43×10^{-9}
$\mu_e = 2.154$	15.05	0.79	3.56×10^{-6}	4.9×10^{-9}
He	18.95	0.68	1.84×10^{-5}	-9.85×10^{-10}
C	0.79	0.69	1.22×10^{-5}	6.7×10^{-12}
O	-27.06	0.76	-1.21×10^{-5}	3.1×10^{-9}

4.2 Fit of the general relativistic mass-radius relation

Keeping in mind the importance of GR for WD, we fit the general relativistic mass-radius relation in order to obtain an analytic expression that better estimate the WD radius, rather than the non-relativistic Newtonian expression

$$\frac{M}{M_\odot} = 2.08 \times 10^{-6} \left(\frac{R}{R_\odot}\right)^{-3}, \tag{4.7}$$

where $R_\odot$ is the radius of the Sun.

The expression we use to fit the general relativistic curve in Fig. 4.1 is given by

$$\frac{M}{M_\odot} = \frac{R}{a + bR + cR^2 + dR^3 + kR^4}, \tag{4.8}$$

where k is the inverse of the constant in the non-relativistic Newtonian mass-radius relation $k = (2.08 \times 10^{-6} R_\odot^3)^{-1}$.

The constants a, b, c and d are parameters that depend on the interior fluid EoS of the star, such that, using the Chandrasekhar EoS for $\mu_e = A/Z = 2$ (Fig. 4.10) we find

$$\begin{aligned} a &= 20.86 \text{ km} \\ b &= 0.66 \\ c &= 2.48 \times 10^{-5} \text{ km}^{-1} \\ d &= 2.43 \times 10^{-9} \text{ km}^{-2}. \end{aligned} \tag{4.9}$$

We employed Eq.(4.8) to depict analytically other mass-radius relations derived using the Salpeter EoS (for He, C and O stars) and the Chandrasekhar EoS for$\mu_e = 2.154$, for details about those EoS, see chapter 2. The values of fitted parameters are given in Tab. 4.4.

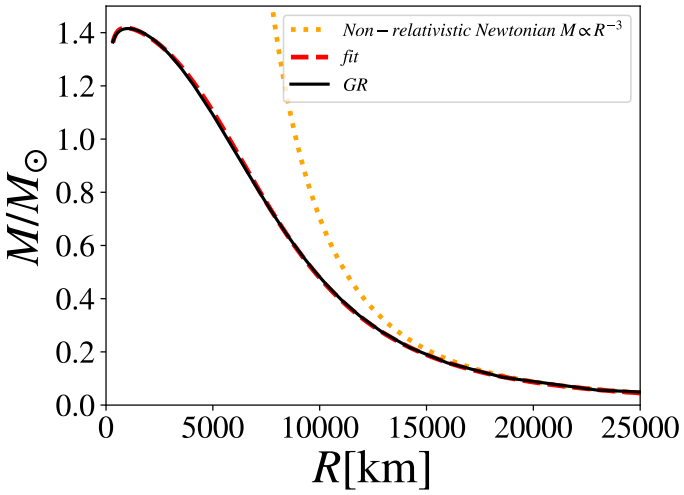

FIGURE 4.10 – Fit of the general relativistic mass-radius diagram with Eq.(4.8) (red dashed line) and the non-relativistic limit (dotted orange line).

4.3 Stellar equilibrium configurations of charged white dwarfs

Effects of strong electric fields on compact objects such as neutron stars, quarks stars and black holes have been intensively investigated, for example, in the references (SUNZU *et al.*, 2014; RAY *et al.*, 2003; ARBAÑIL *et al.*, 2013; NEGREIROS *et al.*, 2009). However, white dwarfs with high electric fields were studied only in (LIU *et al.*, 2014). As we have argued in chapter 1 the charge distribution on the star in (LIU *et al.*, 2014) is supposed to follow a linear relationship with the barium density, i.e., $\rho_e = \alpha\rho$, where α is a constant of proportionality, ρ_e is the charge density, and ρ is the matter energy density.

However, in the context of degenerate matter's EoS several studies show that the thermal and electrical conductivity are larger the greater the degree of degeneracy of the matter, which would imply in turn, as quoted in (MADSEN, 2008), that any existing charge in the interior of white dwarfs and in the outer crust of neutron stars would be arranged in order to be concentrated on the surface of these stars. Therefore, in this section of the present work we will analyze the effects of intense electric fields on the structure of white dwarfs, modeling the charge distribution as a surface distribution that follows the relation

$$\rho_e = C \exp\left[-\frac{(r-R)^2}{b^2}\right], \tag{4.10}$$

being C a constant, R the star's radius as calculated without charge contribution by using (3.61), the constant b is width of the electric charge distribution, in which we consider $b = 10$km, which represents order of magnitude of the WD's atmosphere length. For

smaller b the WD's structure is not significantly changed.

To determine the constant C we use

$$\sigma = \int_0^\infty 4\pi r^2 \rho_e dr, \tag{4.11}$$

with σ being the magnitude proportional to the electric charge distribution. σ would represent the total charge of the star if we were working in a flat space-time situation, however, due to the effects of General Relativity as quoted earlier, we calculated the structure of charged white dwarfs using General Relativity theory. In this case, the total star charge must be computed self-consistently from Equations (3.48), (3.49), (3.50) and (3.51).

It is noteworthy that neutron stars and quark stars with a surface charge distribution, such as (4.10), were studied, respectively, in (JING *et al.*, 2015; NEGREIROS *et al.*, 2009). In both works, we see that the structure of these stars depends on the amount of total charge present on the stars, being a total charge of the order 10^{20}C necessary to produce considerable effects in their structure. Substituting (4.10) into (4.11) we obtain a relation between the constant C and σ

$$8\pi C = \sigma \left(\frac{\sqrt{\pi} b R^2}{2} + \frac{\sqrt{\pi} b^3}{4} \right)^{-1}, \tag{4.12}$$

varying σ we can find different equilibrium configurations as a solution of Bekenstein's equations, in which we show below.

Fig. 4.11 shows the behavior of the total mass $M/M_\odot$ with the central energy density, for six values of σ. The considered central energy densities are in the interval 2×10^6[g/cm^3] to 4×10^{11}[g/cm^3]. The lower limit $\rho_c = 2 \times 10^6$[g/cm^3] is the mean density for white dwarfs and in the upper limit $\rho_c = 4 \times 10^{11}$[g/cm^3] the neutron drip limit is reached, i.e., at this point, the white dwarf becomes to turn into a neutron star. In the cases where $\sigma \leq 1.6 \times 10^{20}$[C], we note that the total mass grows with the central energy density until attain a maximum mass point, after that point, the mass starts to decrease with the grows of the density of energy center. In turn, in the case $\sigma = 2.0 \times 10^{20}$[C] the mass grows monotonically with the central energy density, i.e., we do not found a turning point.

On the other hand, we observe that exist a dependency of the total mass with the parameter σ. For a larger σ more massive stars are obtained. As can be noted in Fig. 4.11, we obtain more massive white dwarfs using $\sigma = 2.0\times10^{20}$[C]. In this case, the mass whose respective electric field saturates the Schwinger limit ($\sim 1.3 \times 10^{16}$[V/cm]) is $2.199M_\odot$, this is attained in the central energy density 1.665×10^{11}[g/cm^3]. This mass is between the masses estimated for the super-Chandrasekhar white dwarfs, 2.1-2.8$M_\odot$ (TAUBENBERGER *et al.*, 2011; SILVERMAN *et al.*, 2011). From this, we understand that a

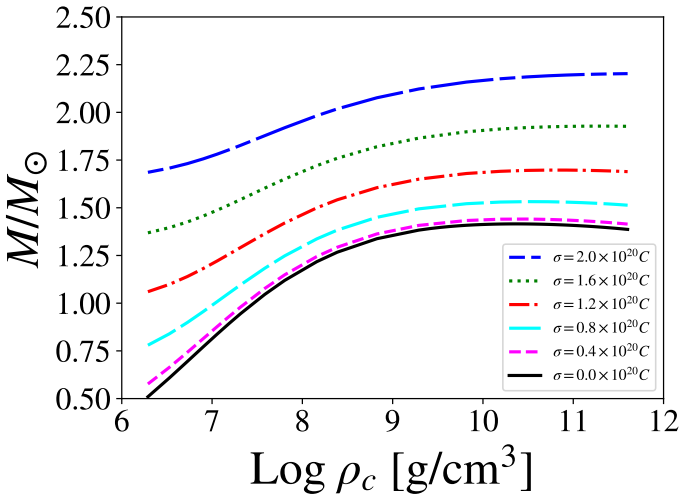

FIGURE 4.11 – Total mass, in Solar masses $M_\odot$, versus central mass density of the star for six values of σ. The unit for the constant σ is [C].

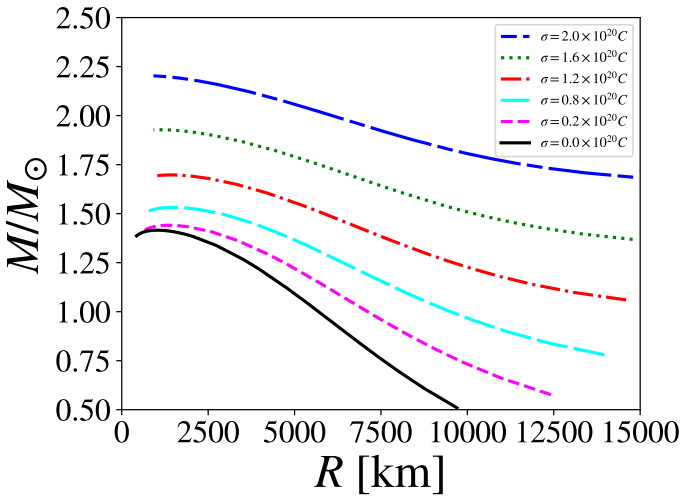

FIGURE 4.12 – The radius of the charged white dwarf as a function of the mass for different values of σ.

surface electric field produces considerable effects in the masses of white dwarfs. In addition, it is important to mention that the grow of the mass with σ can be understood since σ is related with the total charge contained in the star. The charge produces a force which helps to the one generated by the radial pressure to support more mass against the gravitational collapse.

In Fig. 4.12 the total mass as a function of the radius for few values of σ is observed. In the uncharged case $\sigma = 0.0$ the curve is close to attain the typical Chandrasekhar limit, $1.44 M_\odot$ (CHANDRASEKHAR; MILNE, 1931; CHANDRASEKHAR; S., 1935), however,

σ[C]	$M/M_\odot$	R[km]	ρ_c[g/cm^3]	Q[C]	E[V/cm]
0.0×10^{20}	1.416	1021	2.307×10^{10}	-	-
0.4×10^{20}	1.441	1299	3.043×10^{10}	4.055×10^{19}	2.158×10^{15}
0.8×10^{20}	1.532	1539	3.456×10^{10}	8.109×10^{19}	3.078×10^{15}
1.2×10^{20}	1.698	1336	6.613×10^{10}	1.222×10^{20}	6.149×10^{15}
1.6×10^{20}	1.928	1166	1.942×10^{11}	1.637×10^{20}	1.081×10^{16}
2.0×10^{20}	2.203	916.8	4.000×10^{11}	2.058×10^{20}	2.200×10^{16}

TABLE 4.5 – The constant σ and the maximum masses of the electrically charged white dwarfs with their respective radii, central densities, charges and electric fields at the surface of the stars.

in the charged case $\sigma \neq 0$ we found masses that overcome this typical limit. For instance, in the case $\sigma = 2.0 \times 10^{20}$[C] the mass whose electric field saturates the Schwinger limit is around $2.199 M_\odot$. Again, we mention that high values of white dwarf masses (around the super-Chandrasekhar white dwarf masses) can be achieved taking into account a surface electrical charge at the white dwarf.

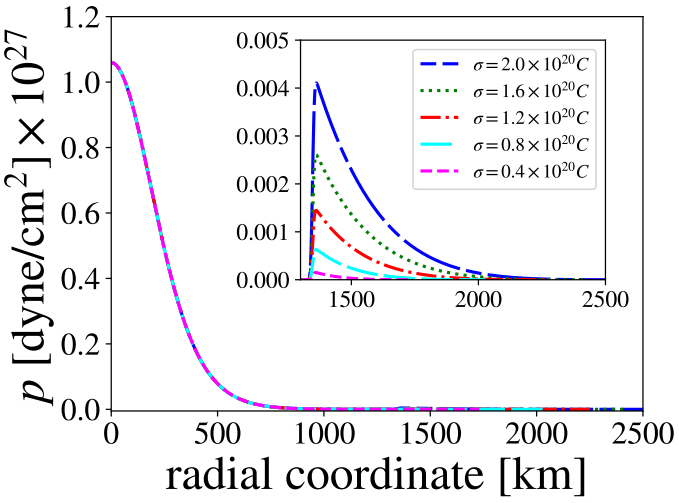

FIGURE 4.13 – Profile of the pressure inside the star as a function of the radial pressure for five different values of σ and for $\rho_c = 10^{10}$[g/cm^3].

With the purpose to observe that the electric charge is only distributed near the star's surface, the pressure profile inside the white dwarf as a function of the radial coordinate is plotted in Fig. 4.13, where few values of σ and $\rho_c = 10^{10}$[g/cm^3] are considered. In figure we can note that the pressure decays monotonically toward the baryonic surface, when this is attained the pressure grows abruptly due to the beginning of the electrostatic layer, after this point the pressure decrease with the radial coordinate until attain the star's surface ($p = 0$). Thus, through this result, we can clearly note that the electric charge is distributed as a spherical shell close to the surface of the white dwarf.

The behavior of the electric field in the star is showed in Fig. 4.14. On figure is employed five different values of σ and $\rho_c = 10^{10}[\mathrm{g/cm^3}]$. As can be seen, in each case presented, the electric field exhibit a very abrupt increase from zero to $10^{15-16}[\mathrm{V/cm}]$, thus indicating that the baryonic surface ends and starts the electrostatic layer. Once the electric surface is distributed like a thin layer close to the surface, the electric field sharply weaken with the grow of the radial coordinate such as is showed in figure.

It is important to emphasize that the electric field could be reduced, once taking into account the change that the electric potential screening may suffer with the increment of the radial distance (see (AKBARI-MOGHANJOUGHI, 2014)). The analysis of such a situation is left for future investigation.

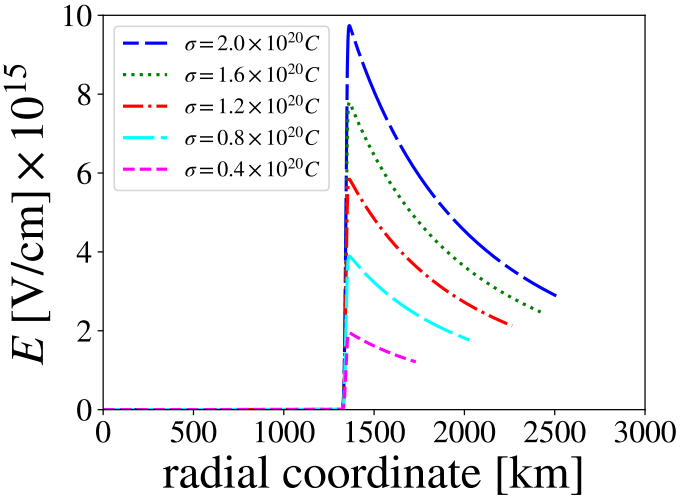

FIGURE 4.14 – Electric field as a function of the radial coordinate inside the charged white dwarf, for five values of σ and one of ρ_c. The central energy density $10^{10}[\mathrm{g/cm^3}]$ is considered.

It is worth mentioning that the electric field found in the charged white dwarfs cases are 10^4 times lower than those found in charged strange stars ones (see, e.g., (NEGREIROS *et al.*, 2009; MALHEIRO *et al.*, 2011a; ARBAÑIL; MALHEIRO, 2015)). This can be understood since white dwarfs have very larger radii than the strange stars.

The values for σ employed, the maximum mass values found in the range of central energy densities considered, with their respective central energy densities, total radius, total charge and electric field are shown in Table 4.5.

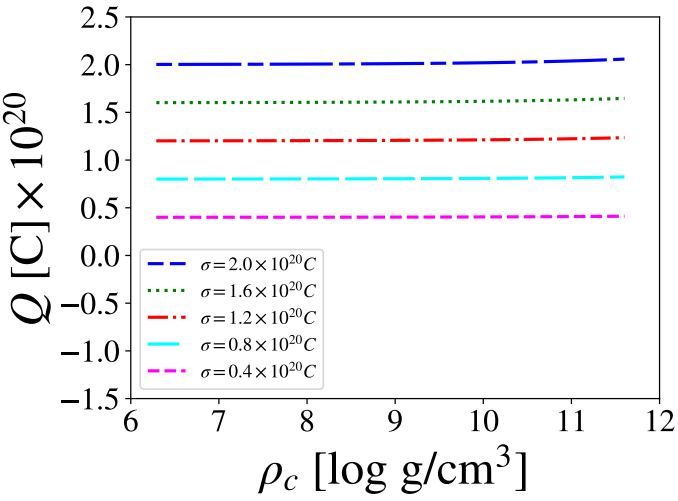

FIGURE 4.15 – Total electric charge against the central energy density for some values of σ.

4.4 About the radial stability of charged white dwarf

Inspired in the study of the turning-point method for axisymmetric stability of uniformly rotating relativistic stars with the angular momentum fixed (FRIEDMAN *et al.*, 1988) (see also (TAKAMI *et al.*, 2011) for a detailed discussion about that theme), in (ARBAÑIL; MALHEIRO, 2015) is shown that the stability of charged objects could be investigated using the results obtained from the hydrostatic equilibrium equation. The authors in (ARBAÑIL; MALHEIRO, 2015) found that along a sequence of charged stars with increasing central energy density and with fixed total charge, the maximum mass equilibrium configuration states the onset of instability. Thus, likewise, in this section we use the results derived from the equilibrium configurations to determine the maximum mass point which marks the start of the instability.

The total charge of white dwarf as a function of the central energy density is plotted in Fig. 4.15, taking into account five different values of σ. In figure we can see that along the sequence of equilibrium configurations with increasing central energy density the total charge is nearly constant. In this case, we understand that the maximum mass point must marks the onset of instability. In other words, the regions made of stable and unstable charged white dwarfs shall be distinguished through the relations $dM/d\rho_c > 0$ and $dM/d\rho_c < 0$, respectively.

Additionally, in Fig. 4.15, it can be observed also that the electrical charge that produce considerable effects in the structure of white dwarfs is around 10^{20}[C]. This amount of charge is similar to those found in the studies, for instance, of polytropic stars (RAY *et al.*, 2003), incompressible stars (FELICE *et al.*, 1995; FELICE *et al.*, 1999; ANNINOS;

ROTHMAN, 2001; ARBAÑIL *et al.*, 2014), strange stars (ARBAÑIL; MALHEIRO, 2015; NEGREIROS *et al.*, 2009; MALHEIRO *et al.*, 2011a) and white dwarfs (LIU *et al.*, 2014), where, certainly, the electric charge is considered.

4.5 Universal charge-radius relation and maximum total charge of white dwarfs

In (MADSEN, 2008), Madsen demonstrates that the electrical charge of a spherically symmetrical static object is limited by the creation of electron-positron pairs in super critical electric fields. Taking into account a timescale $\tau << \infty$, the net positive charge Q is directly proportional to the square of the star's radius $R_{\rm km}$, i.e.,:

$$Q = \beta e R_{\rm km}^2, \tag{4.13}$$

with β and e being the proportionality constant and charge of a proton, respectively. The proportionality constant β is directly related with the timescale chosen τ, for lower timescale a larger β is derived. Madsen found that for a timescale $\tau = 1.0\,s$ is obtained $\beta = 7.0 \times 10^{31}$, and for $\tau = 1.0 \times 10^{-10}\,s$, i.e., a typical weak interaction timescale, $\beta = 1.68 \times 10^{32}$.

For white dwarfs we can consider the electromagnetic interaction, consequently, the timescale can be regarded to be around $10^{-18}\,s$, thereby the constant β becomes equal to 3.34×10^{33}. In this case, we obtain that the more massive white dwarf (see Table I) would allow the maximum charge:

$$Q_{\rm max} \approx 5.0 \times 10^{20}\,[\rm C]. \tag{4.14}$$

Thus, the quantity of charge found in the most massive white dwarf ($Q = 2.045 \times 10^{20}$[C]) is under the maximum charge limit of Eq.(4.14).

4.6 Gravitational instability of white dwarfs in D-dimensions

Using the EoS for an ideal Fermi gas in D-dimensions, we investigated the hydrostatic equilibrium by using the TOV equation previously showed. To solve the equilibrium equations, we also need to define new variables to normalize the TOV. The new variables are $m' = G_D m$, $\rho' = G_D \rho$ and $p' = G_D p$. In order to solve the differential equations we need to define the value of $G_D \epsilon_0^{(D)}$, when defining the value of this quantity we are at the same time defining the value of G_D, in which we suppose that the gravitational

constant G_D may varies according to $G_D = l_D G_4$, where G_4 is the Newtonian gravitational constant, which we set equal to 1, thus working with natural units, and l_D is a parameter that has dimension of km^{D-4}. When we calculate the TOV we obtain the variables m', ρ' and p', and those quantities depend on the choice of the constant G_D. However, after obtained the solutions one can find quantities that do not depend on G_D, i.e, quantities that remains the same for any value of G_D. In the $4D$ case the independent mass, for example, is $MG_D^{3/2}$. The independent mass in the $5D$ case is MG_D^2, and for $D = 6$ it is $MG_D^{5/2}$. Following the pattern one can see that the quantity associated with mass that is independent on the value of G_D is $MG_D^{(D-1)/2}$.

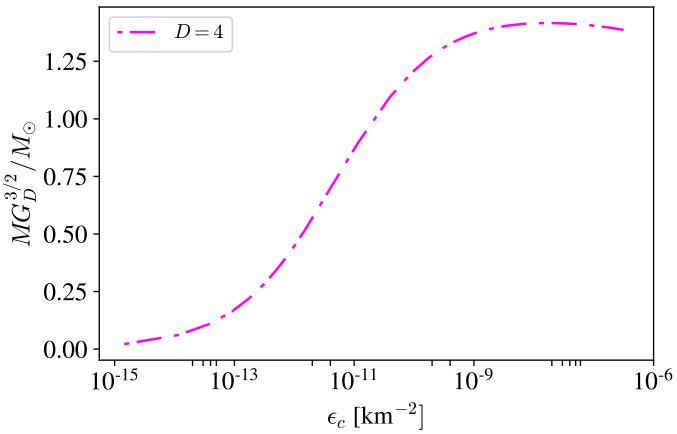

(a) Independent total mass $MG_D^{(D-1)/2}$ as function of the central energy density for white dwarfs in D-dimensions, for $D = 4$.

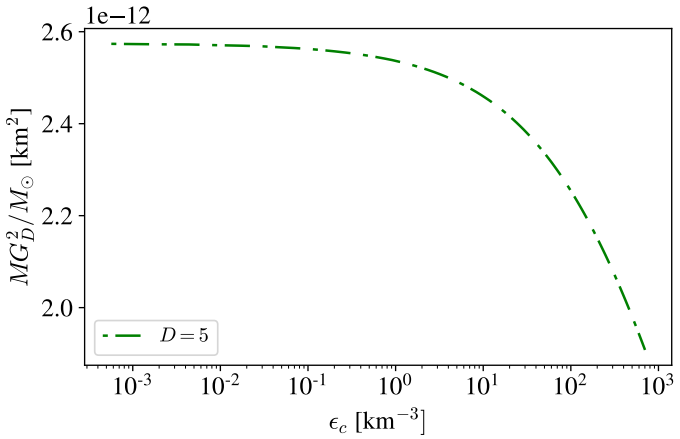

(b) Independent total mass $MG_D^{(D-1)/2}$ as function of the central energy density for white dwarfs in D-dimensions, for $D = 5$.

FIGURE 4.16 – Independent total mass $MG_D^{(D-1)/2}$ as function of the central energy density for white dwarfs in D-dimensions, for $D = 4$ (4.16a) and $D = 5$ (4.16b). As one can see the case $D = 5$ does not present any stability region. It is worth to cite that $G_D = l_D G_4$, where l_D is a parameter with dimension km^{D-4} and G_4 is the Newton's gravitational constant. We also have used natural units $c = 1 = G_4$ with $M_\odot = 1.47\text{km}$.

The Fig. 4.16a shows the mass-central density relation that is independent of the choice of G_D for $D = 4$ and $D = 5$. Since the values of energy density and pressure change drastically depending on the number of space-time dimensions the EoS becomes softer, see Fig. 2.1. After integration we found no stable solutions for $D > 4$, as one can check from the Fig. 4.16b, where we presented the case for $D = 5$. We have checked that for $D \geq 5$ we always find a Mass x ρ_c curve where $\partial M/\partial\rho_c < 0$, which implies that fermion stars are always unstable for extra dimensions, and will collapse to a black hole. The energy conditions of the system are respected, as we will see in the next subsection, being feasible physical solutions, i.e., this matter follows the well-know criteria for normal matter.

4.6.1 Energy conditions

Here we will investigate the energy conditions and see the constrains imposed by the null energy condition (NEC), weak energy condition (WEC), strong energy condition (SEC) and also, dominant energy condition (DEC) at the center of the compact star. It is important to analyze the energy conditions to show that the stellar instability is not due the D-dimensional Fermi gas being an exotic matter (such as the matter in wormholes). Such conditions can be written respectively as,

$$p + \rho \geq 0, \tag{4.15}$$

$$p + \rho \geq 0 \text{ and } \rho \geq 0, \tag{4.16}$$

$$p + \rho \geq 0 \text{ and } T \geq 0, \tag{4.17}$$

$$\rho \geq |p|. \tag{4.18}$$

As we can see in the Fig. 4.17 for any dimension the NEC, WEC, SEC and DEC are satisfied, which implies that the Fermi gas can be stated to be a normal matter in higher dimension. So, as, a normal matter the Fermi gas in D dimensional background would be a feasible physical system. Nevertheless, we shall see latter that the D dimensional Fermi gas does not have gravitational stability even in a Newtonian framework.

Going on to understand the instability in D-dimensional GR and not being aware of Chavanis' work (CHAVANIS, 2007), we have performed the reduction to Newtonian limit by completeness, using the Poisson's equation for the Newtonian gravitational potential, as we can see in the next section.

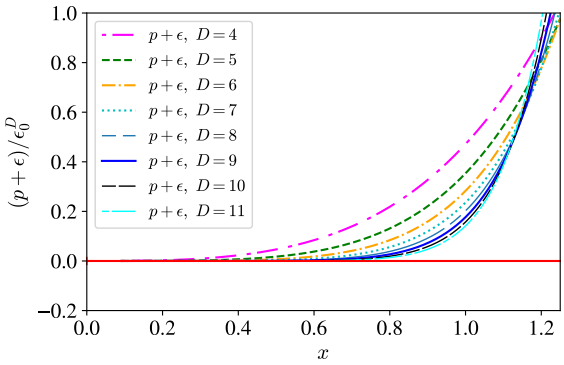

(a) Null energy condition (NEC)

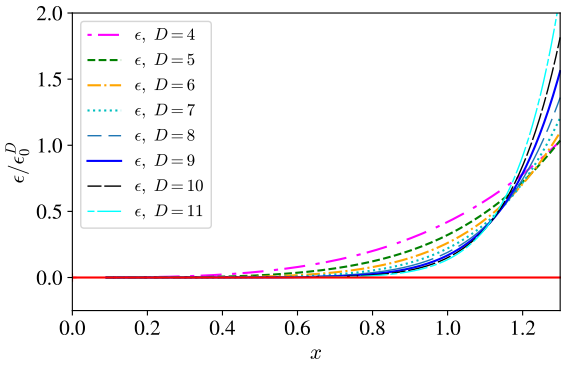

(b) Weak energy condition (WEC)

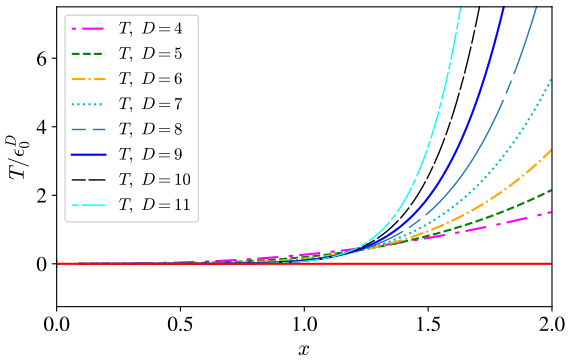

(c) Strong energy condition (SEC)

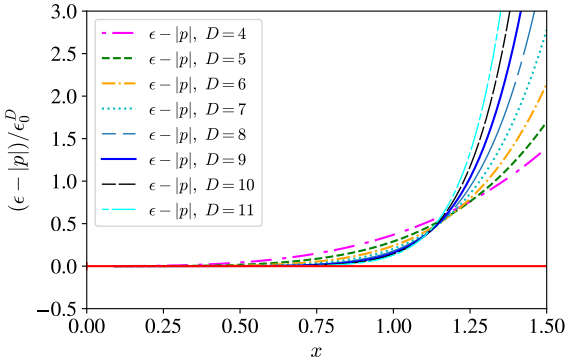

(d) Dominant energy condition (DEC)

FIGURE 4.17 – Energy conditions: in (4.17a) we have the null energy condition (NEC), $p + \rho \geq 0$. In (4.17b) we have the weak energy condition (WEC), $\rho \geq 0$. In (4.17c) the strong energy condition (SEC), $T \geq 0$. And finally in (4.17d) we have the last one, the dominant energy condition (DEC), $\rho \geq |p|$, one can see that for any dimensions, the energy conditions are respected for any value of energy density and pressure.

4.6.2 Lane-Emden equation in D-dimensions (Newtonian instability)

To derive the Lane-Emden equation in a D-dimensional space-time we start by writing the well-known Poisson's equation

$$\nabla^2\phi = 4\pi G\rho, \tag{4.19}$$

where G is the standard gravitational constant, ϕ is the gravitational potential and ρ represents mass density. If one considers the space-time to have spatial extra dimensions the Poisson's equation can be rewritten as

$$\nabla^2\phi_D = \Omega_{D-2}G_D\rho, \tag{4.20}$$

being Ω_{D-2} the solid angle of the hyper-sphere, ϕ_D is the gravitational potential in D dimensions and G_D is the gravitational constant in also arbitrary D space-time dimensions. The D-dimensional Laplace operator ∇^2 in spherical coordinates, disregarding its angular components, now reads

$$\nabla^2 = \frac{\partial^2}{\partial r^2} + \frac{D-2}{r}\frac{\partial}{\partial r}, \tag{4.21}$$

such that, for vacuum, one possible solution of (4.20) for $D \geq 4$ is

$$\phi_D = -\frac{1}{(D-3)}\frac{G_D m}{r^{D-3}}. \tag{4.22}$$

The gravitational field thus becomes,

$$\vec{g} = -\vec{\nabla}\phi_D = -\frac{G_D m}{r^{D-2}}, \tag{4.23}$$

and then the hydrostatic equilibrium equation of a hypersphere in $D-1$ spacial dimensions reads

$$\frac{dp}{dr} = -\frac{G_D m \rho}{r^{D-2}}, \tag{4.24}$$

and the equation of mass continuity is, again, rewritten as

$$\frac{dm}{dr} = \Omega_{D-2}\rho r^{D-2}. \tag{4.25}$$

The assumptions above of universal extra dimensions, and by using the polytropic approximations previously derived, one can obtain the modified Lane-Emden equation, in its dimensionless form, as

$$\frac{1}{\xi^{D-2}}\frac{d}{d\xi}\left(\xi^{D-2}\frac{d\theta}{d\xi}\right) = -\theta^n, \tag{4.26}$$

where we performed the change of variables, $r = a\xi$ and $\rho = \rho_c\theta^n$, with ρ_c being the central mass density, n the polytropic index and $a^2 = \frac{(n+1)K\rho_c^{\frac{1}{n}-1}}{G_D\Omega_{D-2}}$.

The total mass of a spherical object in terms of those new variables thus becomes

$$M = \Omega_{D-2}\rho_c a^{D-1}\int_0^{\xi_{\max}} \xi^{D-2}\theta^n d\xi = \Omega_{D-2}\rho_c a^{D-1}\xi_{\max}^{D-2}\theta'(\xi_{\max}),$$

and by replacing a one get

$$M = \Lambda\rho_c^{\frac{D-1}{2}\left(\frac{1}{n}-1\right)+1}, \tag{4.27}$$

where Λ is a constant defined as

$$\Lambda = \left[\frac{(n+1)K}{G_D \Omega_{D-2}^{\frac{(D-3)}{(D-1)}}}\right]^{\frac{D-1}{2}} \xi_{\max}^{D-2}\theta'(\xi_{\max}). \tag{4.28}$$

In the case of white dwarfs, for $D = 4$ and $n = 3$, one can obtain from Eq. (4.27), for instance, the so-called Chandrasekhar mass limit. However, the assumption that particles may access extra dimensions, such as an ideal Fermi gas in a D dimensional space-time implies that for larger D the mass-central density relation is changed according to (4.27). Thus, considering the stability criterion derived by Chandrasekhar, $\partial M/\partial\rho_c > 0$, we can impose that the mass density exponent in Eq.(4.27) needs to be larger than zero in order the stars to be gravitationally stable. Using the generalized polytropic approximations (2.35) and (2.36), we find

$$\frac{D-1}{2}\left(\frac{1}{n}-1\right)+1>0$$

$$\begin{cases} D<5, \text{non}-\text{relativistic limit } \left(\frac{1}{n}=\frac{2}{D-1}\right) \\ D<4, \text{ultra}-\text{relativistic limit } \left(\frac{1}{n}=\frac{1}{D-1}\right), \end{cases}$$

then, it is a straightforward conclusion that no stable solutions are found for the bunch of fermions in the presence of universal extra dimensions, thus confirming our previous results obtained in a general relativistic framework and also in agreement with (CHAVANIS, 2007).

5 White Dwarfs in $f(\mathcal{R},\mathcal{T})$ Gravity

The application of the gravity $f(\mathcal{R},\mathcal{T})$ for the study of stellar equilibrium is motivated by its recent outcomes in several areas. In particular, it has been shown that from a minimum coupling between matter and geometry, predicted in $f(\mathcal{R},\mathcal{T})$ theories of gravity, it is possible to obtain flat rotation curves for the galaxies' "halo" (ZAREGONBADI *et al.*, 2016). $f(\mathcal{R},\mathcal{T})$ models were also compatible with the description of our solar system (SHABANI; FARHOUDI, 2014; DENG; XIE, 2015). A complete description of the cosmological scenario was constructed from $f(\mathcal{R},\mathcal{T})$ gravity in (MORAES; SANTOS, 2016). In (MORAES; SAHOO, 2017), a cosmological model in agreement with observations was also obtained from a non-minimal coupling between matter and geometry in the framework of the $f(\mathcal{R},\mathcal{T})$ theories. The validity of the first and second laws of thermodynamics in $f(\mathcal{R},\mathcal{T})$ theories were discussed in (SHARIF; ZUBAIR, 2012).

In addition, the hydrostatic equilibrium equations in $f(\mathcal{R},\mathcal{T})$ gravity was originally derived in (MORAES *et al.*, 2016) and it has been used to the study of quarks stars (DAS *et al.*, 2016; SHARIF; WASEEM, 2018; DEB *et al.*, 2018d; DEB *et al.*, 2018a; DEB *et al.*, 2018c; DEB *et al.*, 2018b), and neutron stars (Moraes *et al.*, 2018). In other works the stability and collapse of objects with spherical symmetry were derived in (SHARIF; YOUSAF, 2014; NOUREEN; ZUBAIR, 2015b; NOUREEN; ZUBAIR, 2015a; NOUREEN *et al.*, 2015; ZUBAIR; NOUREEN, 2015).

As we will show below, the $f(\mathcal{R},\mathcal{T})$ gravity can be an important tool for the study of macroscopic properties of white dwarf stars, in the sense that it can increase the maximum stable mass. As well as we will show some advantages of the $f(\mathcal{R},\mathcal{T})$ theory when compared to the results of $f(\mathcal{R})$ theories for such objects. Using the equilibrium equations previously derived for the functional $f(\mathcal{R},\mathcal{T}) = \mathcal{R} + 2\lambda\mathcal{T}$, we calculate the white dwarf equilibrium configurations in this theory.

The mass of the WDs as a function of their total radii is shown in Fig. 5.1 for six different values of λ. $\lambda = 0$ recovers the GR case. From Figure 5.1, we note that the masses of the stars grow and their total radii increase until attain the maximum mass point, which will be represented by full magenta circles. After that, the masses decrease with the total radii. It is important to remark that the total maximum mass grows with

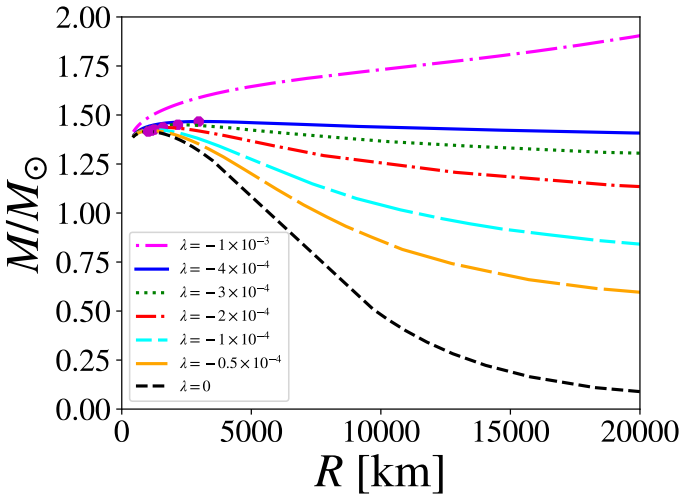

FIGURE 5.1 – Total mass as a function of the total radius for different values of λ. The full magenta circles indicate the maximum mass points.

the decrement of λ and the radius increases much more when we consider a fixed star mass. We also mention that the curves above tend to a plateau when λ is $\approx -4\times10^{-4}$. For smaller values of the parameter λ, all stars are unstable, what can be seen in Figures 5.1 and 5.4 for $\lambda = -1\times10^{-3}$, where $\partial M/\partial R < 0$ and the necessary stability criterion $\partial M/\partial\rho_c > 0$ are not satisfied. So, from the equilibrium configurations, the minimum value allowed for λ is $\sim -4\times10^{-4}$, which defines a limit for the maximum mass of the WD in the $f(\mathcal{R},\mathcal{T})$ gravity to be $\sim 1.467M_\odot$.

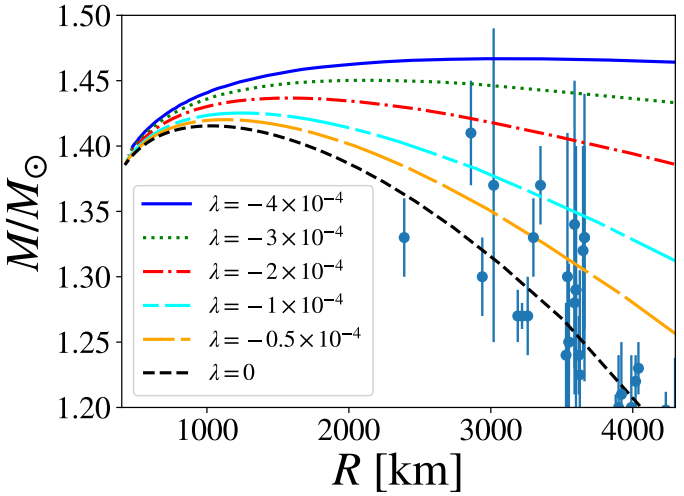

FIGURE 5.2 – Mass as a function of the radius for massive WDs with different values of λ. The blue circles with error bars represent the observational data of a sample of massive WDs taken from the catalogs (VENNES *et al.*, 1997; NALEŻYTY *et al.*, 2004).

In addition, in Fig. 5.2 we highlight the massive WDs region of Fig. 5.1, in which

we have also inserted some observational data taken from the catalogs of References (VENNES *et al.*, 1997; NALEŻYTY *et al.*, 2004). It can be clearly seen from Fig. 5.2 that some of the data can hardly be described purely from General Relativity, while some values of λ can, indeed, predict the existence of massive WDs with larger radii.

Thus, according to observations of some massive WDs, in particular the most massive, WD (1659+440J), found in (VENNES *et al.*, 1997), the inferior limit for λ is $\lambda_{min} \approx -3 \times 10^{-4}$. We regard that this restriction is obtained by neglecting the WD data (0003+436J) with the largest error bar in Fig. 5.2. Such a constraint is more restrictive than the one obtained from Fig. 5.1, with no observational data. It is worth to cite that this observational constrain is not compatible with the one obtained for the $f(\mathcal{R},\mathcal{T}) = \mathcal{R}+2\lambda\mathcal{T}$ cosmology where λ needs to be positive and of the order ~ 1 (VELTEN; CARAMÊS, 2017).

In Fig. 5.3 the energy density, fluid pressure and mass profile in the interior of the star are plotted on the top, central and bottom panels, respectively, as functions of the radial coordinate. We take into account $\rho_c = 10^9$ [g/cm^3] and different values of λ. On the top and central panels, we can observe that the energy density and the fluid pressure decrease monotonically towards the surface of the object.

On the other hand, concerning the bottom panel, it can be noted that the mass profile $m/M_\odot$, with $M_\odot$ representing the Sun's mass, grows until it reaches the surface of the star. It can also be seen that the total mass of the star increases with λ. This is due to the effect caused by the term $2\lambda T$.

Fig. 5.4 shows the behavior of the total mass against the central energy density of the stars. The values considered for the central energy density are between 1.3×10^8 and 4.2×10^{11} [g/cm^3]. The upper limit is the neutron drip limit, i.e., the point where the WD turn into a neutron star. We can note that the total mass grows monotonically with central energy density until it attains a maximum value, except for $\lambda = -1 \times 10^{-3}$. After that point, the stellar mass decreases with the increment of ρ_c and becomes unstable.

Additionally, in Fig. 5.4, we observe an increment of the maximum mass with λ (see also Table 5.1). For example, the maximum mass value found in GR case ($\lambda = 0$) is $1.417M_\odot$, while for $\lambda = -4 \times 10^{-4}$, it is $1.467M_\odot$. A similar effect for λ in the structure of the stars has been found for neutron stars and strange stars (MORAES *et al.*, 2016; MALHEIRO *et al.*, 2003). Moreover, it is remarkable that for lower values of λ, the maximum mass point is reached for lower values of ρ_c, which can be considered an advantage of this approach when compared with $f(R)$ theory of gravity or GR outcomes, as we will argue in the next section.

In Fig. 5.5 the dependence of the total radius with the central energy density is shown. In all cases presented, we can note that the total radius decreases when the central energy

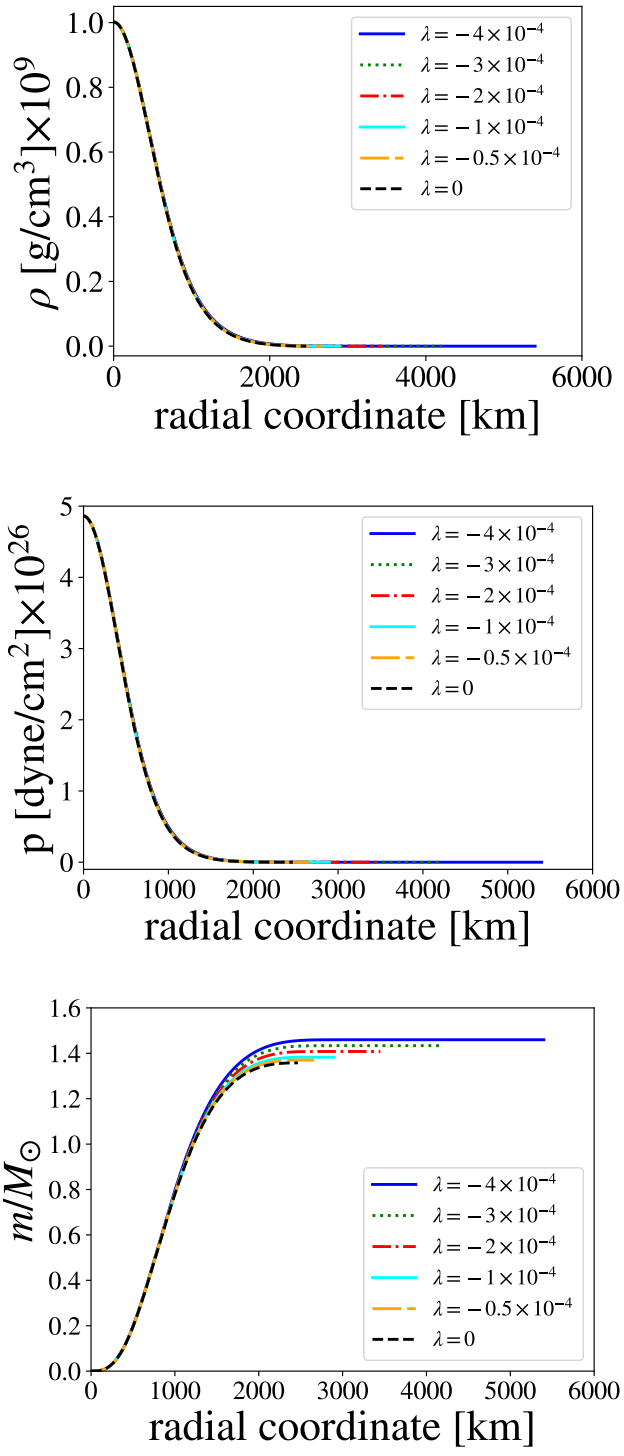

FIGURE 5.3 – On the top panel it is presented the star energy density as a function of the radial coordinate, on the central panel we show the star pressure fluid against the radial coordinate and on the bottom panel we display the mass (in solar masses, $M_\odot$) inside the star versus the radial coordinate. We consider $\rho_c = 10^9$ [g/cm^3] and the displayed values of λ.

density is incremented. Larger radii are found for smaller central energy densities when λ is decreased. This is the most important effect of $f(\mathcal{R},\mathcal{T})$ theory for massive WDs, that

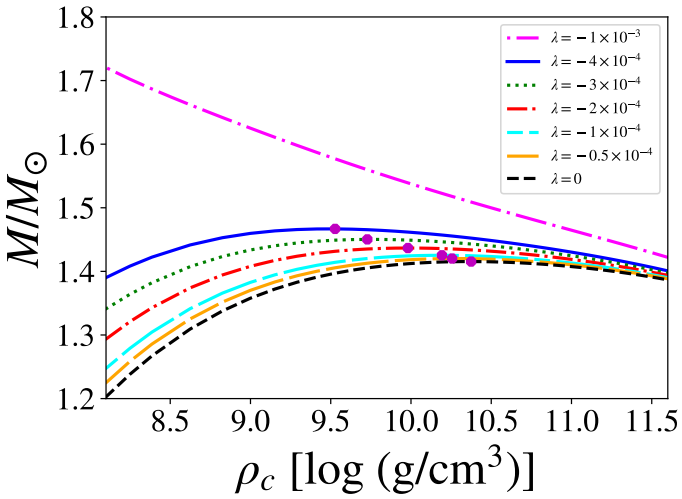

FIGURE 5.4 – The dependence of the total mass of the white dwarfs on central density for different values of λ.

is, the increase of the radius, and as a consequence, the decrease of the central density, in comparison with GR and also $f(\mathcal{R})$ results. This is mainly due to the fact that the sound velocity becomes very small near the surface of the star, so that the term (3.84) weakens the gradient of pressure, yielding to the predicted larger radii.

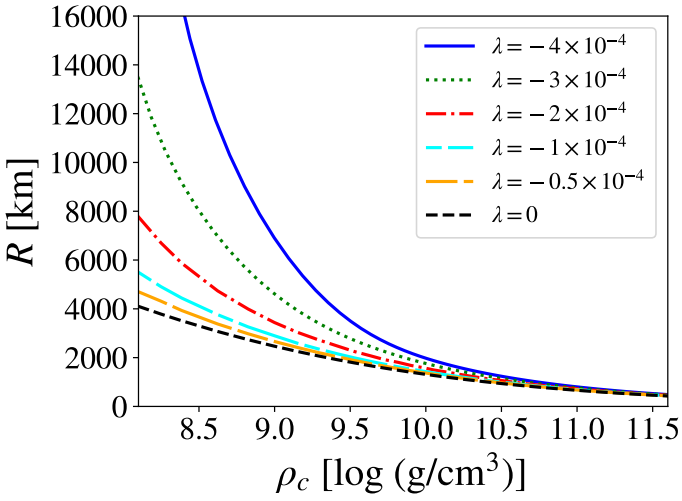

FIGURE 5.5 – The total star radius versus central density for different values of λ.

In Table 5.1 the maximum masses are presented, with their total radii and central energy densities, for each value of λ. We can see that more massive and larger WDs are found with the decrement of λ. The values of maximum masses are obtained for lower central densities (range of $\rho_c \sim 10^9 - 10^{10}$[g/cm^3]) when compared with those predicted in the $f(\mathcal{R})$ gravity or GR scope ($\rho_c \sim 10^{11}$[g/cm^3]) (DAS; MUKHOPADHYAY, 2015b).

λ	$M/M_\odot$	R [km]	ρ_c [g/cm^3]
0.0×10^{-4}	1.416	1021	2.307×10^{10}
-0.5×10^{-4}	1.420	1146	1.803×10^{10}
-1.0×10^{-4}	1.425	1247	1.558×10^{10}
-2.0×10^{-4}	1.437	1590	9.567×10^{9}
-3.0×10^{-4}	1.450	2168	5.345×10^{9}
-4.0×10^{-4}	1.467	2970	3.366×10^{9}

TABLE 5.1 – The maximum masses of the white dwarfs found for each value of λ with their respective total radii and central energy densities.

6 White Dwarfs in Binary Systems

In this chapter we will focus on the study of white dwarf binary systems, in particular, double white dwarf binary systems (for simplicity WD-WD systems). An estimate is that our galaxy host a number of $100 - 300\times(10^6)$ WD-WD binary systems (NELEMANS *et al.*, 2001), but only a few have been detected ~ 100. However, the number of WD-WD binaries has been increased the last few years (NELEMANS *et al.*, 2005) and it is an expectation that this number will increase even more in a near future. In some cases is difficult to determine whether the binary system hosts two white dwarfs or a white dwarf and a neutron star (KULKARNI; KERKWIJK, 2010; KAPLAN *et al.*, 2013), and our plan is that this study hepls to determine the difference between them. Binary systems are of great significance as they are a leading source of gravitational waves, such as the one detected recently by LIGO/VIRGO collaboration (ABBOTT *et al.*, 2017). The large number estimated of WD-WD binaries in our galaxy also indicates that this kind of system can be a leading source of gravitational waves for the LISA detector, which could bring light to a wide variety of physical processes concerning those close binary systems and its evolution (KREMER *et al.*, 2017; BREEDT *et al.*, 2017).

Double white dwarf binary mergers have also been recently introduced as a new subclass of gamma-ray bursts (GRBs) characterized by a prompt gamma-ray emission, an infrared/optical kilonova from the merger ejecta, and an extended X-ray emission from the WD central remnant born in the merger (RUEDA *et al.*, 2018). While the optical and X-ray emission were treated in detail, the gamma-ray emission was only proposed to arise from WD magnetospheric processes. We here estimate the gamma-ray emission as the result of the electric potential induced by the interaction of the magnetic field of the WD.

It has been recently estimated the luminosity generated due to the magnetosphere interaction in a NS-NS merger (LYUTIKOV, 2018). Qualitatively, it is there considered that one of the binary system components possesses a magnetic NS and the companion is a conductor spherical body that is moving into the NS magnetosphere. Under these conditions, the relative motion between the two stars induces an electric potential capable of accelerate particles. Lyutikov estimate applied to WD-WD binaries were shown to power an emission as high as 10^{41}erg/s, however, this estimate is based in a very simple

calculation.

Wu et al. (WU *et al.*, 2002) and Dall'Osso et al. (DALL'OSSO *et al.*, 2006) had applied earlier to WD-WD binary systems, in more details, the above Lyutikov approach - often named as unipolar inductor model (UIM). Wu et al. have considered a binary system composed of a rotating magnetic white dwarf and its companion a non-rotating, non-magnetic white dwarf that behaves like a conductor moving into the primary star's magnetosphere. The system could be asynchronous as the magnetic white dwarf angular velocity Ω can be different from the orbital one, ω_0. The relative velocity is $\vec{v} = r(\omega_0 - \Omega)\hat{\phi}$, where r is the orbital separation. Given the Kepler's third law the velocity becomes

$$\vec{v} = [G(M_1 + M_2)]^{1/3}\omega_0^{1/3}(1-\alpha)\hat{\phi}, \tag{6.1}$$

where the parameter $\alpha = \frac{\Omega}{\omega_0}$ determines how asynchronous is the system.

The induced electric field is

$$\vec{E} = \frac{\vec{v} \times \vec{B}}{c}, \tag{6.2}$$

and its associated electric potential

$$U = 2R_2|E|. \tag{6.3}$$

The total energy dissipation is (DALL'OSSO *et al.*, 2006)

$$\dot{E} = 2I^2\mathcal{R} \tag{6.4}$$

where the factor 2 accounts for the upper and lower similar parts of the circuit (see figure 6.1), $\mathcal{R}$ is the effective resistance of the system and $I = U/\mathcal{R}$ is the electric current. Wu et al. showed that the total resistence for double white dwarf binaries is

$$\mathcal{R} = \frac{1}{2\overline{\sigma}}\left(\frac{H}{\Delta d}\right)\left(\frac{r}{R_1}\right)^{3/2}\frac{j(e)}{R_2}, \tag{6.5}$$

where R_1 and R_2 are the radii of the primary and secondary stars, respectively, $\overline{\sigma}$ is the average conductivity, H is the depth at which the induced currents cross the magnetic field lines and return to the secondary, Δd is the current layer thickness of the arc-like cross section at the primary atmosphere and $j(e)$ is a geometric factor (see (WU *et al.*, 2002)). The luminosity $L = \dot{E}$, then becomes

$$L = \frac{2U^2}{\mathcal{R}} = \left(\frac{\mu_1}{c}\right)^2 \frac{16\overline{\sigma}R_1^{3/2}R_2^3\omega_0^{17/3}(1-\alpha)^2}{(G(M_1+M_2))^{11/6}\,(H/\Delta d)j(e)}, \tag{6.6}$$

where M_1 and M_2 are the respective masses of the primary and secondary stars and

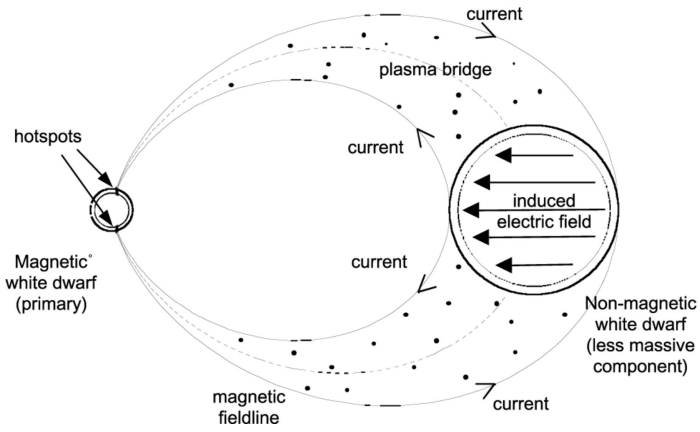

FIGURE 6.1 – Schematic representation of the unipolar inductor model. As the secondary star is a conductor moving in the primary star's magnetosphere an electric field is induced inside the secondary. This electric field could thus accelerate particles from the secondary's surface. In a situation of equilibrium a closed circuit could be set with the charged particles following the magnetic field lines' path. Source: (WU *et al.*, 2002).

$\vec{B} = -(\mu_1/r^3)\hat{z}$, where μ_1 is the magnetic moment of the primary star. As estimated by Wu et al. the ratio $H/\Delta d$ is of the order of 1 and also the geometric factor $j(e) \sim 1$ for orbital periods less than one hour. Wu et al. also estimated the conductivity $\overline{\sigma}$ as $10^{13} - 10^{14}$esu, for a star with electron temperature $T_e = 10^5$K (more details, see (WU *et al.*, 2002)). Using these fiducial parameters derived by Wu et al. we varied the magnetic field strengh to obtain the luminosity as showed in figure 6.2. It is worth to cite that in the work of Wu et al. they fixed the magnetic moment as $\mu_1 = 10^{32}$G cm^3 and varied the parameters of mass and radius of the stars, here we did not fix the magnetic moment, rather we estimate the magnetic moment as $\mu_1 = B_1 R_1^3$, where B_1 is the magnetic field of the primary star and varied the magnetic field. We take into account that the maximum orbital frequency is

$$\omega_0^{\max} = \frac{2\pi}{P_{\min}} = \frac{(G(M_1 + M_2))^{1/2}}{(R_1 + R_2)^{3/2}}, \tag{6.7}$$

and the mass-radius relation is taken from (CARVALHO *et al.*, 2018). According to the model of Wu et al. the unipolar inductor model can power a very high emission 10^{51}ergs/s at instants prior to merger for a magnetic field of 10^9G, see figure 6.2. This is an important result that could explain the gamma-ray emission of some gamma-ray bursts, such as the one associated with the gravitational wave detection GW170817. In particular, the energy observed in GRB 170817A - associated with GW 170817 - is of the order $\sim 10^{46}$erg/s, which could be explained by a magnetic field of a few 10^6G in the present model.

However, Lai showed that in the case of binary systems the magnetic field can be twisted as the dimensionless azimuthal twist of the flux tube $\xi_\phi = -B_{\phi+}/B_z = 16v/c^2\mathcal{R}$ depends on the effective resistance (LAI, 2012). Which means that if the resistance is low enough the magnetic field will be twisted and energy can be released due to disruption of

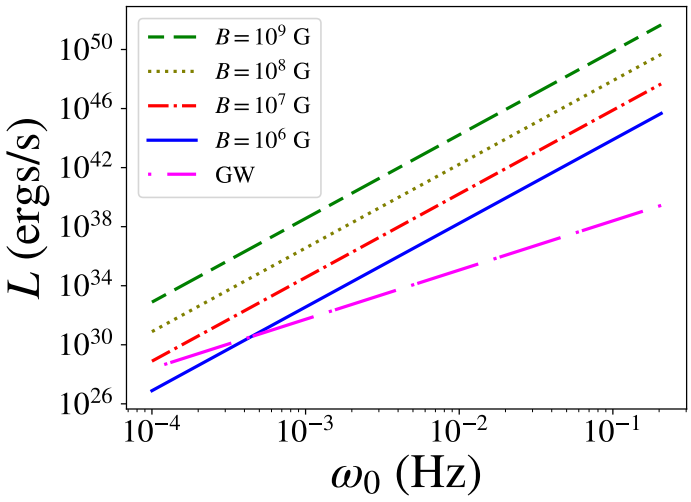

FIGURE 6.2 – Luminosity as a function of the orbit's angular frequency using the results of (WU *et al.*, 2002) (see also Eq. (6.6)). The value of α is 0.9. The masses are $M_1 = M_2 = 0.6M_\odot$ and their respective radii are taken from (CARVALHO *et al.*, 2018). The magnetic field strength ranges from 10^6G to 10^9G. According to the model of Wu et al. the luminosity can be very high at moments close to merger.

the magnetic flux tubes. Using the effective resistance derived by Wu et al. we find that the azimuthal twist is much higher than unity, which implies that the magnetic field is highly twisted and the system is constantly reaching a low energy state by magnetic reconnection. Lai proposes that a quasi-cyclic mechanism can take place (LAI, 2012), where several magnetic recconections may occur. According to (LAI, 2012) the electromagnetic emission can be parameterized by the twist factor ξ_ϕ as

$$L = \xi_\phi \omega_0 (1-\alpha) \frac{\mu_1^2 R_2^2}{2r^5}. \tag{6.8}$$

Using the result of Lai (6.8) with appropriated parameters for WD-WD binary systems the luminosity becomes

$$\begin{aligned} L_{\mathrm{WD-WD}} = 3.84 \times 10^{29} \xi_\phi (1-\alpha) \times \left(\frac{\mu_1}{10^{32}\ \mathrm{G\ cm^3}}\right)^2 \times \\ \left(\frac{R_2}{10^9\ \mathrm{cm}}\right)^2 \times \left(\frac{M}{M_\odot}\right)^{-5/3} \times \left(\frac{P}{10\mathrm{min}}\right)^{-13/3} \mathrm{erg\ s^{-1}}. \end{aligned} \tag{6.9}$$

In figure 6.3 we show the parameterized luminosity with maximum efficiency $\xi_\phi = 1$ and $\alpha = 0.9$. We see that the luminosity drops far below the previous values of figure 6.2, i.e., the luminosity is screened by magnetic stresses. The case of magnetic field $B = 10^9$G the maximum powered emission is 10^{41}erg/s. The GRB 170817A power, 10^{46}erg/s, can be reached now only if the magnetic field is of a few 10^{11}G. This may indicate that GRB

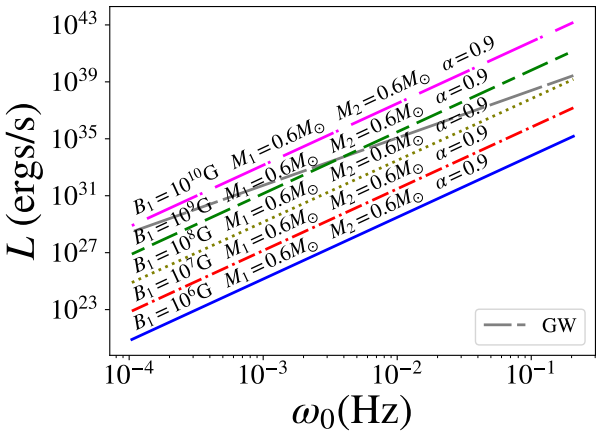

FIGURE 6.3 – Parameterized luminosity as a function of orbital angular frequency (see Eq. 6.9). The masses are $M_1 = M_2 = 0.6M_\odot$. The mass-radius relation is taken from (CARVALHO *et al.*, 2018).

powers may be originated from a high magnetic WD-WD binary at moments close to merger. However, we need to stress that we do not know how much energy can be released in a magnetic reconnection, which could be higher than the parameterized luminosity. It can also be seen from Fig. 6.3 that when the field is larger than 10^9G the electromagnetic (EM) emission is higher than gravitational wave (GW) emission. Since the EM emission also takes energy from the orbital motion the orbital evolution will not be GW driven, rather a coupling between GW and EM emission will drive the binary evolution, for those cases we will use the results of Wu et al. (WU *et al.*, 2002) for the coupling between ω_0 and α

$$\frac{\dot{\omega}_0}{\omega_0} = \frac{1}{g(\omega_0)}\left[L_{\rm GW} - \frac{L_{\rm WD-WD}}{1-\alpha}\right] \tag{6.10}$$

$$\frac{\dot{\alpha}}{\alpha} = \frac{1}{g(\omega_0)}\left[L_{\rm GW} - \frac{L_{\rm WD-WD}}{1-\alpha}\left(1+\frac{g(\omega_0)}{\alpha I_1 \omega_0^2}\right)\right], \tag{6.11}$$

where $L_{\rm GW}$ is the gravitational wave luminosity. In Fig. 6.4 we show the evolution in time of ω_0 considering an initial orbital period of 4 hours. The evolution of ω_0 or equivalently the orbital separation is not sensitive to the initial condition for α. We can see from Fig. 6.4 that for magnetic fields larger than 10^9 the higher the magnetic field the smaller the time necessary to merger, mainly because the magnetic friction takes energy from the orbital motion.

We define now the intrinsic time-domain phase evolution,

$$Q_\omega = \frac{\omega^2}{\dot{\omega}} = 2\pi \frac{dN}{d\ln\omega}, \tag{6.12}$$

where $\omega = 2\omega_0$, is the GW angular frequency, and N the number of GW cycles. From Fig.

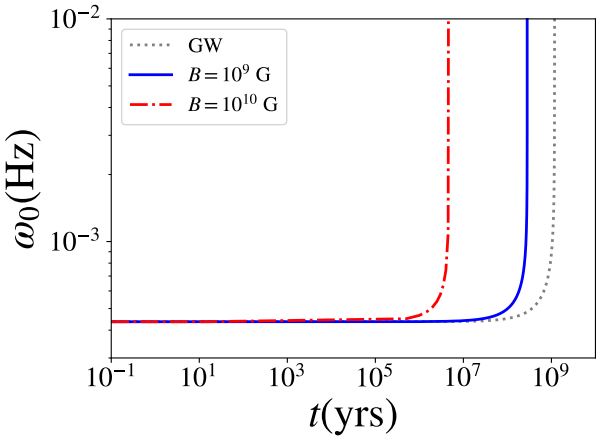

FIGURE 6.4 – Orbital evolution for two values of magnetic field. The parameters were choose such as in Fig. 6.3. The initial period is 4 hours.

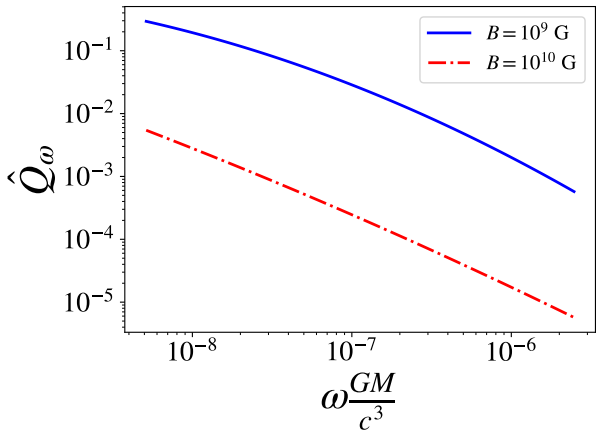

FIGURE 6.5 – Intrinsic time-domain phase evolution normalized by $Q_\omega^{\rm GW}$, $\hat{Q}_\omega \equiv Q_\omega/Q_\omega^{\rm GW}$.

6.5 we can see that the intrinsic time-domain is largely affected according the magnetic field is increased for $B > 10^9$G, which implies a different number of cycles N for an appreciable changing in frequency. This effect can be measured by gravitational wave detectors, such as LISA, and may be a possible way to estimate the magnitude of the high magnetic fields in WD-WD binary systems.

Another important quantity is the delay time distribution (DTD), which is defined as the "hypotetical supernova rate versus time that would follow a brief burst of star formation" (MAOZ; MANNUCCI, 2012), or simply the number of systems as a function of the time elapsed to form them. The DTD is important because it can provide clues about the progenitors of type Ia supernovae. The DTD is related to lifetimes, i.e., the binary evolution timescale. As we have shown the binary evolution is affected by the UIM and one would expect as a result a different scenario for the DTD. The theoretical DTD can be derived by simple physical considerations. For example, if the orbital evolution is

governed by energy loss from gravitational wave emission, we have then

$$\frac{dr}{dt} = -\frac{\kappa}{4r^3}, \quad \kappa = \frac{256}{5}\frac{G^3}{c^5}M_1M_2(M_1+M_2), \tag{6.13}$$

integrating (6.13) we have that after a time t the system evolves from an orbital distance r' to r as

$$r'^4 - r^4 = \kappa t. \tag{6.14}$$

Now, supposing an initial separation distribution $n'(r')$, systems with separations in the range of r' to $r'+dr'$ migrates after a time t to a shell from r to $r+dr$ in the evolved distribution $n(r,t)$. Number conservation, except for those systems who reaches merger, yields

$$n(r,t)dr = n'(r')dr'. \tag{6.15}$$

If the initial separation distribution is a power law $n' \propto r'^{\alpha}$, we have

$$n(r,t) \propto r^3(r^4+\kappa t)^{(\alpha-3)/4}. \tag{6.16}$$

The evolved distribution can be broke into two parts, where both can be given also by a power law. First we may have systems with $r >> (\kappa t)^{1/4}$, and the distribution will have the same power law as the original, i.e., $n(r) \sim r^{\alpha}$. For orbital separations $r << (\kappa t)^{1/4}$, then we have $n(r) \sim r^3$. Binaries with short separations will control the DTD, the DTD then becomes,

$$\frac{dn}{dt} = \frac{dn}{dr}\frac{dr}{dt} \propto \frac{n(r,t)}{r^4} \sim t^{(\alpha-3)/4}. \tag{6.17}$$

These above calculations is a review from (MAOZ *et al.*, 2012). According to (MAOZ; MANNUCCI, 2012) a consistent consideration is $\alpha = -1$, which leads to the well know result for the DTD as proportional to $\sim t^{-1}$ and this is also in good agreement with the observational data for delays between the range 1Gyr $< t <$ 10Gyr. However, for smaller delays $t <$ 1Gyr the observational data show some discrepance with the typical result $\sim t^{-1}$. As the magnetic friction changes the orbital evolution we fit it and its respective separation distributions and DTDs could be derived, the results are showed in Tab. 6.1. The parameterized DTDs for magnetic WD-WD binaries show that they all provide the standard result $\sim t^{-1}$ for $\alpha = -1$. However, the power law is changed for small separations. In Fig. (6.6a) we show the separations distributions versus orbital separation. From the figure we can see that the similar power-law shape is reached in a different position when considering magnetic WD-WD binary systems. On the other hand systems with short separations have its power law for n changed.

Taking now a series of WD populations, all of them with an inital separation distribution $n' \propto r'^{\alpha}$ and produced with a rate $\tau(t)$ between $t = 0$ and the age of the Galaxy

TABLE 6.1 – Parameterized orbital evolution, separation distribution and delay time distribution for WD-WD binaries.

B (G)	dr/dt	$n(r,t) \propto$	$dn/dt \propto$
0	$-4.05 \times 10^{26} a^{-3}$	$(r^4 + 1.62 \times 10^{27} t)^{(\alpha-3)/4} r^3$	$n/r^4 \sim t^{(\alpha-3)/4}$
10^9	$-7.06 \times 10^{37} a^{-3.97}$	$(r^{4.97} + 3.5 \times 10^{38} t)^{(\alpha-3.97)/4.97} r^{3.97}$	$n/r^{4.97} \sim t^{(\alpha-3.97)/4.97}$
10^{10}	$-1.7 \times 10^{45} a^{-4.48}$	$(r^{5.48} + 1.92 \times 10^{46} t)^{(\alpha-4.48)/5.48} r^{4.48}$	$n/r^{5.48} \sim t^{(\alpha-4.48)/5.48}$

$t = t_0$ we have, as a total present-day distribution

$$N(r) = \int_0^{t0} \tau(t_0 - t) n(r,t) dt. \tag{6.18}$$

In the case of binaries which have their orbital evolution driven by gravitational wave emission, we have

$$N(r) \propto \int_0^{t_0} r^3 (r^4 + \kappa t)^{(\alpha-3)/4} dt, \quad \rightarrow N(x) \propto x^{4+\alpha} \left[(1 + x^{-4})^{(\alpha+1)/4} - 1 \right], \text{ if } \alpha \neq -1$$
$$\rightarrow N(x) \propto x^3 \ln (1 + x^{-4}), \text{ if } \alpha = -1 \tag{6.19}$$

where we considered the rate τ as a constant and $x = r/(\kappa t_0)^{1/4}$ is the normalized separation. Similar to the DTD, the present day distribution N will be affected if we consider magnetic WD-WD binaries whose orbital evolution is affected by the UIM. The present day distribution for magnetic WD-WD binaries can be obtained from (6.18) and they are showed in Fig. 6.6, where we show that the power-law shape for N is changed only for systems with small orbital separations. These results may also affect the merger rate dN/dt, but we left this for future analysis.

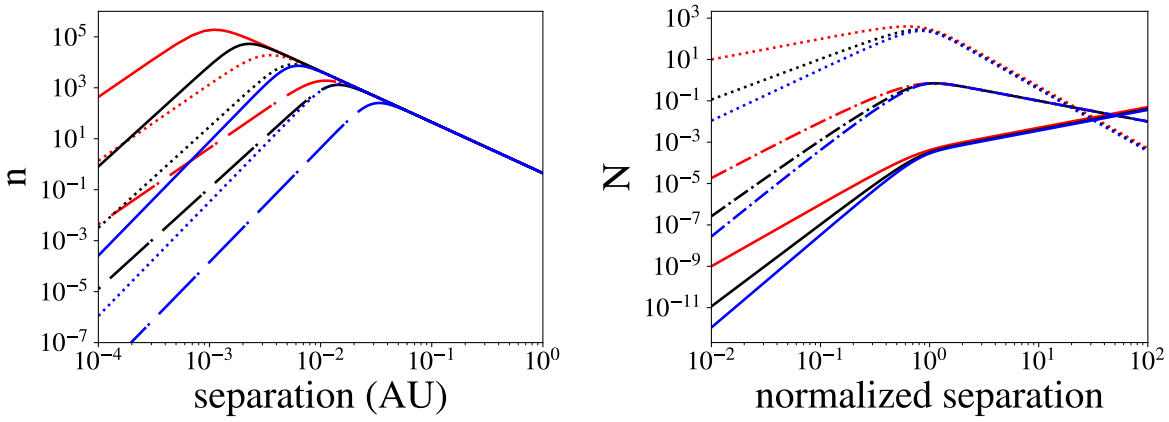

(a) Separation distibutions.

(b) Present day distributions.

FIGURE 6.6 – Left: Evolution of the separation distributions n for WD-WD binaries with an initial power-law where $\alpha = -2$. Red, black and blue lines correspond to magnetic fields of 0, 10^9G and 10^{10}G, respectively. Solid, dotted and dashed-dotted lines corresponds to a time t of 1Myr, 100Myr and 10Gyr. Right: Present day distributions N for a timescale $t_0 = 10$Gyr. Colors follow the same representation as in the left panel, solid, dashed-dotted and dotted lines now represent α equals to 1, -1 and -3, respectively.

7 Conclusions

- *General relativistic effects on white dwarfs*

  In this part of this thesis we showed that General Relativity is very important to estimate correctly the radius of a massive WD ($M > 1.3M_{\odot}$) and, consequently, to calculate the surface gravity and any other property who depends on the mass and radius of the star. We also showed that the minimum radii are very different within either Newtonian or general relativistic cases (about 200% at most).

  We demonstrate that for fixed values of total mass there is a large deviation from Newtonian WD radius to general relativistic WD radius, for example, for a mass close to the value $M = 1.42M_{\odot}$ the Newtonian radius is about 50% larger than the general relativistic one. For the most massive WD found in literature $M = 1.41 \pm 0.04$ (VENNES *et al.*, 1997) the Newtonian value of radius is 37% larger than the general relativistic one (or at least 6% for a mass of $1.37M_{\odot}$). Due to those deviations in radius the surface gravity is expected to be 55% smaller in Newtonian case in comparison with the result from GR for a fixed total mass of about $M = 1.42M_{\odot}$.

  Briefly, the GR effects produces a different correlation between surface gravity and radius, what may induce changes in the values of observational parameters. In particular, if we measured the surface gravity for a massive WD that we know the mass, the correct radius obtained by GR is going to be smaller than the one we would obtain if we do not take into account general relativity, because of the different mass-radius relation of the two cases.

  The WD structure in a general relativistic, finite temperature case was studied in (CARVALHO *et al.*, 2014), in which was showed that the finite temperature effects are more significant the less massive the star is. The deviations arising from thermal effects are negligible for stars with $M < 1.2M_{\odot}$. On the other hand the main effects of GR appears for stars with $M > 1.3M_{\odot}$, what turns both effects crucial for the determination of the WD mass-radius relation from observations.

  We also found a novel analytic mass-radius relation by fitting the general relativistic mass-radius relationship obtained numerically. We suggest that it can be useful to

calculate other properties of the stars like magnetic dipole field, moment of inertia, gravitational red-shift and so on.

- *Surface charge effects on white dwarfs*

  The static equilibrium configurations and the stellar radial stability of charged white dwarfs were investigated. Both studies were analyzed through the results derived from the hydrostatic equilibrium equation, the Tolman-Oppenheimer-Volkoff equation, modified to include the electrical part. For the interior of white dwarfs, we consider that the equation of state follows the employed for the fully degenerated electron gas (CHANDRASEKHAR, 1967; SHAPIRO; TEUKOLSKY, 1983). In addition, we assume a Gaussian distribution of charge of ~ 10 [km] thickness close the star's surface. It is important to mention that the interior solution match smoothly to the exterior Reissner-Nordström vacuum solution.

  We observe that for larger total charge, more massive stellar objects are found. For instance, the increment of the total charge from 0 to 2.058×10^{20}[C] allows to increase the total mass in approximately 55.58%, growing from $1.416\, M_{\odot}$ to $2.203\, M_{\odot}$. This increment in the mass of the star is explained since the electric charge acts as an effective pressure, thus helping the hydrodynamic pressure to support more mass against the gravitational collapse. It is worth mentioning that for the total electric charge 2.058×10^{20}[C], we found that the Schwinger limit is saturated for a white dwarf with $\sim 2.2\, M_{\odot}$. This total mass is within the interval of white dwarf considered as super-Chandrasekhar white dwarfs (TAUBENBERGER *et al.*, 2011; SILVERMAN *et al.*, 2011). From the aforementioned, we can understand that a surface distribution of charge could plays an important role in the existence of the super-Chandrasekhar white dwarfs.

  On the other hand, the stability against small radial perturbations of charged white dwarfs are analyzed using a sequence of equilibrium configurations with increasing central energy density, where these spherical objects are constituted by an equal total electric charge. In this types of sequences, the maximum mass point marks the onset of the instability, see (ARBAÑIL; MALHEIRO, 2015). From this, we can say that the regions where lay stable and unstable white dwarfs can be distinguished by the inequalities $dM/d\rho_c > 0$ and $dM/d\rho_c < 0$, respectively.

- *$f(\mathcal{R}, \mathcal{T})$ gravity effects on white dwarfs*

  In this section we investigated the effects of an extended theory of gravity, namely $f(R, T)$ gravity, in WDs, by developing the hydrostatic equilibrium analysis for such a theory. Our main goal was to check the imprints of the extra material terms - coming from the $T-$dependence of the theory - on WD properties.

The hydrostatic equilibrium configurations of WDs in alternative gravity theories others than $f(R,T)$ gravity can be seen in the recent literature. In (DAS; MUKHOPADHYAY, 2015b) the consequences of modifications in GR were deeply analyzed in the WDs perspective. A similar approach is presented in reference (DAS; MUKHOPADHYAY, 2015a). In (JAIN *et al.*, 2016) it was shown that WDs provide a unique setup to constrain Horndeski theories of gravity. In (BANERJEE *et al.*, 2017), it was explored the effects that WDs suffers when described in various modified gravity models, such as scalar-tensor-vector, Eddington inspired Born-Infeld and $f(R)$ theories of gravity. Furthermore, WDs have been used to constrain hypothetical variations on the gravitational constant (ALTHAUS *et al.*, 2011; GARCÍA-BERRO *et al.*, 2011; CÓRSICO *et al.*, 2013).

The equilibrium configurations of WDs were analyzed for $f(R,T) = R + 2\lambda T$ with different values of λ and central energy densities. We showed that the extended theory of gravity affects the maximum mass and radius of WDs depending on the value of λ. Since gravitational fields are smaller for WDs than for neutron stars or quarks stars, the scale parameter λ used here is small when compared to the values used in Ref. (MORAES *et al.*, 2016). In this way, WDs data can be used as a tool to constrain an inferior limit on λ, which is $\lambda_{min} \approx -3 \times 10^{-4}$.

The values of the parameter λ used in the present work are clearly small when compared to those of reference (MORAES *et al.*, 2016), in which the hydrostatic equilibrium configurations of neutron and quark stars were calculated in $f(R,T)$ gravity. This may be due to the fact that the compactness M/R of WDs is small when compared to those of neutron and quark stars. In fact, it can be seen in (MORAES *et al.*, 2016) that the values of λ needed to get stable quark stars are greater than the values used for neutron stars, as a probable consequence of the higher compactness of quarks stars in relation to neutron stars. In this way, these analysis indicate that higher compactness objects would need higher deviations from GR.

We found that for $\lambda = -4 \times 10^{-4}$, the maximum mass of the WD is $1.47 M_{\odot}$. This value is determined in a central energy density $\sim 85\%$ lower and radius $\sim 110\%$ greater than those values used to find the maximum mass value in the GR case ($\lambda = 0$). The outcomes for the central energy density are also smaller than those obtained in $f(R) = R + \alpha R^2$ gravity, for different values of α (DAS; MUKHOPADHYAY, 2015b).

We argue about the advantages of having WDs with lower central energy densities in the following. In (MIKHEEV; TSVETKOV, 2016) some constraints on the central density of a WD were obtained. The authors have derived a system of equations and inequalities that allows one to determine constraints on ρ_c. They have found

that $\rho_c \leq 10^9$ g/cm^3 for the star RX J0648.0-4418. Moreover, in a seminal paper by Hamada and Salpeter (HAMADA; SALPETER, 1961), it was found that for the maximum masses of WDs, $\rho_c \sim 10^9 - 10^{10}$ g/cm^3. Recently, WD calculations in GR also showed that central energy densities are limited by nuclear fusion reactions (CHAMEL *et al.*, 2013; BOSHKAYEV *et al.*, 2013; OTONIEL *et al.*, 2016). It is worth quoting that the values of the central energy densities that we have obtained for the $f(R,T)$ gravity respect these constraints. In contrast, what has been found for the central energy density of WDs in $f(R)$ gravity is $\rho_c \sim 10^{11}$ g/cm^3 (DAS; MUKHOPADHYAY, 2015b).

As a direct extension of the present work, one can also consider quadratic terms on T for the functional form of $f(R,T)$, that is, $f(R,T) = R + 2\lambda T + \xi T^2$, with ξ being a free parameter. Since the extra material terms seem to yield an increment on the mass of WDs, one may expect the presence of the quadratic term T^2 to significantly elevate the Chandrasekhar limit and predict the existence of super-Chandrasekhar WDs (HOWELL *et al.*, 2006; SCALZO *et al.*, 2010), which still require convincing physical explanation.

- *Effects of extra dimensions on white dwarfs*

  We investigate the equilibrium configurations of self-gravitating spherically symmetric fluid composed by a relativistic free Fermi gas in the framework of higher dimensional gravity. It is considered the hydrostatic equilibrium equation within General Relativity (GR) and Newtonian theories of gravitation under the presence of universal extra dimensions (UED). We generalize the equation of state (EoS) of an ideal relativistic Fermi gas in the presence of such UEDs, obtain for the first time analytic expressions for the energy density and pressure in D-dimensions, and solve the generalized D-dimensional Tolman-Oppenheimer-Volkoff stellar equilibrium equation. Interesting properties of the D-dimensional relativistic free Fermi gas such as sound velocity, and polytropic limits were also presented. In particular, we show that the adiabatic index Γ for the non-relativistic and ultra-relativistic limits of a degenerated free fermi gas in D-dimensions is related only to the space-time dimension. Thus, the sound velocity in these two cases is always constant and decreases with the increase of the spacial number of dimensions, since goes with $1/(D-1)$. We also find that there is no gravitationally stable fermion compact star solution for the D-dimensional ideal Fermi gas considering GR, when $D > 4$. Furthermore, this important result is independent of the fermion mass, and also of the gravitational constant value G_D in D dimensions. We performed an analysis of the energy conditions of the equation of state, and also considered the Newtonian limit by completeness. We found that for any number of dimensions the energy conditions are all respected, which implies that the ideal relativistic Fermi gas in D-dimensions

can be stated to be a normal matter. Concerning the Newtonian limit, we derive the generalized Lane-Emden equation, and again, we did not found stable solutions, meaning that even in a Newtonian theory of gravity it is not possible to have stable fermion compact stars constituted by an ideal Fermi gas with $D > 4$, which is in agreement with the literature. Since, the main source of the internal pressure inside white dwarfs is due to the degenerate free electron gas, this class of compact objects cannot exist in more dimensions, even in the GR theory, which is important to take into account for Super-Chandrasekhar white dwarfs, in order to obtain the correct star radius (CARVALHO *et al.*, 2018). Thus, the existence of white dwarfs in our universe is one more observational evidence that extended extra spatial dimensions do not exist, and extra dimensions must be compactified, as proposed, for instance, in brane-word gravity where the "normal" matter can only propagate in the 4-D brane.

- *Effects of unipolar inductor model on double white dwarf binaries*

  We take into account the magnetic friction between double white dwarf binaries by using the so called unipolar inductor model (UIM). We showed that the UIM may produce high energy emission, being possible to achieve the GRB powers, nevertheless when we consider the twist of the magnetic field we note that the magnetic field lines can be opened and flares due to disruption of magnetic flux tubes occurs with certain frequency, thus we consider a parameterized emission proposed in the literature yielding a much smaller electromagnetic emission. We stress that the energy released as flares due to disruption of magnetic flux tubes were not calculated here and it may also be related somehow to GRBs, and we plan to address this question in a near future. Moreover, we showed that the parameterized UIM can affect the orbital evolution for magnetic fields $B > 10^9$G, thus changing the time needed to merger. Consequently, the separation distribution, delay time distribution and possibly the merger rate are also affected. It is worth to cite that this is a work in progress, so the conclusions presented here are not definitive.

Bibliography

ABBOTT, B. P.; ABBOTT, R.; ABBOTT, T.; ACERNESE, F.; ACKLEY, K.; ADAMS, C.; ADAMS, T.; ADDESSO, P.; ADHIKARI, R.; ADYA, V. *et al.* Gw170817: observation of gravitational waves from a binary neutron star inspiral. **Physical Review Letters**, APS, v. 119, n. 16, p. 161101, 2017. 71

ABRAMOWITZ, M.; STEGUN, I. A. **Handbook of mathematical functions: with formulas, graphs, and mathematical tables**. [S.l.]: Courier Corporation, 1965. v. 55. 28

AKBARI-MOGHANJOUGHI, M. Generalized charge-screening in relativistic thomas–fermi model. **Physics of Plasmas**, AIP Publishing, v. 21, n. 10, p. 102702, 2014. 57

ALTHAUS, L. G.; CÓRSICO, A. H.; TORRES, S.; LORÉN-AGUILAR, P.; ISERN, J.; GARCÍA-BERRO, E. The evolution of white dwarfs with a varying gravitational constant. **Astronomy & Astrophysics**, EDP Sciences, v. 527, p. A72, mar 2011. ISSN 0004-6361. 82

ALVARENGA, F. G.; CRUZ-DOMBRIZ, A. de la; HOUNDJO, M. J. S.; RODRIGUES, M. E.; SÁEZ-GÓMEZ, D. Dynamics of scalar perturbations in f (R , T) gravity. **Physical Review D**, American Physical Society, v. 87, n. 10, p. 103526, may 2013. ISSN 1550-7998. 41

ANNINOS, P.; ROTHMAN, T. Instability of extremal relativistic charged spheres. **Physical Review D**, APS, v. 65, n. 2, p. 024003, 2001. 58, 59

ARBAÑIL, J. D.; LEMOS, J. P.; ZANCHIN, V. T. Incompressible relativistic spheres: Electrically charged stars, compactness bounds, and quasiblack hole configurations. **Physical Review D**, APS, v. 89, n. 10, p. 104054, 2014. 58, 59

ARBAÑIL, J. D.; MALHEIRO, M. Equilibrium and stability of charged strange quark stars. **Physical Review D**, APS, v. 92, n. 8, p. 084009, 2015. 20, 57, 58, 59, 81

ARBAÑIL, J. D. V.; LEMOS, J. P. S.; ZANCHIN, V. T. Polytropic spheres with electric charge: Compact stars, the Oppenheimer-Volkoff and Buchdahl limits, and quasiblack holes. **Physical Review D**, American Physical Society, v. 88, n. 8, p. 084023, oct 2013. ISSN 1550-7998. 20, 53

BAIKO, D. A.; YAKOVLEV, D. G. Thermal and Electric Conductivities of Coulomb Crystals in Neutron Stars and White Dwarfs. **Astronomy Letters**, v. 21, p. 702–709, apr 1995. 20

BANERJEE, S.; SHANKAR, S.; SINGH, T. P. Constraints on modified gravity models from white dwarfs. **Journal of Cosmology and Astroparticle Physics**, IOP Publishing, v. 2017, n. 10, p. 004–004, oct 2017. ISSN 1475-7516. 20, 21, 82

BARRIENTOS, J.; RUBILAR, G. F. Comment on "f(R,T) gravity". **Physical Review D**, American Physical Society, v. 90, n. 2, p. 028501, jul 2014. 41

BECHHOEFER, J.; CHABRIER, G. On the fate of stars in high spatial dimensions. **American journal of physics**, AAPT, v. 61, n. 5, p. 460–462, 1993. 30

BERA, P.; BHATTACHARYA, D. Mass-radius relation of strongly magnetized white dwarfs: nearly independent of Landau quantization. **Monthly Notices of the Royal Astronomical Society**, Oxford University Press, v. 445, n. 4, p. 3951–3958, dec 2014. ISSN 1365-2966. 43

BOSHKAYEV, K.; RUEDA, J. A.; RUFFINI, R. General Relativistic White Dwarfs and Their Astrophysical Implications. **Journal of the Korean Physical Society**, v. 65, n. 6, p. 855–860, 2014. 20

BOSHKAYEV, K.; RUEDA, J. A.; RUFFINI, R.; SIUTSOU, I. ON GENERAL RELATIVISTIC UNIFORMLY ROTATING WHITE DWARFS. **The Astrophysical Journal**, v. 762, n. 2, p. 117, jan 2013. ISSN 0004-637X. 20, 83

BRANCH, D.; TAMMANN, G. A. Type Ia Supernovae as Standard Candles. **Annual Review of Astronomy and Astrophysics**, Annual Reviews 4139 El Camino Way, P.O. Box 10139, Palo Alto, CA 94303-0139, USA, v. 30, n. 1, p. 359–389, sep 1992. ISSN 0066-4146. 19

BREEDT, E.; STEEGHS, D.; MARSH, T.; FUSILLO, N. G.; TREMBLAY, P.-E.; GREEN, M.; PASQUALE, S. D.; HERMES, J.; GÄNSICKE, B. T.; PARSONS, S. *et al.* Using large spectroscopic surveys to test the double degenerate model for type ia supernovae. **Monthly Notices of the Royal Astronomical Society**, Oxford University Press, v. 468, n. 3, p. 2910–2922, 2017. 71

CAMERON, A. G. W. **Chalk River Rep.** [S.l.]: Atomic Energy Can. ltd., 1957. 27

CARVALHO, G.; LOBATO, R.; MORAES, P.; ARBAÑIL, J. D.; OTONIEL, E.; MARINHO, R.; MALHEIRO, M. Stellar equilibrium configurations of white dwarfs in the f (r, t) gravity. **The European Physical Journal C**, Springer, v. 77, n. 12, p. 871, 2017. 20, 21

CARVALHO, G.; MARINHO, R.; MALHEIRO, M. General relativistic effects in the structure of massive white dwarfs. **General Relativity and Gravitation**, Springer, v. 50, n. 4, p. 38, 2018. xi, 43, 73, 74, 75, 84

CARVALHO, G. A.; JR, R. M. M.; MALHEIRO, M. Mass-radius relation for white dwarfs models at zero temperature. **Journal of Physics: Conference Series**, IOP Publishing, v. 706, n. 5, p. 052016, apr 2016. ISSN 1742-6588. 43, 45

CARVALHO, G. A.; JR, R. M. M.; MALHEIRO, M.; MARINHO, R.; MALHEIRO, M. Mass-Radius diagram for compact stars. **Journal of Physics: Conference Series**, IOP Publishing, v. 630, n. 1, p. 012058, jul 2015. ISSN 1742-6588. 45

CARVALHO, G. A.; Marinho Jr, R. M.; MALHEIRO, M. General Relativistic effects in the structure of massive white dwarfs. **arXiv:1709.01635 [gr-qc]**, sep 2017. 43

CARVALHO, G. A.; MARINHO, R.; MALHEIRO, M. The importance of GR for the radius of massive white dwarfs. In: **THE SECOND ICRANet CÉSAR LATTES MEETING: Supernovae, Neutron Stars and Black Holes**. [S.l.: s.n.], 2015. v. 1693, p. 030004. ISBN 9780735413405. 45

CARVALHO, G. A.; MARINHO, R. M.; MALHEIRO, M. The importance of general relativity for the radius of super-Chandrasekhar white dwarfs. In: **The Fourteenth Marcel Grossmann Meeting**. [S.l.]: WORLD SCIENTIFIC, 2017. p. 4319–4324. ISBN 978-981-322-659-3. 43, 45

CARVALHO, S. M. de; ROTONDO, M.; RUEDA, J. A.; RUFFINI, R. Relativistic Feynman-Metropolis-Teller treatment at finite temperatures. **Physical Review C - Nuclear Physics**, American Physical Society, v. 89, n. 1, p. 1–10, jan 2014. ISSN 05562813. Disponível em: <https://link.aps.org/doi/10.1103/PhysRevC.89.015801>. 22, 27, 80

CHAMEL, N.; FANTINA, A. F.; DAVIS, P. J. Stability of super-Chandrasekhar magnetic white dwarfs. **Physical Review D**, American Physical Society, v. 88, n. 8, p. 081301, oct 2013. ISSN 1550-7998. 22, 27, 83

CHANDRASEKHAR, S. The Dynamical Instability of Gaseous Masses Approaching the Schwarzschild Limit in General Relativity. **The Astrophysical Journal**, v. 140, p. 417, aug 1964. ISSN 0004-637X. 28

CHANDRASEKHAR, S. **An Introduction to the Study of Stellar Structure**. Dover: [s.n.], 1967. 528 p. 18, 43, 81

CHANDRASEKHAR, S.; MILNE, E. A. The Highly Collapsed Configurations of a Stellar Mass. **Monthly Notices of the Royal Astronomical Society**, Oxford University Press, v. 91, n. 5, p. 456–466, mar 1931. ISSN 0035-8711. 55

CHANDRASEKHAR, S.; S. The Maximum Mass of Ideal White Dwarfs. **The Astrophysical Journal**, v. 74, p. 81, jul 1931. ISSN 0004-637X. 22

CHANDRASEKHAR, S.; S. The Highly Collapsed Configurations of a Stellar Mass. (Second Paper.). **Monthly Notices of the Royal Astronomical Society**, v. 95, n. 3, p. 207–225, jan 1935. ISSN 0035-8711. 18, 55

CHANDRASEKHAR, S.; TOOPER, R. F. The dynamical instability of the white-dwarf configurations approaching the limiting mass. **The Astrophysical Journal**, v. 139, p. 1396, 1964. 43

CHAVANIS, P.-H. White dwarf stars in d dimensions. **Physical Review D**, APS, v. 76, n. 2, p. 023004, 2007. 61, 64

COELHO, J. G.; MALHEIRO, M. Magnetic dipole moment of soft gamma-ray repeaters and anomalous X-ray pulsars described as massive and magnetic white dwarfs. **Publications of the Astronomical Society of Japan**, v. 66, n. 1, p. 14–14, feb 2014. ISSN 0004-6264. 19

CÓRSICO, A. H.; ALTHAUS, L. G.; GARCÍA-BERRO, E.; ROMERO, A. D. An independent constraint on the secular rate of variation of the gravitational constant from pulsating white dwarfs. **Journal of Cosmology and Astroparticle Physics**, IOP Publishing, v. 2013, n. 06, p. 032–032, jun 2013. ISSN 1475-7516. 82

DALL'OSSO, S.; ISRAEL, G. L.; STELLA, L. Astrophysical unipolar inductors powered by gw emission. **Astronomy & Astrophysics**, EDP Sciences, v. 447, n. 3, p. 785–796, 2006. 72

DAS, A.; RAHAMAN, F.; GUHA, B. K.; RAY, S. Compact stars in f (R , T) gravity. **The European Physical Journal C**, Springer Berlin Heidelberg, v. 76, n. 12, p. 654, dec 2016. ISSN 1434-6044. 65

DAS, U.; MUKHOPADHYAY, B. New mass limit for white dwarfs: Super-Chandrasekhar type Ia supernova as a new standard candle. **Physical Review Letters**, v. 110, n. February, p. 1–4, 2013. ISSN 00319007. 19, 20

DAS, U.; MUKHOPADHYAY, B. Maximum mass of stable magnetized highly super-Chandrasekhar white dwarfs: stable solutions with varying magnetic fields. **Journal of Cosmology and Astroparticle Physics**, v. 2014, n. 06, p. 050–050, 2014. ISSN 1475-7516. 19, 20

DAS, U.; MUKHOPADHYAY, B. Imprint of modified Einstein's gravity on white dwarfs: Unifying Type Ia supernovae. **International Journal of Modern Physics D**, World Scientific Publishing Company, v. 24, n. 12, p. 1544026, oct 2015. ISSN 0218-2718. 20, 21, 82

DAS, U.; MUKHOPADHYAY, B. Modified Einstein's gravity as a possible missing link between sub- and super-Chandrasekhar type Ia supernovae. **Journal of Cosmology and Astroparticle Physics**, v. 2015, n. 05, p. 045–045, may 2015. ISSN 1475-7516. 20, 21, 69, 82, 83

DEB, D.; GUHA, B.; RAHAMAN, F.; RAY, S. Anisotropic strange stars under simplest minimal matter-geometry coupling in the f (r,t) gravity. **Physical Review D**, APS, v. 97, n. 8, p. 084026, 2018. 65

DEB, D.; KETOV, S. V.; KHLOPOV, M.; RAY, S. Study on charged strange stars in f(r,t) gravity. **arXiv preprint arXiv:1812.11736**, 2018. 65

DEB, D.; KETOV, S. V.; MAURYA, S.; KHLOPOV, M.; MORAES, P.; RAY, S. Exploring physical features of anisotropic strange stars beyond standard maximum mass limit in f(r,t) gravity. **arXiv preprint arXiv:1810.07678**, 2018. 65

DEB, D.; RAHAMAN, F.; RAY, S.; GUHA, B. Strange stars in f (r, t) gravity. **Journal of Cosmology and Astroparticle Physics**, IOP Publishing, v. 2018, n. 03, p. 044, 2018. 65

Del Popolo, A.; Le Delliou, M. Small Scale Problems of the ΛCDM Model: A Short Review. **Galaxies**, Multidisciplinary Digital Publishing Institute, v. 5, n. 1, p. 17, feb 2017. ISSN 2075-4434. 19

DENG, X.-M.; XIE, Y. Solar system's bounds on the extra acceleration of f(r,t) gravity revisited. **International Journal of Theoretical Physics**, Springer, v. 54, n. 6, p. 1739–1749, 2015. 65

D'INVERNO, R. **Introducing Einstein's relativity**. [S.l.]: Clarendon Press, 1992. 383 p. ISBN 0198596863. 32, 35, 36

FELICE, F. de; SIMING, L.; YUNQIANG, Y. Relativistic charged spheres: Ii. regularity and stability. **Classical and Quantum Gravity**, IOP Publishing, v. 16, n. 8, p. 2669, 1999. 58, 59

FELICE, F. de; YU, Y.; FANG, J. Relativistic charged spheres. **Monthly Notices of the Royal Astronomical Society**, Oxford University Press Oxford, UK, v. 277, n. 1, p. L17–L19, 1995. 58, 59

FOWLER, R. H. On Dense Matter. **Monthly Notices of the Royal Astronomical Society**, Oxford University Press, v. 87, n. 2, p. 114–122, dec 1926. ISSN 0035-8711. 22

FRANZON, B.; SCHRAMM, S. Effects of strong magnetic fields and rotation on white dwarf structure. **Physical Review D**, American Physical Society, v. 92, n. 8, p. 083006, oct 2015. ISSN 1550-7998. 19, 20

FRENKEL, Y. I. No Title. **Zeit. fur Phys.**, v. 50, p. 234, 1928. 26

FRIEDMAN, J. L.; IPSER, J. R.; SORKIN, R. D. Turning-point method for axisymmetric stability of rotating relativistic stars. **The Astrophysical Journal**, v. 325, p. 722–724, 1988. 58

FRIEMAN, J. A.; TURNER, M. S.; HUTERER, D. Dark Energy and the Accelerating Universe. **Annual Review of Astronomy and Astrophysics**, Annual Reviews, v. 46, n. 1, p. 385–432, sep 2008. ISSN 0066-4146. 19

GARCÍA-BERRO, E.; LORÉN-AGUILAR, P.; TORRES, S.; ALTHAUS, L. G.; ISERN, J. An upper limit to the secular variation of the gravitational constant from white dwarf stars. **Journal of Cosmology and Astroparticle Physics**, IOP Publishing, v. 2011, n. 05, p. 021–021, may 2011. ISSN 1475-7516. 82

GHOSH, S.; RAHAMAN, F.; GUHA, B.; RAY, S. Charged gravastars in higher dimensions. **Physics Letters B**, Elsevier, v. 767, p. 380–385, 2017. 29

GLENDENNING, N. K. Compact Stars. Springer, p. 475, 2000. 24, 26

HAMADA, T.; SALPETER, E. E. Models for Zero-Temperature Stars. **The Astrophysical Journal**, v. 134, p. 683, 1961. ISSN 0004-637X. 22, 83

HARKO, T. Oppenheimer-volkoff equation ind space-time dimensions. **Acta Physica Hungarica**, Springer, v. 72, n. 2-4, p. 253–258, 1992. 38, 39

HARKO, T.; LOBO, F. S. N.; NOJIRI, S.; ODINTSOV, S. D. f (R , T) gravity. **Physical Review D**, American Physical Society, v. 84, n. 2, p. 024020, jul 2011. ISSN 1550-7998. 40

HERRERA, L. The weyl tensor and equilibrium configurations of self-gravitating fluids. **General Relativity and Gravitation**, Springer, v. 35, n. 3, p. 437–448, 2003. 43

HICKEN, M.; GARNAVICH, P. M.; PRIETO, J. L.; BLONDIN, S.; DEPOY, D. L.; KIRSHNER, R. P.; PARRENT, J. The luminous and carbon-rich supernova 2006gz: A double degenerate merger? **The Astrophysical Journal**, v. 669, n. 1, p. L17–L20, nov 2007. ISSN 0004-637X. 19

HILLEBRANDT, W.; NIEMEYER, J. C. Type Ia Supernova Explosion Models. **Annual Review of Astronomy and Astrophysics**, Annual Reviews 4139 El Camino Way, P.O. Box 10139, Palo Alto, CA 94303-0139, USA, v. 38, n. 1, p. 191–230, sep 2000. ISSN 0066-4146. 18

HOWELL, D. A.; SULLIVAN, M.; NUGENT, P. E.; ELLIS, R. S.; CONLEY, A. J.; Le Borgne, D.; CARLBERG, R. G.; GUY, J.; BALAM, D.; BASA, S.; FOUCHEZ, D.; HOOK, I. M.; HSIAO, E. Y.; NEILL, J. D.; PAIN, R.; PERRETT, K. M.; PRITCHET, C. J. The type Ia supernova SNLS-03D3bb from a super-Chandrasekhar-mass white dwarf star. **Nature**, v. 443, n. 7109, p. 308–311, sep 2006. ISSN 1476-4687. 19, 83

JAIN, R. K.; KOUVARIS, C.; NIELSEN, N. G. White Dwarf Critical Tests for Modified Gravity. **Physical Review Letters**, American Physical Society, v. 116, n. 15, p. 151103, apr 2016. ISSN 0031-9007. 20, 21, 82

JI, P.; QU, S.; BAI, Y. Modified surface redshift of pulsars produced by magnetoplasma. **General Relativity and Gravitation**, Springer, v. 40, n. 1, p. 131–138, 2008. 50

JING, Z.; WEN, D.; ZHANG, X. Electrically charged: An effective mechanism for soft EOS supporting massive neutron star. **Science China Physics, Mechanics & Astronomy**, Science China Press, v. 58, n. 10, p. 109501, oct 2015. ISSN 1674-7348. 20, 54

JING, Z.-Z.; WEN, D.-H. A New Solution in Understanding Massive White Dwarfs. **Chinese Physics Letters**, IOP Publishing, v. 33, n. 5, p. 050401, may 2016. ISSN 0256-307X. 20, 21

KAPLAN, D. L.; MARSH, T. R.; WALKER, A. N.; BILDSTEN, L.; BOURS, M. C.; BREEDT, E.; COPPERWHEAT, C. M.; DHILLON, V. S.; HOWELL, S. B.; LITTLEFAIR, S. P. *et al.* Properties of an eclipsing double white dwarf binary nltt 11748. **The Astrophysical Journal**, IOP Publishing, v. 780, n. 2, p. 167, 2013. 71

KEPLER, S. O.; ROMERO, A. D.; PELISOLI, I.; OURIQUE, G. White Dwarf Stars. **International Journal of Modern Physics: Conference Series**, v. 45, p. 1760023, jan 2017. ISSN 2010-1945. 18, 19

KLEINMAN, S. J.; KEPLER, S. O.; KOESTER, D.; PELISOLI, I.; PEÇANHA, V.; NITTA, A.; COSTA, J. E. S.; KRZESINSKI, J.; DUFOUR, P.; LACHAPELLE, F. R.; BERGERON, P.; YIP, C.-W.; HARRIS, H. C.; EISENSTEIN, D. J.; ALTHAUS, L.; CÓRSICO, A. SDSS DR7 White Dwarf Catalog. **The Astrophysical Journal Supplement Series**, IOP Publishing, v. 204, n. 1, p. 5, 2013. ISSN 0067-0049. 18, 19

KNUTSEN, H. On the instability of an isentropic model for a gaseous relativistic star. **General Relativity and Gravitation**, Springer, v. 20, n. 4, p. 317–325, 1988. 43

KREMER, K.; BREIVIK, K.; LARSON, S. L.; KALOGERA, V. Accreting double white dwarf binaries: Implications for lisa. **The Astrophysical Journal**, IOP Publishing, v. 846, n. 2, p. 95, 2017. 71

KRORI, K.; BORGOHAIN, P.; DAS, K. Interior schwarzschild-like solution in higher dimensions. **Physics Letters A**, v. 132, p. 321–323, 1988. 38

KULKARNI, S.; KERKWIJK, M. V. The (double) white dwarf binary sdss 1257+ 5428. **The Astrophysical Journal**, IOP Publishing, v. 719, n. 2, p. 1123, 2010. 71

LAI, D. Dc circuit powered by orbital motion: magnetic interactions in compact object binaries and exoplanetary systems. **The Astrophysical Journal Letters**, IOP Publishing, v. 757, n. 1, p. L3, 2012. 73, 74

LEMOS, J. P.; ZANCHIN, V. T. Bonnor stars in d spacetime dimensions. **Physical Review D**, APS, v. 77, n. 6, p. 064003, 2008. 38

LIEBERT, J. White Dwarf Stars. **Annual Review of Astronomy and Astrophysics**, v. 18, n. 1, p. 363–398, 1980. ISSN 0066-4146. 26

LIU, H.; ZHANG, X.; WEN, D. One possible solution of peculiar type ia supernovae explosions caused by a charged white dwarf. **Physical Review D**, American Physical Society, v. 89, n. 10, p. 104043, may 2014. ISSN 1550-7998. 20, 53, 59

Lobato, R. V.; Carvalho, G. A.; Martins, A. G.; Moraes, P. H. R. S. Energy nonconservation as a link between $f(R,T)$ gravity and noncommutative quantum theory. **arXiv e-prints**, p. arXiv:1803.08630, Mar 2018. 40

LOBATO, R. V.; COELHO, J.; MALHEIRO, M. Particle acceleration and radio emission for SGRs/AXPs as white dwarf pulsars. **Journal of Physics: Conference Series**, v. 630, n. 1, p. 012015, 2015. ISSN 1742-6596. 19

LYUTIKOV, M. Electrodynamics of double neutron star mergers. **arXiv preprint arXiv:1809.10478**, 2018. 71

MADSEN, J. Universal Charge-Radius Relation for Subatomic and Astrophysical Compact Objects. **Physical Review Letters**, American Physical Society, v. 100, n. 15, p. 151102, apr 2008. ISSN 0031-9007. 53, 59

MALHEIRO, M.; FIOLHAIS, M.; TAURINES, A. Metastable strange matter and compact quark stars. **Journal of Physics G: Nuclear and Particle Physics**, IOP Publishing, v. 29, n. 6, p. 1045, 2003. 67

MALHEIRO, M.; NEGREIROS, R. P.; WEBER, F.; USOV, V. The effects of charge on the structure of strange stars. In: IOP PUBLISHING. **Journal of Physics: Conference Series**. [S.l.], 2011. v. 312, n. 4, p. 042018. 57, 59

MALHEIRO, M.; RUEDA, J. A.; RUFFINI, R. SGRs and AXPs as rotation powered massive white dwarfs. **arXiv:1102.0653 [astro-ph.SR]**, feb 2011. 19

MAOZ, D.; BADENES, C.; BICKERTON, S. J. Characterizing the galactic white dwarf binary population with sparsely sampled radial velocity data. **The Astrophysical Journal**, IOP Publishing, v. 751, n. 2, p. 143, 2012. 77

MAOZ, D.; MANNUCCI, F. Type-ia supernova rates and the progenitor problem: a review. **Publications of the Astronomical Society of Australia**, Cambridge University Press, v. 29, n. 4, p. 447–465, 2012. 76, 77

MIKHEEV, S. A.; TSVETKOV, V. P. Constraints on the central density and chemical composition of the white dwarf RX J0648.0-4418 with a record period of rotation in a model with the equation of state of an ideal degenerate electron gas. **Physics of Particles and Nuclei Letters**, Pleiades Publishing, v. 13, n. 4, p. 442–450, jul 2016. ISSN 1547-4771. 82

MORAES, P. Cosmology from induced matter model applied to 5d f(r,t) theory. **Astrophysics and Space Science**, Springer, v. 352, n. 1, p. 273–279, 2014. 41

MORAES, P. Cosmological solutions from induced matter model applied to 5d gravity and the shrinking of the extra coordinate. **The European Physical Journal C**, Springer, v. 75, n. 4, p. 168, 2015. 41

Moraes, P.; Arbañil, J. D. V.; Carvalho, G.; Lobato, R.; Otoniel, E.; Marinho R.M., J.; Malheiro, M. Compact Astrophysical Objects in f(R,T) gravity. **arXiv e-prints**, p. arXiv:1806.04123, Jun 2018. 65

MORAES, P.; ARBANIL, J. D.; MALHEIRO, M. Stellar equilibrium configurations of compact stars in f (R , T) theory of gravity. **Journal of Cosmology and Astroparticle Physics**, IOP Publishing, v. 2016, n. 06, p. 005–005, jun 2016. ISSN 1475-7516. 41, 65, 67, 82

MORAES, P. H. R. S.; SAHOO, P. K. The simplest non-minimal matter-geometry coupling in the f(R, T) cosmology. **The European Physical Journal C**, Springer Berlin Heidelberg, v. 77, n. 7, p. 480, jul 2017. ISSN 1434-6044. 65

MORAES, P. H. R. S.; SANTOS, J. R. L. A complete cosmological scenario from f (R , T) gravity theory. **The European Physical Journal C**, Springer Berlin Heidelberg, v. 76, n. 2, p. 60, feb 2016. ISSN 1434-6044. 41, 65

NALEŻYTY, M.; MADEJ, J.; NALEZYTY, M.; MADEJ, J. A catalogue of isolated massive white dwarfs. **Astronomy & Astrophysics**, EDP Sciences, v. 420, n. 2, p. 507–513, jun 2004. ISSN 0004-6361. xi, 66, 67

NEGREIROS, R. P.; WEBER, F.; MALHEIRO, M.; USOV, V. Electrically charged strange quark stars. **Physical Review D**, American Physical Society, v. 80, n. 8, p. 083006, oct 2009. ISSN 1550-7998. 20, 53, 54, 57, 59

NELEMANS, G.; NAPIWOTZKI, R.; KARL, C.; MARSH, T.; VOSS, B.; ROELOFS, G.; IZZARD, R.; MONTGOMERY, M.; REERINK, T.; CHRISTLIEB, N. *et al.* Binaries discovered by the spy project-iv. five single-lined da double white dwarfs. **Astronomy & Astrophysics**, EDP Sciences, v. 440, n. 3, p. 1087–1095, 2005. 71

NELEMANS, G.; YUNGELSON, L. R.; ZWART, S. P.; VERBUNT, F. Population synthesis for double white dwarfs-i. close detached systems. **Astronomy & Astrophysics**, EDP Sciences, v. 365, n. 3, p. 491–507, 2001. 71

NOJIRI, S.; ODINTSOV, S. Unified cosmic history in modified gravity: From F(R) theory to Lorentz non-invariant models. **Physics Reports**, North-Holland, v. 505, n. 2-4, p. 59–144, aug 2011. ISSN 0370-1573. 40

NOUREEN, I.; ZUBAIR, M. Dynamical instability and expansion-free condition in f (R,T) gravity. **The European Physical Journal C**, Springer Berlin Heidelberg, v. 75, n. 2, p. 62, feb 2015. ISSN 1434-6044. 65

NOUREEN, I.; ZUBAIR, M. On dynamical instability of spherical star in f(R,T) gravity. **Astrophysics and Space Science**, Springer Netherlands, v. 356, n. 1, p. 103–110, mar 2015. ISSN 0004-640X. 65

NOUREEN, I.; ZUBAIR, M.; BHATTI, A. A.; ABBAS, G. Shear-free condition and dynamical instability in f(R,T) gravity. **The European Physical Journal C**, Springer Berlin Heidelberg, v. 75, n. 7, p. 323, jul 2015. ISSN 1434-6044. 65

OPPENHEIMER, J. R.; VOLKOFF, G. M. On Massive Neutron Cores. **Physical Review**, v. 55, n. 4, p. 374–381, feb 1939. ISSN 0031-899X. 35, 42

OSTRIKER, J. P.; BODENHEIMER, P. Rapidly rotating stars. ii. massive white dwarfs. **The Astrophysical Journal**, v. 151, p. 1089, mar 1968. ISSN 0004-637X. 20

OTONIEL, E.; FRANZON, B.; MALHEIRO, M.; SCHRAMM, S.; WEBER, F. Very Magnetized White Dwarfs with Axisymmetric Magnetic Field and the Importance of the Electron Capture and Pycnonuclear Fusion Reactions for their Stability. **arxiv**, sep 2016. 27, 83

PATHRIA, R. K. **Statistical Mechanics**. Segunda ed. Oxford: [s.n.], 1996. 540 p. 23

PENROSE, R. "golden oldie": Gravitational collapse: The role of general relativity. **General Relativity and Gravitation**, Springer, v. 34, n. 7, p. 1141–1165, 2002. 43

PERLMUTTER, S.; ALDERING, G.; GOLDHABER, G.; KNOP, R. A.; NUGENT, P.; CASTRO, P. G.; DEUSTUA, S.; FABBRO, S.; GOOBAR, A.; GROOM, D. E.; HOOK, I. M.; KIM, A. G.; KIM, M. Y.; LEE, J. C.; NUNES, N. J.; PAIN, R.; PENNYPACKER, C. R.; QUIMBY, R.; LIDMAN, C.; ELLIS, R. S.; IRWIN, M.; MCMAHON, R. G.; RUIZ-LAPUENTE, P.; WALTON, N.; SCHAEFER, B.; BOYLE, B. J.; FILIPPENKO, A. V.; MATHESON, T.; FRUCHTER, A. S.; PANAGIA, N.; NEWBERG, H. J. M.; COUCH, W. J.; PROJECT, T. S. C. Measurements of and from 42 High-Redshift Supernovae. **The Astrophysical Journal**, IOP Publishing, v. 517, n. 2, p. 565–586, jun 1999. ISSN 0004-637X. 19

R. ADLER, M. B. M. S. **Introduction to General Relativity**. Segunda ed. Tokio: [s.n.], 1975. 566 p. 50

RAY, S.; ESPINDOLA, A. L.; MALHEIRO, M.; LEMOS, J. P.; ZANCHIN, V. T. Electrically charged compact stars and formation of charged black holes. **Physical Review D**, APS, v. 68, n. 8, p. 084004, 2003. 20, 53, 58

RIESS, A. G.; FILIPPENKO, A. V.; CHALLIS, P.; CLOCCHIATTIA, A.; DIERCKS, A.; GARNAVICH, P. M.; GILLILAND, R. L.; HOGAN, C. J.; JHA, S.; KIRSHNER, R. P.; LEIBUNDGUT, B.; PHILLIPS, M. M.; REISS, D.; SCHMIDT, B. P.; SCHOMMER, R. A.; SMITH, R. C.; SPYROMILIO, J.; STUBBS, C.; SUNTZEFF, N. B.; TONRY, J. Observational Evidence from Supernovae for an Accelerating Universe and a Cosmological Constant. **The Astronomical Journal, Volume 116, Issue 3, pp. 1009-1038.**, v. 116, p. 1009–1038, may 1998. ISSN 0004-6256. 19

RUEDA, J.; RUFFINI, R.; WANG, Y.; BIANCO, C.; BLANCO-IGLESIAS, J.; KARLICA, M.; LORÉN-AGUILAR, P.; MORADI, R.; SAHAKYAN, N. Electromagnetic emission of white dwarf binary mergers. **arXiv:1807.07905**, 2018. 71

SALPETER, E. E.; E., E. Energy and Pressure of a Zero-Temperature Plasma. **The Astrophysical Journal**, v. 134, p. 669, nov 1961. ISSN 0004-637X. 22, 27

SCALZO, R. A.; ALDERING, G.; ANTILOGUS, P.; ARAGON, C.; BAILEY, S.; BALTAY, C.; BONGARD, S.; BUTON, C.; CHILDRESS, M.; CHOTARD, N.; COPIN, Y.; FAKHOURI, H. K.; GAL-YAM, A.; GANGLER, E.; HOYER, S.; KASLIWAL, M.; LOKEN, S.; NUGENT, P.; PAIN, R.; PÉCONTAL, E.; PEREIRA, R.; PERLMUTTER, S.; RABINOWITZ, D.; RAU, A.; RIGAUDIER, G.; RUNGE, K.; SMADJA, G.; TAO, C.; THOMAS, R. C.; WEAVER, B.; WU, C. NEARBY SUPERNOVA FACTORY OBSERVATIONS OF SN 2007if: FIRST TOTAL MASS MEASUREMENT OF A SUPER-CHANDRASEKHAR-MASS PROGENITOR. **The Astrophysical Journal**, IOP Publishing, v. 713, n. 2, p. 1073–1094, apr 2010. ISSN 0004-637X. 19, 83

SHABANI, H.; FARHOUDI, M. Cosmological and solar system consequences of f (R , T) gravity models. **Physical Review D**, American Physical Society, v. 90, n. 4, p. 044031, aug 2014. ISSN 1550-7998. 65

SHAMIR, M. F. Locally rotationally symmetric Bianchi type I cosmology in f(R, T) gravity. **The European Physical Journal C**, Springer Berlin Heidelberg, v. 75, n. 8, p. 354, aug 2015. ISSN 1434-6044. 41

SHAPIRO, S. L.; TEUKOLSKY, S. A. **Black Holes, White Dwarfs, and Neutron Stars**. Weinheim, Germany: WILEY-VCH, 1983. 629 p. ISBN 0471873160. 18, 26, 27, 81

SHARIF, M.; WASEEM, A. Anisotropic quark stars in f (r, t) gravity. **The European Physical Journal C**, Springer, v. 78, n. 10, p. 868, 2018. 65

SHARIF, M.; YOUSAF, Z. Dynamical analysis of self-gravitating stars in f(R,T) gravity. **Astrophysics and Space Science**, Springer Netherlands, v. 354, n. 2, p. 471–479, dec 2014. ISSN 0004-640X. 65

SHARIF, M.; ZUBAIR, M. Thermodynamics in f (R , T) theory of gravity. **Journal of Cosmology and Astroparticle Physics**, IOP Publishing, v. 2012, n. 03, p. 028–028, mar 2012. ISSN 1475-7516. 65

SILVERMAN, J. M.; GANESHALINGAM, M.; LI, W.; FILIPPENKO, A. V.; MILLER, A. A.; POZNANSKI, D. Fourteen months of observations of the possible super-chandrasekhar mass type ia supernova 2009dc. **Monthly Notices of the Royal Astronomical Society**, Oxford University Press, v. 410, n. 1, p. 585–611, jan 2011. ISSN 00358711. 19, 54, 81

SUNZU, J. M.; MAHARAJ, S. D.; RAY, S. Quark star model with charged anisotropic matter. **Astrophysics and Space Science**, v. 354, n. 2, p. 517–524, dec 2014. ISSN 0004-640X. 53

TAKAMI, K.; REZZOLLA, L.; YOSHIDA, S. A quasi-radial stability criterion for rotating relativistic stars. **Monthly Notices of the Royal Astronomical Society: Letters**, The Royal Astronomical Society, v. 416, n. 1, p. L1–L5, 2011. 58

TANAKA, M.; KAWABATA, K. S.; YAMANAKA, M.; MAEDA, K.; HATTORI, T.; AOKI, K.; NOMOTO, K.; IYE, M.; SASAKI, T.; MAZZALI, P. A.; PIAN, E. SPECTROPOLARIMETRY OF EXTREMELY LUMINOUS TYPE Ia SUPERNOVA 2009dc: NEARLY SPHERICAL EXPLOSION OF SUPER-CHANDRASEKHAR MASS WHITE DWARF. **The Astrophysical Journal**, IOP Publishing, v. 714, n. 2, p. 1209–1216, may 2010. ISSN 0004-637X. 19

TAUBENBERGER, S.; BENETTI, S.; CHILDRESS, M.; PAKMOR, R.; HACHINGER, S.; MAZZALI, P. A.; STANISHEV, V.; ELIAS-ROSA, N.; AGNOLETTO, I.; BUFANO, F.; ERGON, M.; HARUTYUNYAN, A.; INSERRA, C.; KANKARE, E.; KROMER, M.; NAVASARDYAN, H.; NICOLAS, J.; PASTORELLO, A.; PROSPERI, E.; SALGADO, F.; SOLLERMAN, J.; STRITZINGER, M.; TURATTO, M.; VALENTI, S.; HILLEBRANDT, W. High luminosity, slow ejecta and persistent carbon lines: SN 2009dc challenges thermonuclear explosion scenarios. **Monthly Notices of the Royal Astronomical Society**, Oxford University Press, v. 412, n. 4, p. 2735–2762, apr 2011. ISSN 00358711. 19, 54, 81

TOLMAN, R. C. Static solutions of einstein's field equations for spheres of fluid. **Physical Review**, v. 55, n. 4, p. 364–373, feb 1939. ISSN 0031-899X. 35, 42

VELTEN, H.; CARAMÊS, T. R. Cosmological inviability of f (r, t) gravity. **Physical Review D**, APS, v. 95, n. 12, p. 123536, 2017. 67

VENNES, S.; THEJLL, P. A.; Genova Galvan, R.; DUPUIS, J. Hot White Dwarfs in the Extreme Ultraviolet Explorer Survey. II. Mass Distribution, Space Density, and Population Age. **The Astrophysical Journal**, IOP Publishing, v. 480, n. 2, p. 714–734, may 1997. ISSN 0004-637X. ix, x, xi, 19, 44, 45, 49, 51, 66, 67, 80

WANG, L.; WHEELER, J. C. Spectropolarimetry of Supernovae. **Annual Review of Astronomy and Astrophysics**, v. 46, n. 1, p. 433–474, sep 2008. ISSN 0066-4146. 18

WEN, D.-H.; LIU, H.-L.; ZHANG, X.-D. The mass limit of white dwarfs with strong magnetic fields in general relativity. **Chinese Physics B**, IOP Publishing, v. 23, n. 8, p. 089501, aug 2014. ISSN 1674-1056. 43

WOLF, C. The binding energy of a schwarzschild sphere in d space-time dimensions. **Astronomische Nachrichten**, Wiley Online Library, v. 312, n. 5, p. 299–306, 1991. 38, 39

WOOSLEY, S. E.; HEGER, A. THE REMARKABLE DEATHS OF 9-11 SOLAR MASS STARS. **The Astrophysical Journal**, IOP Publishing, v. 810, n. 1, p. 34, aug 2015. ISSN 1538-4357. 18

WU, K.; CROPPER, M.; RAMSAY, G.; SEKIGUCHI, K. An electrically powered binary star? **Monthly Notices of the Royal Astronomical Society**, Blackwell Science, Ltd Oxford, UK, v. 331, n. 1, p. 221–227, 2002. xi, 72, 73, 74, 75

YAKOVLEV, D. G.; URPIN, V. A. Astronomy reports. **Soviet Astronomy, Vol. 24, P. 303, 1980**, American Institute of Physics, v. 24, p. 303, 1993. ISSN 0038-5301. 20

YAMANAKA, M.; KAWABATA, K. S.; KINUGASA, K.; TANAKA, M.; IMADA, A.; MAEDA, K.; NOMOTO, K.; ARAI, A.; CHIYONOBU, S.; FUKAZAWA, Y.; HASHIMOTO, O.; HONDA, S.; IKEJIRI, Y.; ITOH, R.; KAMATA, Y.; KAWAI, N.; KOMATSU, T.; KONISHI, K.; KURODA, D.; MIYAMOTO, H.; MIYAZAKI, S.; NAGAE, O.; NAKAYA, H.; OHSUGI, T.; OMODAKA, T.; SAKAI, N.; SASADA, M.; SUZUKI, M.; TAGUCHI, H.; TAKAHASHI, H.; TANAKA, H.; UEMURA, M.; YAMASHITA, T.; YANAGISAWA, K.; YOSHIDA, M. EARLY PHASE OBSERVATIONS OF EXTREMELY LUMINOUS TYPE Ia SUPERNOVA 2009dc. **The Astrophysical Journal**, IOP Publishing, v. 707, n. 2, p. L118–L122, dec 2009. ISSN 0004-637X. 19

ZAREGONBADI, R.; FARHOUDI, M.; RIAZI, N. Dark matter from f (R , T) gravity. **Physical Review D**, American Physical Society, v. 94, n. 8, p. 084052, oct 2016. ISSN 2470-0010. 65

ZUBAIR, M.; NOUREEN, I. Evolution of axially symmetric anisotropic sources in f(R,T) gravity. **The European Physical Journal C**, Springer Berlin Heidelberg, v. 75, n. 6, p. 265, jun 2015. ISSN 1434-6044. 65

ZWIEBACH, B. **A first course in string theory**. [S.l.]: Cambridge University Press, 2009. 673 p. ISBN 9780521880329. 40

Appendix A - Some derivations and important mathematical identities

Using the definition of the energy-momentum tensor one find for its covariant derivative

$$\begin{aligned}\nabla^{\mu}T_{\mu\nu} &= \nabla^{\mu}(-pg_{\mu\nu}) + \nabla^{\mu}[(p+\rho)u_{\mu}u_{\nu}] && \text{(A.1)}\\ &= -\nabla_{\nu}p + g^{\alpha\mu}\nabla_{\alpha}[(p+\rho)u_{\mu}u_{\nu}] && \text{(A.2)}\\ &= -\nabla_{\nu}p + g^{\alpha\mu}\partial_{\alpha}[(p+\rho)u_{\mu}u_{\nu}] - g^{\alpha\mu}(p+\rho)[\Gamma^{\beta}_{\mu\alpha}u_{\beta}u_{\nu} + \Gamma^{\beta}_{\nu\alpha}u_{\beta}u_{\mu}], && \text{(A.3)}\end{aligned}$$

however, for the static case $u_{\mu} = \{\sqrt{g_{00}}, 0, 0, 0\}$, and using $\nu = 1$, we have

$$-\partial_1 p - g^{00}(p+\rho)\Gamma^{0}_{10}(u_0)^2 = 0 \quad \text{(A.4)}$$

$$-p' - g^{00}(p+\rho)\frac{\phi'}{2}\frac{1}{g^{00}} = 0 \quad \text{(A.5)}$$

$$-p' - (p+\rho)e\frac{\phi'}{2} = 0. \quad \text{(A.6)}$$

To derive the field equations for the $f(\mathcal{R},\mathcal{T})$ gravity we follow the same procedure such as in chapter 3, i.e., we take the variation of the action with respect to the metric $g_{\mu\nu}$. To perform the derivation of the field equations of the $f(\mathcal{R},\mathcal{T})$ gravity we need to consider the action

$$s = \int\left(\frac{f(\mathcal{R},\mathcal{T})}{16\pi}\sqrt{-g} + \sqrt{-g}L_m\right)d^4x. \quad \text{(A.7)}$$

Taking the variation of (A.7), we obtain

$$\delta s = \frac{1}{16\pi}\int\left[f_{\mathcal{R}}\delta R + f_{\mathcal{T}}\frac{\delta T}{\delta g^{\mu\nu}}\delta g^{\mu\nu} - \frac{1}{2}g_{\mu\nu}f(\mathcal{R},\mathcal{T})\delta g^{\mu\nu} + \frac{16\pi}{\sqrt{-g}}\frac{\delta(\sqrt{-g}L_m)}{\delta g^{\mu\nu}}\delta g^{\mu\nu}\right]\sqrt{-g}d^4x, \quad \text{(A.8)}$$

where we have used the notation $f_{\mathcal{R}} = \frac{\partial f(\mathcal{R},\mathcal{T})}{\partial\mathcal{R}}$ and $f_{\mathcal{T}} = \frac{\partial f(\mathcal{R},\mathcal{T})}{\partial\mathcal{T}}$. Now, knowing that

$$\delta\mathcal{R} = R_{\mu\nu}\delta g^{\mu\nu} + g_{\mu\nu}\Box\delta g^{\mu\nu} - \nabla_{\mu}\nabla_{\nu}\delta g^{\mu\nu}, \quad \text{(A.9)}$$

we obtain,

$$\delta s = \frac{1}{16\pi}\int\Bigg[f_{\mathcal{R}}(R_{\mu\nu}\delta g^{\mu\nu} + g_{\mu\nu}\Box\delta g^{\mu\nu} - \nabla_\mu\nabla_\nu\delta g^{\mu\nu}) + f_{\mathcal{T}}\frac{\delta(g^{\alpha\beta}T_{\alpha\beta})}{\delta g^{\mu\nu}}\delta g^{\mu\nu} - \frac{1}{2}g_{\mu\nu}f(\mathcal{R},\mathcal{T})\delta g^{\mu\nu} - 8\pi T_{\mu\nu}\delta g^{\mu\nu}\Bigg]\sqrt{-g}d^4x, \quad \text{(A.10)}$$

with $T_{\mu\nu} \equiv -2\frac{\delta(\sqrt{-g}L_m)}{\delta g^{\mu\nu}}$ being the definition of the energy-momentum tensor. Integrating by parts the second and third term of the right hand side of (A.10), one can obtain the field equations, by taking $\delta s = 0$, as

$$f_{\mathcal{R}}R_{\mu\nu} - \frac{1}{2}f(\mathcal{R},\mathcal{T})g_{\mu\nu} + (g_{\mu\nu}\Box - \nabla_\mu\nabla_\nu)f_{\mathcal{R}} = 8\pi T_{\mu\nu} - f_{\mathcal{T}}(T_{\mu\nu} + \Theta_{\mu\nu}), \quad \text{(A.11)}$$

where $\Theta_{\mu\nu} \equiv g^{\alpha\beta}\frac{\delta T_{\alpha\beta}}{\delta g^{\mu\nu}}$. If we consider that the function $f(\mathcal{R},\mathcal{T})$ is reduced to $f(\mathcal{R})$ one can obtain from (A.11) the field equations of the $f(\mathcal{R})$ gravity.

Now, applying ∇^μ in (A.11)

$$f_{\mathcal{R}}\nabla^\mu R_{\mu\nu} + R_{\mu\nu}\nabla^\mu f_{\mathcal{R}} - \frac{1}{2}g_{\mu\nu}\nabla^\mu f(\mathcal{R},\mathcal{T}) + (\nabla_\nu\Box - \Box\nabla_\nu)f_{\mathcal{R}} = 8\pi T_{\mu\nu} - f_{\mathcal{T}}\nabla^\mu T_{\mu\nu} - f_{\mathcal{T}}\nabla^\mu\Theta_{\mu\nu} - (T_{\mu\nu} + \Theta_{\mu\nu})\nabla^\mu f_{\mathcal{T}}. \quad \text{(A.12)}$$

and making use of the following mathematical identities

$$\nabla^\mu G_{\mu\nu} = 0 \quad \text{(A.13)}$$

$$(\Box\nabla_\nu - \nabla_\nu\Box)\phi = R_{\mu\nu}\nabla^\mu\phi \quad \text{(A.14)}$$

$$\nabla^\mu f(\mathcal{R},\mathcal{T}) = f_{\mathcal{R}}\nabla^\mu R + f_{\mathcal{T}}\nabla^\mu T, \quad \text{(A.15)}$$

one can achieve that

$$\nabla^\mu T_{\mu\nu} = \frac{f_{\mathcal{T}}}{8\pi - f_{\mathcal{T}}}\left(\nabla^\mu\Theta_{\mu\nu} + (T_{\mu\nu} + \Theta_{\mu\nu})\nabla^\mu \ln f_{\mathcal{T}} - \frac{1}{2}\nabla_\nu T\right), \quad \text{(A.16)}$$

if we take $f_{\mathcal{T}} = 0$, the conservation of the energy-momentum tensor is recovered as in GR and $f(\mathcal{R})$ theories of gravity.

FOLHA DE REGISTRO DO DOCUMENTO

1. CLASSIFICAÇÃO/TIPO	2. DATA	3. REGISTRO N°	4. N° DE PÁGINAS
TD	11 de abril de 2019	DCTA/ITA/TD-006/2019	98

5. TÍTULO E SUBTÍTULO:

White dwarfs in general relativity, modified theories of gravity and binary systems.

6. AUTOR(ES):

Geanderson Araújo Carvalho

7. INSTITUIÇÃO(ÕES)/ÓRGÃO(S) INTERNO(S)/DIVISÃO(ÕES):

Instituto Tecnológico de Aeronáutica – ITA

8. PALAVRAS-CHAVE SUGERIDAS PELO AUTOR:

Compact stars; White dwarfs; Gravitation; Modified theories of gravity; Binary systems; Gravitational waves.

9.PALAVRAS-CHAVE RESULTANTES DE INDEXAÇÃO:

Estrelas anãs; Gravitação; Estrelas massivas; Ondas gravitacionais; Relatividade; Física.

10. APRESENTAÇÃO: **X Nacional** **Internacional**

ITA, São José dos Campos. Curso de Doutorado. Programa de Pós-Graduação em Física. Área de Física Nuclear. Orientador: Prof. Dr. Rubens de Melo Marinho Júnior; coorientador: Jorge Armando Rueda Hernández. Defesa em 09/04/2019. Publicada em (2019).

11. RESUMO:

In this work we perform, initially, a comparative study of the hydrostatic equilibrium of white dwarfs (WD) in different approaches, namely, Newtonian and general relativistic. We obtain that the structure of these stars suffer effects from both special and general relativistic corrections for stars with mass $M>1.3M_\odot$. We also consider the inclusion of effects in the structure of WD from strong electric fields, for such we suppose a superficial net charge distribution in those stars. We find that the total charge necessary to appreciate considerable effects in the structure of WD is of the order of $10^{19-20} {\rm C}$, whose electric fields at the surface $E\sim 10^{17-18}{\rm V/m}$ are mostly below the Schwinger critical field limit $1.3\times 10^{18} {\rm V/m}$. In this case, even with fields smaller than the critical one we obtain super-Chandrasekhar WD masses in the order of $\sim 2M_{\odot}$, being in this way consistent with estimated masses measured from supernova Ia observations. We consider also a modified gravity model, in which in the Einstein-Hilbert Lagrangian the Ricci scalar is replaced by an arbitrary function of the form $f(\R,\T)$, where $\R$ and $\T$ represent the Ricci scalar and trace of the energy-momentum tensor, respectively. We showed from the hydrostatic equilibrium, for the specific functional form $f(\R,\T)=\R+2\lambda \T$, that the maximum mass of WD is modified according to the variation of the parameter λ. The larger the magnitude of λ the larger and more massive stars are found. We also find for the suggested model that the maximum mass stars' central densities are smaller than the ones obtained in General Relativity and other modified theories of gravity. We investigated also some properties of the D-dimensional Fermi gas to show that WD are gravitationally unstable due the presence of extra spatial dimensions. Moreover, we showed that the electric field induced by magnetic friction in double WD binaries can power a high electromagnetic emission (for $B>10^{9}$G) and it can also change the orbital evolution of the binaries.

12. GRAU DE SIGILO:

(X) OSTENSIVO **( ) RESERVADO** **( ) SECRETO**